ScuDo

Scuola di Dottorato ~ Doctoral School

WHAT YOU ARE, TAKES YOU FAR

Doctoral Dissertation

Doctoral Program in Electronics Engineering (29^{th}cycle)

Analysis and Modulation of Molecular Quantum-dot Cellular Automata (QCA) Devices

By

Ruiyu Wang

******

Supervisor(s):

Prof. Gianluca.Piccinini., Supervisor

Prof. Mariagrazia.Graziano., Co-Supervisor

Doctoral Examination Committee:

Prof. Csaba György, Referee, Pázmány Péter Catholic University

Dr. Pavel Jelinek, Referee, Czech Academy of Sciences

Politecnico di Torino

2017

Declaration

I hereby declare that, the contents and organization of this dissertation constitute my own original work and does not compromise in any way the rights of third parties, including those relating to the security of personal data.

Ruiyu Wang
2017

* This dissertation is presented in partial fulfillment of the requirements for **Ph.D. degree** in the Graduate School of Politecnico di Torino (ScuDo).

I would like to dedicate this thesis to my loving parents

Acknowledgements

And I would like to acknowledge ...

Abstract

Since its introduction, the traditional CMOS technology has been through a remarkable growth and development. It has led, till recent years, to double the number of devices on a chip every eighteen month, according to the Moore's law. This has been possible thanks to the scaling of the devices. The scaling is a particular important process, that allows to obtain faster devices, with a reduced power consumption and a greater density on chip.

The quickening pace of scaling for MOSFET technology accelerates the introduction of many new technologies to extend CMOS into nanoscale MOSFET structure. In particular, in 2014, the first 14*nm* scale devices were shipped to consumers by *Intel*. Meanwhile the *International Technology Roadmap for Semiconductors (ITRS)* also defines the 5 nanometer (5*nm*) node as the technology node following the 7*nm* node that may be achieved by the end of this decade (2020), when the Moore's law may reach the end. This is due to the fact that these technologies of scaling process have serious drawbacks: first of all, the size reduction brings major technological problems. For example the interconnections, whose scaling rate is much less substantial than the devices themselves, also the photolitography techniques are not sufficiently developed to satisfy the required resolution and throughput; then, with the increasing device density, the power consumption thus becomes voracious.

For all these reasons, with a cautious optimism, several completely new approaches to information-processing and data-storage have been addressed as beyond CMOS study. Rather than vying to "replace" CMOS with the current roadmap, these embryonic paradigms could extend to new applications domains in nanometer size where is currently not accessible to CMOS. As one of these successful new proposals, the *Field-Coupled Nano-computing (FCN)* bypasses the traditional

CMOS transistor and utilizes local field interactions between interconnected primitive nanoscale logic blocks to transfer and process digital information.

As a leading solution of FCN, the *Quantum-dot Cellular Automata (QCA)*, is an emerging technology introduced for digital computation with the aim of simultaneously reducing both device size and power consumption. In particular, it offers an alternative way for implementing molecular electronic, in which information transmission and processing depend on electrostatic interactions between charges in arrays of cells composed of six quantum dots. For each six-dot cell, there are two mobile charges localized inside and depending on the free charges position inside, the binary information could be encoded. No current flows between QCA devices during operation thus strongly reducing the power dissipation.

Regarding the physical implementation of the QCA technology, different solutions were proposed in literature as well as prototype or more advanced circuits were developed. Among all, its molecular solution, the so-called *Molecular Quantum-dot Cellular Automata (MQCA)* is found to be the most promising, since high operating frequency (THz) and ambient working temperature could be allowed due to nanometer size of a molecular system, though a molecular prototype is not yet demonstrated. Importantly, in literature preliminary attempts to demonstrate the MQCA feasibility were carried out from both theoretical and experimental point of view.

This work focused on developing the methodology to characterize the feasibility of an artificially synthesized molecule (named *Bis-ferrocene*) as an element to build MQCA devices and realize QCA operation. Moreover, the behavior of MQCA functional logic blocks made of this candidate molecule has also been demonstrated and analyzed from an electronic point of view.

To be specific, the procedure of characterizing single bis-ferrocene molecule, which could be recognized as half QCA cell, includes quantum chemistry ab-initio simulations and post-processing of simulation data. During the simulations, biasing conditions like externally applied electric fields (write-in system or clock) and point charges are adopted for simulating the working environment of MQCA, e.g., adiabatic switching of molecules, thus completing the characterizing procedure. In addition, different from previous literature, in order to represent the characterization results which describe the physical or chemical property of molecule into quantities that could be measured by electronic instrumentation for further read-out system

design, new figures of merits like *Aggregated Charge* and *Equivalent Input Voltage* V_{IN} were defined through mathematical equations.

Whereas for of MQCA functional logic blocks, they could be demonstrated aligning a group of molecules together following the designed patterns. Binary information is transmitted via electrostatic interaction between groups of atoms on molecules. However, regarding simulation the classic quantum chemistry show its limitation in terms of optimizing molecular system as a whole. As a consequence of that we have proposed an alternative new method of analysis based on a novel algorithm implemented *MATLAB*. This algorithm for MQCA device study relies on data obtained from ab-initio simulation that describes single molecule reaction to another molecule in presence, i.e., the trans-characteristic (charge vs. applied E-field) relation, and on models of describing and superposing the electrostatic interactions among all molecules distributed. In detail, every molecule along the MQCA structure will arrange its charge configuration according to the influence of neighboring molecules. Such re-arranged charge continues on its turn to affect back the other molecules. The algorithm iterates these steps of *Cause and Effect* in a sequence, e.g. their positions, for all molecules in presence, and then superposes all counted interactions among molecules until reaching convergence in a self-consistent way. Eventually the aggregated charges of molecules are obtained as output data. Such quantitative data foresee the information propagated inside MQCA devices thus describing their performance. However, it is necessary to mention that the electrostatic interaction among neighboring molecules considered here is ideal neglecting the so-called *Screening Effects*, which exists between molecules and metal nanowires or among molecules themselves, for the sake of approximation and reducing intensive computation resource. The influence caused by the screening effects is out of the main goal of current work. On the other hand, although our study is based on bis-ferrocene molecule, the proposed methodology and analysis procedure is not only concentrated on one specific candidate molecule. The whole analyzing package discussed above is both fundamental and generic, which provides also the possibility to examine other potential candidate molecules that might be suitable or not with purpose of MQCA computation. More importantly, as future work, more precise molecular interaction modeling mechanism, screening effects between molecules and conduction metal nanowires or among molecule themselves as well as dynamic switching response of molecules should be involved increasing the accuracy of our modeling methods. Furthermore, some applications

have been run with the new method of MQCA analysis to emulate some disturbances that might occur during operation, such as thermal noises or experimental related defects, e.g. mis-alignments or missing molecules. These results could provide important feedback to both circuit designers and technologists facilitating the fabrication of MQCA prototype.

As a summary, this work is organized as follows:

- **Chapter 1: Introduction**:
  The state-of-the-art technology of FCN and QCA are introduced here. This chapter also discusses the general working principle of QCA based on its cell structures, and the clock system used for realizing adiabatic switching and possible solutions for realizing clock system are present at the end.

- **Chapter 2: QCA Device Implementation**:
  Possible physical implementations of QCA technology are discussed, including the metal-dot solution, the semiconductor solution, the magnetic and molecular solution.

- **Chapter 3: Review of Molecular QCA**:
  Here a review of molecular solution of QCA is presented in detail. Based on the requirements for MQCA candidate, the ad-hoc synthesized molecule (named *Bis-ferrocene*) is thus introduced. Meanwhile, the binary information encoding and switching mechanism based on applied biasing conditions inside molecules are also mentioned.

- **Chapter 4: Bis-ferrocene Molecule Analysis as QCA Device**:
  In this chapter, the two-stage methodology envisaged for single bis-ferrocene molecule analysis, which is recognized as half a MQCA cell, has been described. It is based on quantum chemistry ab-initio simulation (*Gaussian 09* simulation) and post-processing of data. A brief introduction of quantum chemistry simulation and the usage of *Gaussian 09* are provided.

- **Chapter 5: Molecular Characterization Results**:
  Results regarding single bis-ferrocene molecule analysis are obtained and discussed here. These results include molecular reaction to externally applied biasing conditions that emulate proper working environment, e.g. electric field as write-in stage and clock system, or point charges that represent the

presence of another molecule nearby. At the end, similar analysis has been performed for case of a complete MQCA cell with two molecules together. Therefore, the MQCA cell response is also illustrated.

- **Chapter 6: MQCA Binary Wire Analysis**:
  This chapter demonstrates the limitation of using quantum chemistry method to analyze a binary MQCA wire, which is the most straightforward functional block for building digital circuit. Then a method based on iterative steps of ab-initio simulations between two molecules is present as another attempt for understanding molecule switching mechanism along wire to forwarding information. At last, an alternatively new method of wire analysis is proposed based on a novel algorithm for modeling and computing electrostatic interaction among molecules, based on which information encoding and processing throughout the wire is determined. Furthermore, in this method, the clock zones and multi-phase clock signals for adiabatic switching is firstly considered.

- **Chapter 7: MQCA Functional Block Analysis**:
  In this chapter, the proposed algorithm for analyzing MQCA wire has been extended to two-dimensional structure analysis in cases like MQCA inverter, three-input majority gate, etc.

- **Chapter 8: New Method of Analysis Application**:
  Some applications have been performed here using the new method of analysis with the aim of determining the tolerance of MQCA device with respect to external disturbances and exploring its potential of high throughput of information.

- **Chapter 9: Ongoing and Future Work**:
  At last, some ongoing and future work has been mentioned regarding the enhancement of new method as well as the novel algorithm. In addition, some experimental trials have also performed for eventual demonstration of MQCA device.

- **Chapter 10: Conclusion**:
  This chapter summarizes all work and strengthens the main contributions of this work.

Contents

List of Figures

List of Tables

Chapter 1

Introduction

1.1 State-Of-The-Art: Beyond CMOS Technology

In the world of electronics, the famous Moore's prediction has been proved accurate for several decades, meanwhile it has also been used in the semiconductor industry to guide long-term planning as well as to set targets for research and development [1]. Moore's law is not so much a physical law as an observation or projection. Although it held steady from 1975 until around 2012, its rate was more rapid during the first decade. In fact, it might not be logically sound to extrapolate from the historical growth rate into the indefinite future for electronics growth. For example, the updated International Technology Roadmap for Semiconductors in 2010 has predicted that such growth would slow around 2013 [2] and in the year of 2015 Gordon Moore foresaw and announced that the rate of technological progress would reach the final saturation: "I see Moore's law dying here in the next decade or so [3]."

Therefore, with the generally acknowledged sunsetting of Moore's Law, in April 2014, the ITRS committee announced it would be reorganizing the ITRS Roadmap to better suit the needs of the industry. The idea was to summarize all the elements related to the seventeen technical working groups and allocate them into seven focus topics [4], among which two trends have been followed since then by the technological development in electronics. The first one is the so-called *More Moore* trend, this optimistic group sticks on Moore's law and aims at the continued shrinking of the CMOS transistor size till reaching the nanometer size. The main advantages

of CMOS transistor scaling are the better increased performance in terms of ultra fast operating frequencies and the increased device density. However, this miniaturization leads to a voracious appetite for power consumption and in a chip with high device density the power dissipation becomes a problem. The second trend is called *Beyond CMOS* or *More than Moore* which refers to the possible future digital logic technologies beyond the CMOS scaling problems that limits device density and speeds due to heating effects [5]. In particular, this technological trend aims alternatively on devices that provide electronics but aren't CMOS based. Inside this judicious new paradigm both logic state encoding and digital computation are performed without current flow. As a consequence of that, the amount of power consumption is strongly reduced and it is related only to the leakage of interface circuitry.

In the *Emerging Research Devices* (ERD) section of the International Technology Roadmap for Semiconductors (ITRS,[6]), beyond CMOS, several completely new approaches to information-processing and data-storage technologies and architectures are emerging to address the timeframe beyond the current roadmap. Among all of these embryonic solutions, the so-called *Field-Coupled Nano-computing (FCN)*, a new family of nano-devices for binary computation, starts to exhibit its huge potential for vying to "replace" CMOS technology.

1.2 Field-Coupled Nano-Computing

As one of the new approaches for emerging technology beyond CMOS, Field-Coupled Nano-computing (FCN) bypasses the transistor paradigm and utilizes local field interactions between nanoscale building blocks in patterned arrays that are carefully organized to transfer information and implement digital logic, which do not use transistors or involve charge transport. Each of the leading FCN paradigms - Quantum-dot Cellular Automata (QCA), Molecular Quantum-dot Cellular Automata (MQCA), NanoMagnetic Logic (NML) and Atomic Quantum-dot Cellular Automata (AQCA) is a potential candidate for post-CMOS nanocomputing because of their promising and unique features, and each faces also critical challenges to realization [7].

1.3 General Principle Of QCA

The theory of Quantum-dot Cellular Automata (QCA) was proposed by C.S. Lent and his co-worker at early 1990s [8]. QCA is a means of representing binary information in its basic units, known as cells, through which no current flows. The device performance is achieved by the coupling of such QCA cells through field interaction, either electrostatic or magnetic. Binary information is stored in the arrangement of polarized charge (or magnetic dipoles) within the QCA cell. More importantly, inside these cells there is no monopole moment and they are destined to be bi-stable having two low energy states, with different dipole or quadrupole orientation which can encode a classic logic state 1 or 0.

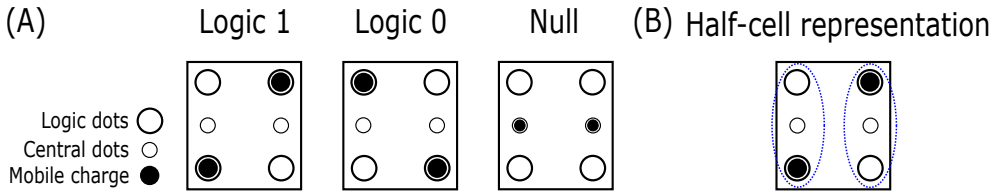

Figure 1.1 QCA cell structure and logic state encoding. (A) In QCA, the logic state is encoded in terms of different arrangement of mobile charges inside the six-dot structure: if two mobile charges labeled with black spheres are distributed along one of the antipodal site of the cell, the traditional logic state "0" or "1" is achieved, whereas if thus charges occupy the central dots thus forming the *NULL* state; (B) The complete QCA cell is divided into two half-cells, and because of Coulombic interaction, two single charges distribute opposite logic dots in these two half-cells.

According to this new paradigm demonstrated in [9–11], digital devices are possible to be designed with arranged cells and inside each cell there are six quantum dots (or four quantum dots depending the implementation technology) together with two mobile charges. Such QCA cell has a shape of square with four quantum dots localized in the corner of the square, named working or logic dots and two quantum dots in the middle, i.e., the central dots. Therefore, the quantum mechanics and the Coulomb interaction lead to a natural charge confinement of those free charges on antipodal sites, occupying one of the two diagonals formed by the logic dots. As shown in Figure 1.1(A), these two probable configurations of charges are demonstrated thus encoding binary logic states. Moreover, if the two mobile charges are forced to occupy the two central dots, such configuration of charges does not represent a real logic state, nevertheless it is essential for realizing adiabatic switching issue, thus it is called *NULL* state [12]. Note that Figure 1.1(B) depicts that the full

six-dot cell can also be viewed as a pair of half-cells (with two dots each) in which the sign of the dipole alternates, i.e., the single mobile charge localized on different logic dots inside these two half-cells.

Due to confining potential barriers and coupling mechanisms, in principle the free charges can tunnel between dots inside the cell, but not outside. Then, the state change of the cell is provided by the internal charge re-arrangement. The ideal distance between two neighboring QCA cells is equal to the width of a single cell, which is the distance *d* between two corner logic dots along the same side highlighted in Figure 1.2. Whereas concerning the propagation of the logic state encoded by the cell, electrostatic repulsion among free charges inside each cell is responsible for creating the interactions among QCA cells, every QCA cell distributes its charge with respect to the presence of other nearby cells so that the digital computation is performed with involving current flow.

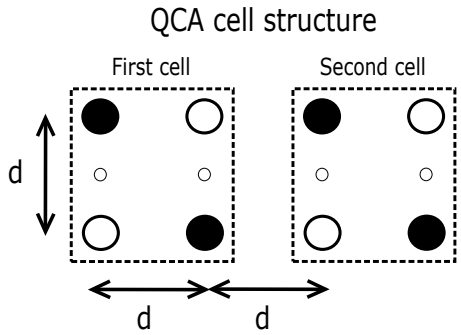

Figure 1.2 Interaction between two neighboring QCA cells: the second cell on the right is located with a distance of *d* away from the first cell on the left and it will re-arrange itself in terms of forming the same charge configuration as the first cell minimizing the electrostatic repulsion as well as the total energy.

Consequently, this remarkable simple interaction enables general purpose computing, e.g., fundamental logic blocks for QCA circuits could be implemented by means of suitable layouts of those QCA cells arrays [13]. For example, data can be moved in a QCA circuit with a row of QCA cells aligned together with identical distance in between, i.e., a binary QCA wire. A binary signal propagated from left to right of the wire because of electrostatic interactions between adjacent cells, the scheme of a QCA wire is reported in Figure 1.3(A)(B). Although in traditional CMOS transistor based electronic circuitry the wire is just a simple metal line, in QCA technology it is considered to be a computational element since the correct propagation of the binary information depends on the proper states encoded by all

the cell along the line. Other basic logic gates like majority voter and inverters could be also schematically implemented [14], as depicted in Figure 1.3(C)(D). In particular, inside the majority voter, the three input cell vote for the logic state of the output cell. The majority voting function can be also reduced to an OR or AND function by forcing the logic state of one input cell to a 1 state or a 0 state. Meanwhile, inversion of binary information is also possible and hence the QCA's logic set complete in terms of functionality. In literature, a lot of works have been already proposed for the design of many complex QCA systems, such as arithmetical units, e.g., adders and multipliers, mentioned in [13, 15–17] and even microprocessors, like in [18, 19].

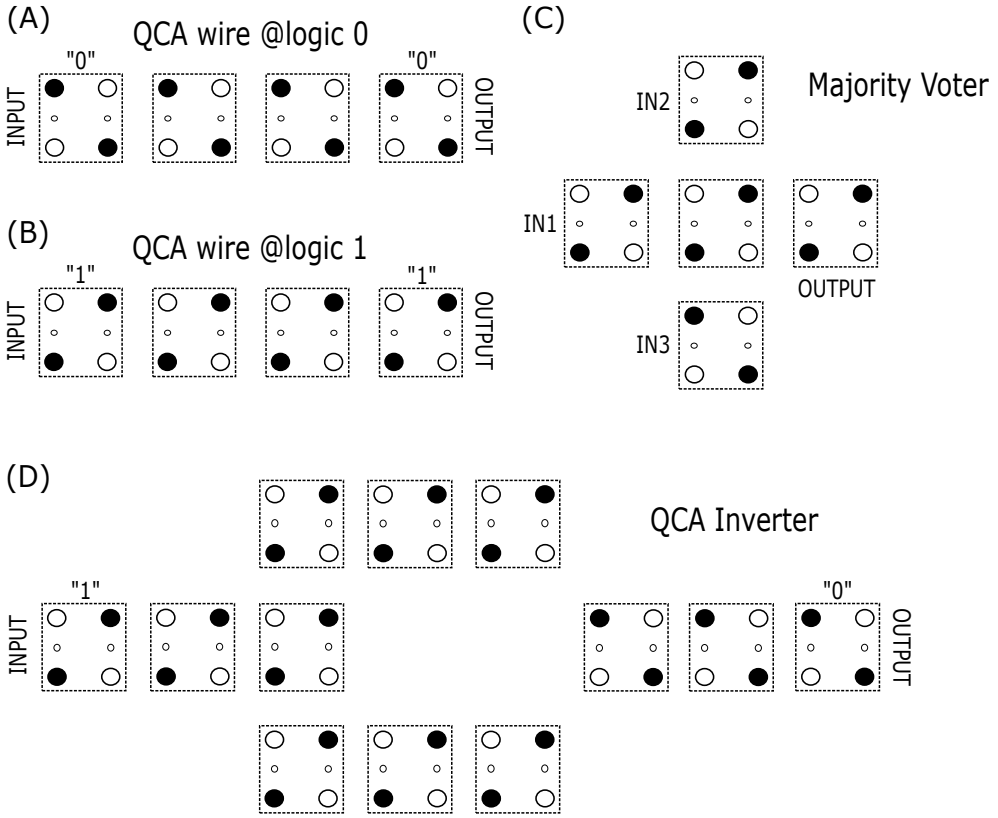

Figure 1.3 Fundamental QCA devices: (A, B) QCA wire with both logic state considered at the input cell on the left, the binary wire transmits information between the input and the output cell. (C) The three-input majority gate of QCA, which is the fundamental logic element of the QCA architecture. The logic state of the output cell is determined by two or more of the logic states of the total three inputs. (D) The QCA inverter uses the electrostatic interaction of diagonally aligned QCA cells to invert the logic state come from the input cell and to propagate it to the output.

1.4 Clock Of QCA

According to a complete analysis of the quantum phenomena and the thermodynamics mechanism involved in a QCA circuit mentioned in [10], there is a maximum number of QCA cells allowed in the circuit to warranty the proper QCA computation. This number increases with the decreasing size of the cell or with lowering temperature. Moreover, the authors in [20] mentioned that the abrupt switching of the QCA cell state could lead to meta-stability problems along the circuits. Thus with the aim of overcoming these limits during computation guaranteeing the quality of information transfer, it is suggested to adopt a different mode of switching for QCA circuits with large number of cell involved, which is the so-called *Adiabatic Switching* [12, 20–22]. The adiabatic switching is the quantum version of adiabatic theorem. In particular, adiabatic switching mechanism between different logic states of cells consists of three main stages:

- Lowering the inter-dot potential barriers in order to remove the old logic state encoded by the charges of the cell thus leaving the cell in *NULL* state;
- Applying the new logic signal to the cell;
- Raising again the potential barriers in order to lock the cell in the new logic state.

It is necessary to stress that, these transition stages should be performed gradually avoiding those cells falling into meta-stable states.

Concerning the physical implementation of adiabatic switching mechanism, a possible solution in terms of using a multi-phase clock system to guide the switching interactions was proposed in [20] from a technological point of view. Firstly, the QCA circuit system is needed to be partitioned into small areas, named *Clock Zones* and inside each clock zone an external reference signal, i.e., *Clock*, is applied with four phases to help the state transition of the cells during each stage of the adiabatic switching mechanism, e.g., switching the cells between a *NULL* state and an active logic state (either 0 or 1) enabling the computation.

Figure 1.4(A)(B) illustrates in principle a natural sequence of three clock signals applied to a majority voter that is correspondingly partitioned into three clock zones marked by different intensity of grey. It also highlights the data flow through three

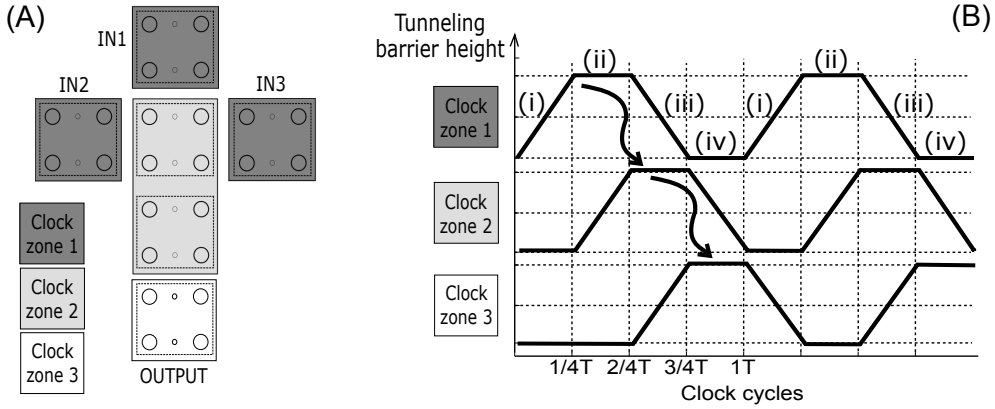

Figure 1.4 Scheme of QCA clock zones: (A) Clock zones partitioned on a clocked QCA three-input majority voter; (B) A periodic waveform of applied multi-phase clock signal on each clock zone of the majority voter. The clock signals for three clock zones repeat the same pattern with a fixed difference of one quarter of the period between each other, whereas the arrows demonstrate the flow of information from one zone to the next inside the circuit [22].

adjacent clocking zones by well-designed timing of the multi-phase clock signals [23]. Each clock signal is in four adjacent and periodic phases and these clock signals will be attached to every cell of the QCA device. The clock signals adopted here possess the ability to control the tunneling barriers of all dots within each cell, and they are switched quasi-adiabatically. In particular, the tunneling barriers of each cell are raised and lowered smoothly to determine how and when each cell reacts to its neighbors. As discussed in [22, 24], these tunneling barriers which guided by the clock signals are representatively modulated in terms of four phases, as depicted in Figure 1.5 and they are called *Switch*, *Hold*, *Release* and *Relax*.

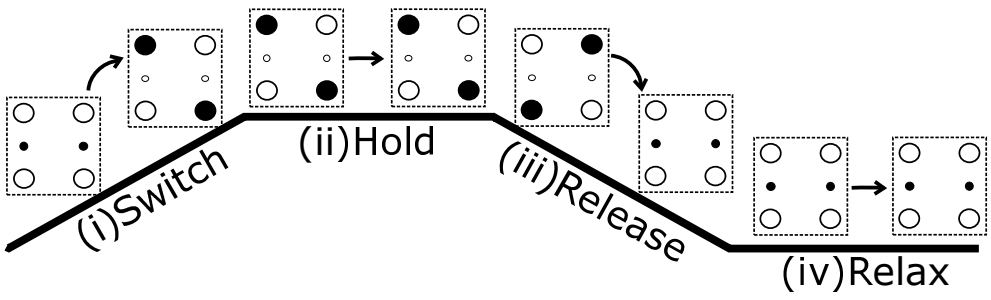

Figure 1.5 Detailed description of the applied four phases QCA clock signal waveform.

During the *Switch* phase, the potential barrier is increasing and the mobile charges inside the cell are naturally localized on the dots along one of the two diagonals, so

the cell arranges its state becoming polarized according to the neighboring cells, thus the binary information is encoded and propagated. Then, in the *Hold* phase, the inter-dot potential barriers are raised to the highest value so that the cells are locked in their previous logic states and act as a driver for the cells of the nearby clock zone, no further switching phenomena is observed. The states of cells in this phase are locked, thus at this point the effective tunneling element between the logic state "1" and logic state "0" is negligible. Next, in the *Release* phase, the inter-dot potential barriers are lowered and the free charges are thus forced to move to the central dots of the cell, hence these cells lose their polarities. Finally, in the *Relax* phase, the potential barrier reaches and keeps its lowest value and the cells are retained in unpolarized state, i.e., *NULL* state, where the free charges are kept in the central dots of the cell. In this way the cells inside this clock zone have no influence to the cells of the other clock zones.

Applying a clock signal with these above mentioned four clock phases to each clock zone and considering a difference in phase in terms of a quarter of the period between two adjacent clock zones, the multi-phase clock system is physically obtained. Possible clock signal waveform for all clock zones are schematically illustrated in Figure 1.5(B). Alternating the multi-phase clock signal in each zone ensures the proper information propagation as well as correct QCA computation following the directions of arrows. For example, if a QCA wire is partitioned into several zones and the same clock mechanism is applied, this binary wire will transmit the data along itself like a shifted register.

As another example of complex clocked QCA logic structure, Figure 1.6 depicts an 8-to-1 multiplexer implemented with QCA cells [24]. The whole circuit layout is divided into multiple clock zones and each clock zone is identified by a gradation of grey and the four clock phases are alternated inside. Applying the clock signals to this circuit, the state of the QCA cells are managed in terms of only few cells per phase could switch and the information chosen by the select signals propagates from the eight inputs at the left to the single output located at the right.

In addition, clock system not only permits control of information flow around the circuit via adiabatic switching, it also enable true power gain in QCA devices [25]. As binary information is encoded by localization of charges and when it moves from part to part inside the circuit, the signal energy is lost to the outside environment due to unavoidable dissipative processes (e.g. phonon emission or inelastic

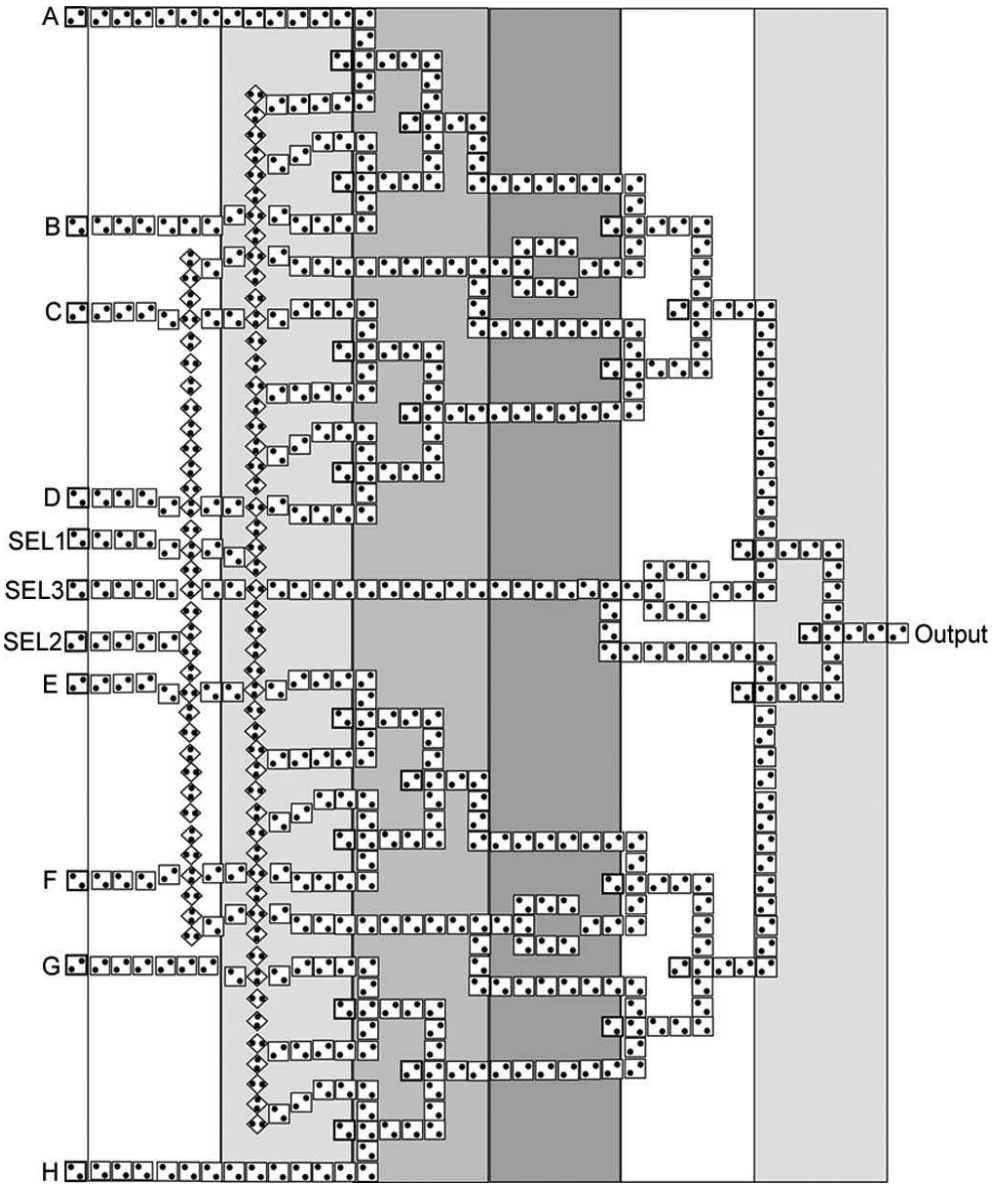

Figure 1.6 Clocking scheme is applied to a 8-to-1 multiplexer based on QCA cells [24].

losses). That amount of energy must be recovered otherwise the information itself propagated through will heavily decay or eventually be lost. Thus during the transition of each clock phase the actual power gain must exist, compensating the fact that a weak input signal is insufficient for retaining logic levels throughout the whole device. In conventional CMOS transistor-based circuits, the current from the power supply is responsible for the recovery of energy loss in the signal path. Whereas in the case of clocked QCA paradigm, such energy comes from the externally ap-

plied clock system without involving any current flow. The clock system favors the cell in order to restore cells to the fully polarized logic states. Theoretical analysis regarding power gain in QCA circuit has been performed in detail for both the metal-dot [26] and molecular cases [27]. Meanwhile, the power gain has been also experimentally measured in metal-dot QCA devices with clock applied [26].

Chapter 2

QCA DEVICE IMPLEMENTATION

QCA is not only a paradigm for computing from a theoretical point of view, but its corresponding devices have been experimentally demonstrated. Concerning physically implementing QCA technology, many solutions have been proposed and implemented over nearly two decades. Among them, some outstanding examples have been listed as follows.

2.1 Metal-Dot Solution

Inside this solution scheme, the dots in the QCA are represented by metal islands (for example Al) as shown in Figure 2.1, and the these metal islands are connected to each other by means of tunnel junctions allowing electrons to move freely [12, 21, 28–30]. This kind QCA cell is divided into two half-cells and between two half-cells there are capacitors coupled inside to prevent charge exchanging.

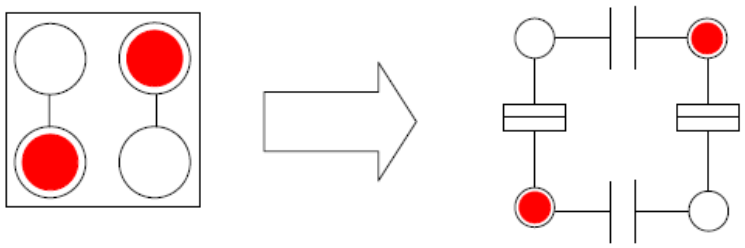

Figure 2.1 QCA cell and its equivalent QCA device circuit implemented with metal islands [29].

The metal-dot implementation was the first fabrication technology created to demonstrate the concept of QCA computing paradigm. A prototype of QCA cell based on this solution was built with the aim of showing QCA functionality [29]: the schematic cell structure is shown in Figure 2.2(A), whereas Figure 2.2(B) depicts the corresponded Scanning Electron Microscopy (SEM) image. However, because of the relatively large-sized dots that realized by metal islands and the associated thermal energy, such implementation system could work only when the environment temperature is kept extremely low, i.e., cryogenic temperature around tens of mK, for quantum effects (electron switching) to be observed and its structural properties are not suitable for scalable design of circuitry. In the meantime, the maximum operating frequency is limited in the range of MHz.

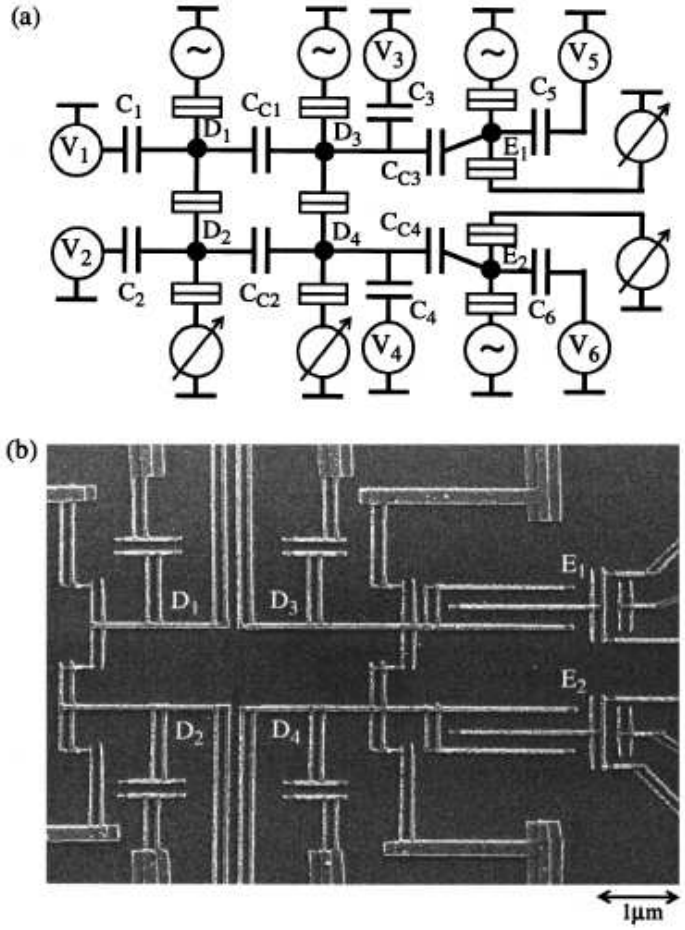

Figure 2.2 (A) A schematic diagram of QCA cell structure implemented with metal-dot solution; (B) The associated scanning electron micrograph of the implemented QCA cell [29].

2.2 Semiconductor-Dot Solution

Another idea proposed was based on a semiconductor structure [20]. Some possible implementations have been carried out using semiconductors like silicon [31] or GaAs/AlGaAs heterostructure [32].

In particular, the authors in [31] have experimentally demonstrated a four-dot QCA cell in an ion-implanted phosphorus-doped (Si:P) silicon system, as shown in Figure 2.3 with the SEM images. These four implanted (n^+) Si:P dots are distributed into tunnel-coupled pairs A and B, while each tunnel path has been coupled to an electron reservoir. In order to confine the charge movement within each pair A or B, the two dot pairs are coupled by means of two capacitors (Figure 2.3(A)) and meanwhile there is a gap sufficient to forbid electron to transfer between pairs. Moreover, the reservoirs at the source and drain make possible to characterize the cell via direct current and to determine the total electron occupancy of the cell. Inside Si:P system, the cell dimension reduction could also be down to the single donor level and the direct measurement of cell switching is also feasible thanks to a readout system realized with Single-Electron-Transistor (SET) of the cell.

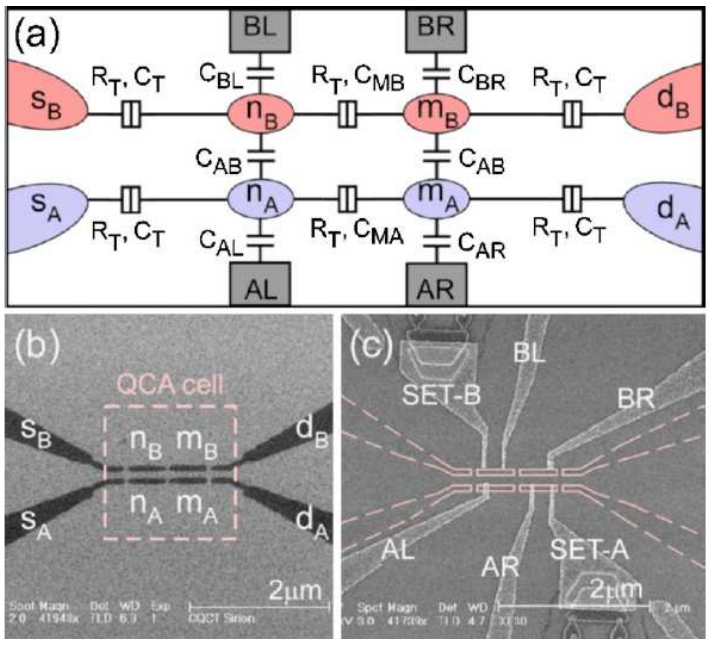

Figure 2.3 (A) Schematic equivalent circuit of the QCA cell based on ion-implanted phosphorus-doped (Si:P) silicon system; (B) SEM image of phosphorus-implanted n^+ regions which is highlighted as dark stripes in the image; (C) SEM image of completed QCA cell, whereas the dashed lines represents the buried n^+ dots and leads [31].

Regarding the solution with GaAs/AlGaAs heterostructure, Figure 2.4(a)(b) sketches the QCA cell electron micrograph as well as the equivalent circuit of the QCA unit cell. Four logic quantum dots are defined by top metal gates depleting 2 dimensional electron gas (DEG). There is also coupling between two half-cells using capacitors and measurement of cell switching is also achievable using direct current and locked-in measurement through the Ohmic contacts between source and drain [32].

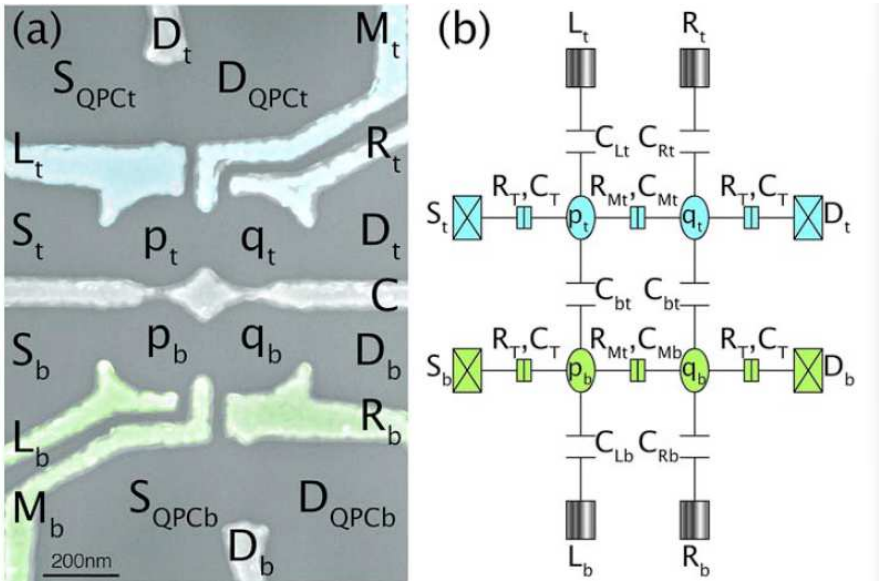

Figure 2.4 (A) The SEM image of a QCA cell implemented by means of GaAs/AlGaAs heterostructures; (B) Schematic equivalent circuit of the four-dot QCA cell [32].

Semiconductor (or solid state) QCA implementations could potentially be used to implement QCA devices with the same highly advanced semiconductor fabrication processes used to implement CMOS devices. Cell polarization is encoded as charge position, and quantum-dot interactions rely on electrostatic coupling. However, current semiconductor processes have not yet reached a point where scaling down the dot dimension up to nanometer size level is feasible.

Nevertheless, due to the low performance and extremely low working temperature which compared to standard CMOS based technology, both metal-dot and semiconductor approached were early abandoned.

2.3 Magnetic Solution

Another physical solution suitable for building QCA device is based on nanomagnet logic [33] which is the so-called magnetic QCA. The dots are realized by magnetic domains. Unlike traditional QCA paradigm that the logic states are encoded in terms of different configurations of mobile charges contained in the cells, the binary information in magnetic QCA is represented by the magnetization vector (up or down) of these nanomagnets. Instead of electron-tunneling effects, the term "Quantum" refers to the quantum-mechanical nature of the magnetic exchange interactions. Thus information propagates among magnetic QCA devices due to the magnetic field coupling interaction (ferromagnetic or anti-ferromagnetic) and devices implemented in this way could work at room temperature.

The magnetic QCA implementation is the most explored and developed since some preliminary experiments have been already carried out [34, 35]. Figure 2.5 reports some possible schematic logic blocks based on magnetic QCA and Figure 2.6 illustrates a three-input majority voter realized with these nanomagnets [34]. In particular, Figure 2.6(A) displays a SEM image of the equivalent circuit of majority voter, while Figure 2.6(B) and Figure 2.6(C) illustrate the magnetic force microscope images of magnetic ordering in the same circuit for two orientations of horizontal clocking field, as indicated by the red arrows [34].

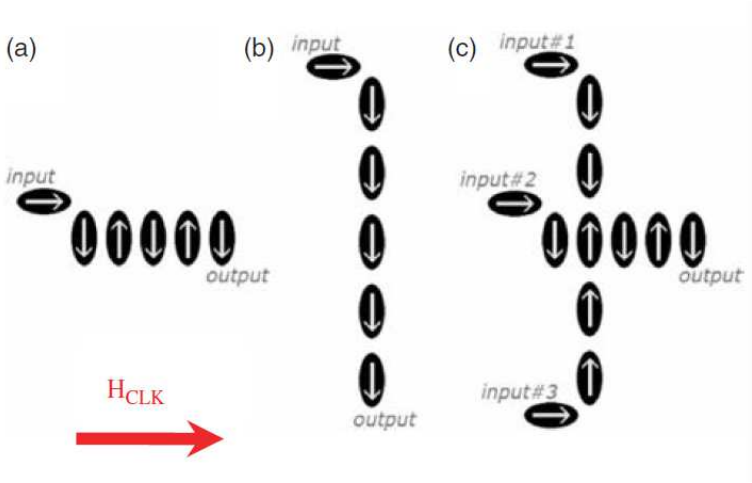

Figure 2.5 (A) Anti-ferromagnetically coupled binary wire; (B) Ferromagnetically coupled binary wire; (C) A combination of a majority voter and three binary wires: two, driven by inputs 1 and 3, are ferromagnetically coupled; one, driven by input 2 is anti-ferromagnetically coupled [34].

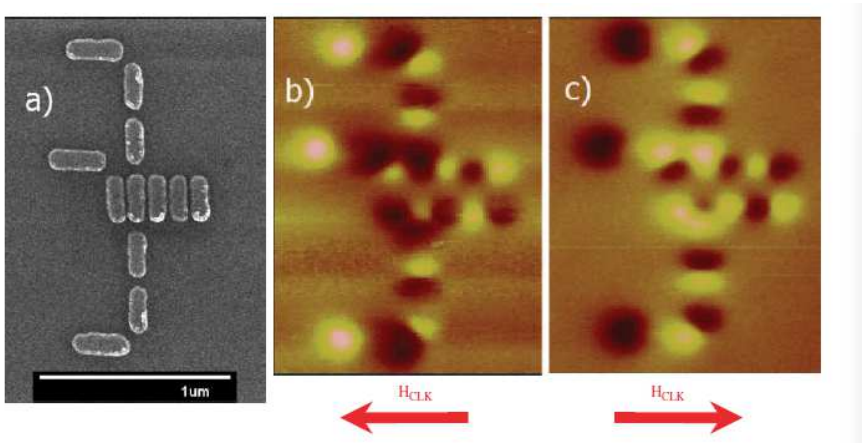

Figure 2.6 A QCA three-input majority voter implemented with nanomagnets [34].

2.4 Molecular Solution

Alternatively to those mentioned approaches, a proposed but not yet implemented method consists of building QCA devices out of single molecules, known as the Molecular QCA (MQCA) [14, 36–38]. The expected advantages of MQCA solution which make it superior to others are the highly symmetric cell structure, ultra-high switching speeds, extremely high device density, operation at room temperature, and even the possibility of mass-producing devices by means of self-assembly of molecules. However, a number of technical challenges, including choice of molecules, the design of proper interfacing mechanisms, and the clocking technology remain to be solved before this approach can be experimentally demonstrated. A detailed description of Molecular QCA solution and its performance will be discussed in the following chapter.

Chapter 3

REVIEW OF MOLECULAR QCA

3.1 Molecular QCA

Since the QCA paradigm is particularly well-matched to the challenge of molecular electronics, it is more natural to implement QCA devices using molecules. Molecuar QCA is found to be the most promising among all proposed emerging technologies due to this down to molecular size (nanoscale level) of device which could allow the computation to be performed at room temperature. Meanwhile the switching speed could also achieve the expected high operating frequencies (up to THz) as well as the high device density [39]. In particular, MQCA approach is an analogue of metal-dot QCA implementation and they both utilize configuration of mobile charges to determine logic states and binary information is transmitted via electrostatic interaction.

However, inside MQCA the quantum dots are served by redox sites of the molecules as charge containers. This is because a redox site can add an electron (be reduced) or loose an electron (be oxidized) without breaking the chemical bonds [25]. Therefore, the redox center could be characterized by low-lying non-bonding (π or d) orbitals. Generally speaking, a molecule is in its neutral form, whereas the performance of the MQCA computing could be enhanced if such molecule is in oxidized or reduced form. In the oxidized molecule, an electron is missing and its net charge is positive; in the reduced form, the molecule has attracted an electron resulting a negative net charge. As a consequence of that, the molecule and its corresponded counterion form a neutral system. Regarding the presence and influence of

the counterion of molecules, a solid description is discussed by the authors of [40] and [48]. Another feasible method to oxidize or reduce a molecule is provided by the cyclic-voltammetry (CV), hence the redox sites processes are electrically carried out.

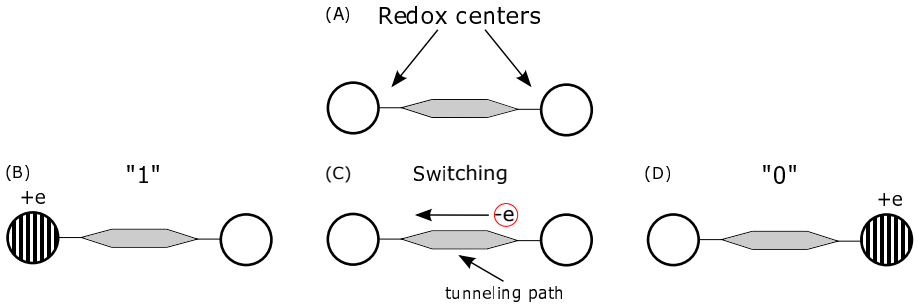

Figure 3.1 QCA Implementation of oxidized molecule with two redox sites: (A) molecule sketch; (B)logic state "1" encoding; (C) transient state for switching and (D) logic state "0" encoding.

Figure 3.1 shows a schematically simplified oxidized molecule with two redox centers (two dots), an electron is free move along the tunneling path and eventually localizes into one of the two redox sites available of the molecule [41]. Encoding of binary information corresponds to the charge configuration of the molecule: e.g., when the unit positive charge $+e$ is in the redox site on the left (the circle with internal blue pattern in Figure 3.1(B)), the molecule is, for example, in logic state "1". If the positive charge $+e$ occupies the right site (the circle with internal blue pattern in Figure 3.1(D)), then the molecule is in the opposite logic state "0". Apart from these charge configurations for information encoding, a transient switching state corresponding to the free electron $-e$ moving along the tunneling path from one dot to the other is also highlighted in Figure 3.1(C). The intermediate symbol (stretched exagon) represents the central part of the molecule which is slightly active from an electrostatic point of view. Furthermore, it acts like a channel to favor charge movement as well as a separator to favor the positive charge to entirely distribute on one of the two dots.

As mentioned in Section 1.4, motivated by the adiabatic switching mode, a single molecule should have more charge configurations adopted in MQCA circuit with more molecules to avoid meta-stability problem during switching of states [22, 42]. Therefore a single QCA cell must dispose six dots. Since a single molecule is naturally treated as half cell and a complete MQCA cell requires two identical

molecule juxtaposing together, a molecule now should possesses three dots, i.e., redox sites, as depicted in Figure 3.2. The extra third redox site is necessary for encoding the *NULL* state in which, for oxidized molecule, the positive charge $+e$ occupies the central dot. The half-cell representation by three-dot molecule and the complete MQCA cell with two molecules aligned together are shown in Figure 3.3. Specifically, the two half-cells interact with each other through the electrostatic forces among the free charges which tend to localize within each molecule in order to minimize the energy of the cell. Hence the free charges are able to occupy the dots along the antipodal sites of the square cell, as described in Section 1.3. By the same logic, the electrostatic interactions also determine the charge configurations (or logic state) of neighboring cells.

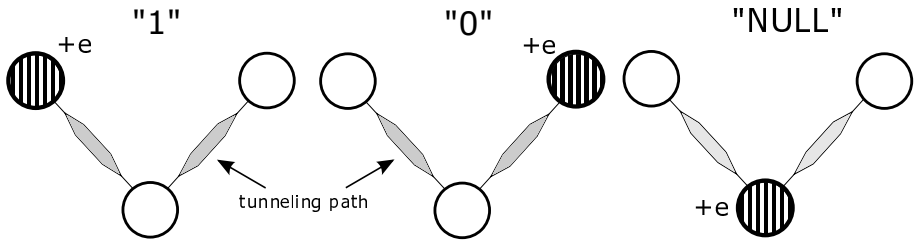

Figure 3.2 State encoding of a 3-dot molecule for QCA computation.

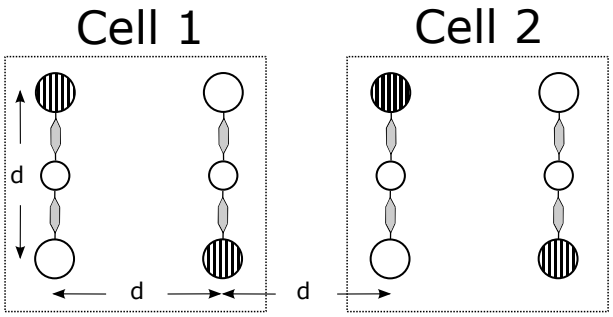

Figure 3.3 Complete MQCA cell and interaction between cells (top view).

3.2 Molecule Candidate: Bis-Ferrocene

Molecules with at least two redox sites are called mixed-valence compounds. Between the redox sites there is a bridging ligands acting as a tunneling path that allows an electron to move within the molecule [43]. However, unlike the construction of a half-cell with a single molecule and single mobile charge, some other

implementations could have four redox sites in single molecule, resulting in one molecule per one QCA cell with two mobile charges. For simplicity we will focus on the former mode for which there are two molecules in each full QCA cell.

A considerable literature have examined this class of mixed-valence compounds for the sake of seeking molecular candidates for MQCA realization, including both ideal and ad-hoc synthesized molecules. For example, the diallyl butane molecule mentioned in [14], the decatriene molecule reported in [44], the mixed-valence complex based on one iron atom (Fe) and one ruthenium atom (Ru) described in [45], the the self-doping mixed-valence zwitterion demonstrated in [46], the mixed-valence meta-Fe2 based on iron atoms (Fe) mentioned in [47] and the bis-ferrocene molecule discussed in [48].

3.2.1 Molecular Structure

During the journey of choosing suitable candidates for implementing MQCA devices, the candidate molecule on which this thesis focused is the so-called *Bis-ferrocene* molecule, as proposed and described in [48–52]. In specific, see Figure 3.4, this molecule has been synthesized ad-hoc for the purpose of QCA computation by a group of the chemistry department at the University of Bologna (Italy), in the frame of a collaboration among ST Microelectronics (Italy), University of Bologna and Politecnico di Torino (Italy).

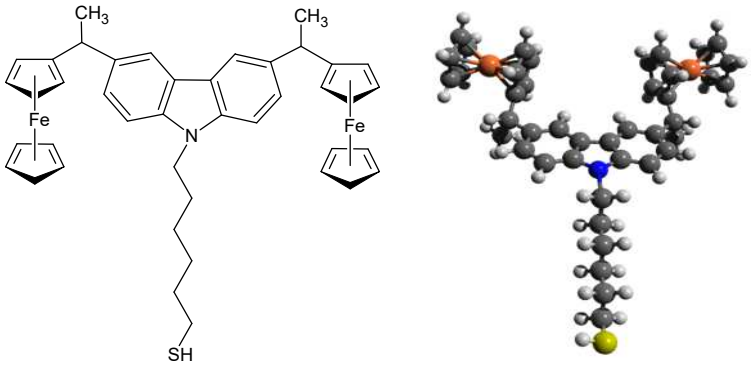

Figure 3.4 Bis-Ferrocene: (left)chemical structure; (right)ball-and-stick model.

The detailed physical structure and the associate simplified scheme of dot presentation for the bis-ferrocene molecule is reported in Figure 3.5(A)(B). According the requirement of molecules for QCA computation discussed at the end of Section

3.1, the molecule is constituted of two ferrocenes groups which are redox sites and functioned as logic dots (*Dot1* and *Dot2*), then a central carbazole bridge, i.e., the third redox site, that acts as middle dot (*Dot3*) for representing the *NULL* state.

With the aim of fabrication and demonstration, this molecule is also equipped with an alkyl chain as a binding element in order to connect the molecule to the ending thiol (-SH) group. Whereas this ending group is used to anchor molecules to real substrates, e.g., gold surface, by means of Self-Assembled-Monolayer (SAM) formation [48]. Regarding the dimension of the molecule, the distance between the two logic dots, measured between the centers of two iron atoms inside ferrocenes groups, is 1.0*nm*, whereas the total height is 1.8*nm*, as sketched in Figure 3.5(A). As mentioned in Section 1.3 and Figure 1.1(B), single bis-ferrocene molecule, as well as its three simplified dots, is considered as half MQCA cell, thus aligning two molecules together with a distance of 1.0*nm* forms a complete square MQCA cell (Figure 3.5(C)).

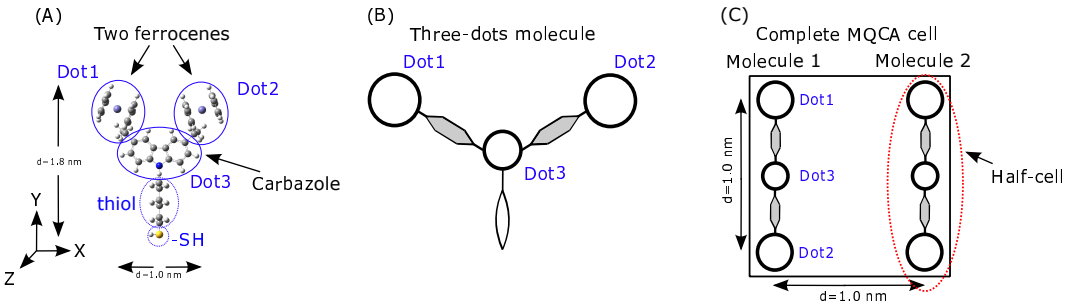

Figure 3.5 The bis-ferrocene molecule: (A) molecular structure; (B) simplified 3-dot scheme; (C) MQCA cell based on bis-ferrocene molecule.

About the molecular features, the authors in [48] have proposed and synthesized three isomers of the bis-ferrocene molecule: two diastereoisomers (the (S, S) and (R, R) chiral compounds) and the mesoisomer, as depicted in Figure 3.6. The difference among them is determined by the position of the ferrocenes with respect to the carbazole plane. According to Section 3.1, the bis-ferrocene possesses similar three molecular forms, which are neutral, oxidized and reduced. Detailed analysis about these three forms of molecules as QCA devices is reported in [53]. Whereas an oxidization process of bis-ferrocene molecule could be also performed in two ways: (1)chemical oxidization via introducing the atom of iodine (I) as counterions; (2)electrical oxidization by means of cyclic-voltammetry (CV) [48]. In addition, the author of [48] has also performed experiments for demonstrating the possibility of

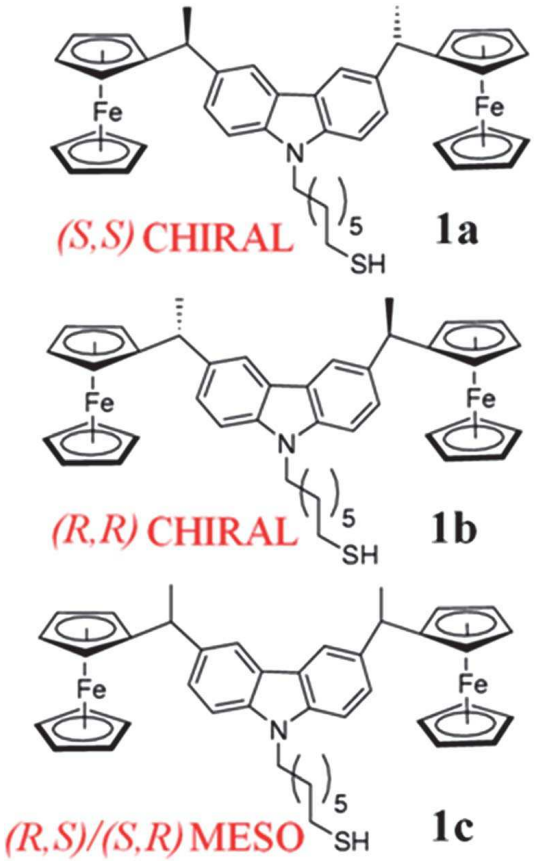

Figure 3.6 The bis-ferrocene molecule: structure of the synthesized two diastereoisomers and the meso isomer [48].

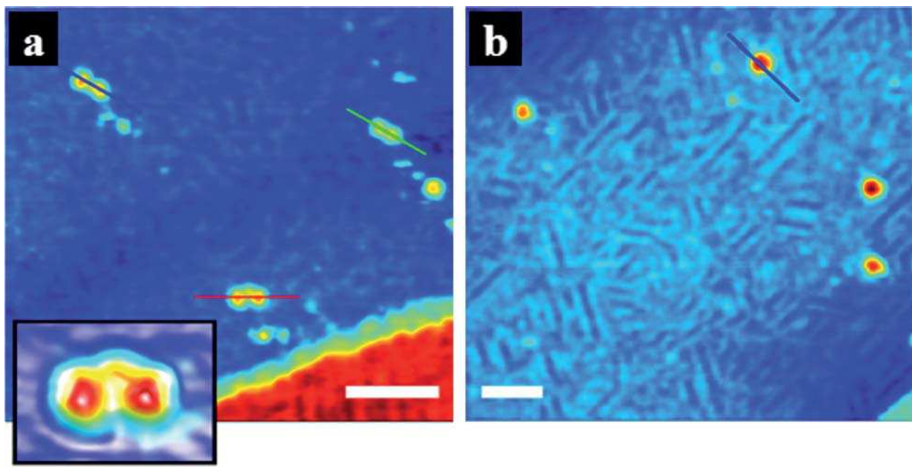

Figure 3.7 The STM imaging of bis-ferrocene molecules deposited on Au(111) substrate [48].

binding bis-ferrocene molecules on real substrates, the obtained data is highlighted in terms of Scanning Tunneling Microscopy (STM) image shown in Figure 3.7.

In particular, regarding the preparation of the solid-state film of bis-ferrocene molecule, characterizations have been carried out on mixed self-assembled monolayers (SAMs) of bis-ferrocenes and hexane-1,6-dithiols on Au (111) substrate. Such arrangement was designed to prevent orientational rearrangements of molecules, which would have deleterious consequences on the MQCA application. Relevant solid-state electrochemistry and STM measurement have confirmed the achievement of this goal, as discussed and demonstrated in [48]. Meanwhile, its functionality both as single half QCA cell and candidate for building MQCA circuits will be simulated and validated in Chapter 4 and Chapter 5.

Based on bis-ferrocene molecules, similar QCA logic blocks discussed in Section 1.3 can be also implemented through designed patterns of molecular layouts, as shown in Figure 3.8. For example, a MQCA wire could be implemented in principle aligning a group of bis-ferrocene molecules together with identical distance d in between. Hence once the input cell or the input molecule of the wire is forced with defined logic state ("0" or "1"), the Coulombic interactions will make the charge moves within each molecule until total molecular system reaches the minimum energy. As a consequence of that, the two neighboring MQCA cells have the same charge configuration that representing the same cell polarity (logic state). But within a cell, the two mobile charges localize, as expected, at the two diagonal corners meaning that the two nearby bis-ferrocene molecules have just the opposite polarities, see Figure 3.8(A). Figure 3.8(B)(C)(D) illustrate some other functional schemes of MQCA, like majority voters, inverters and a bus made of three parallel wires.

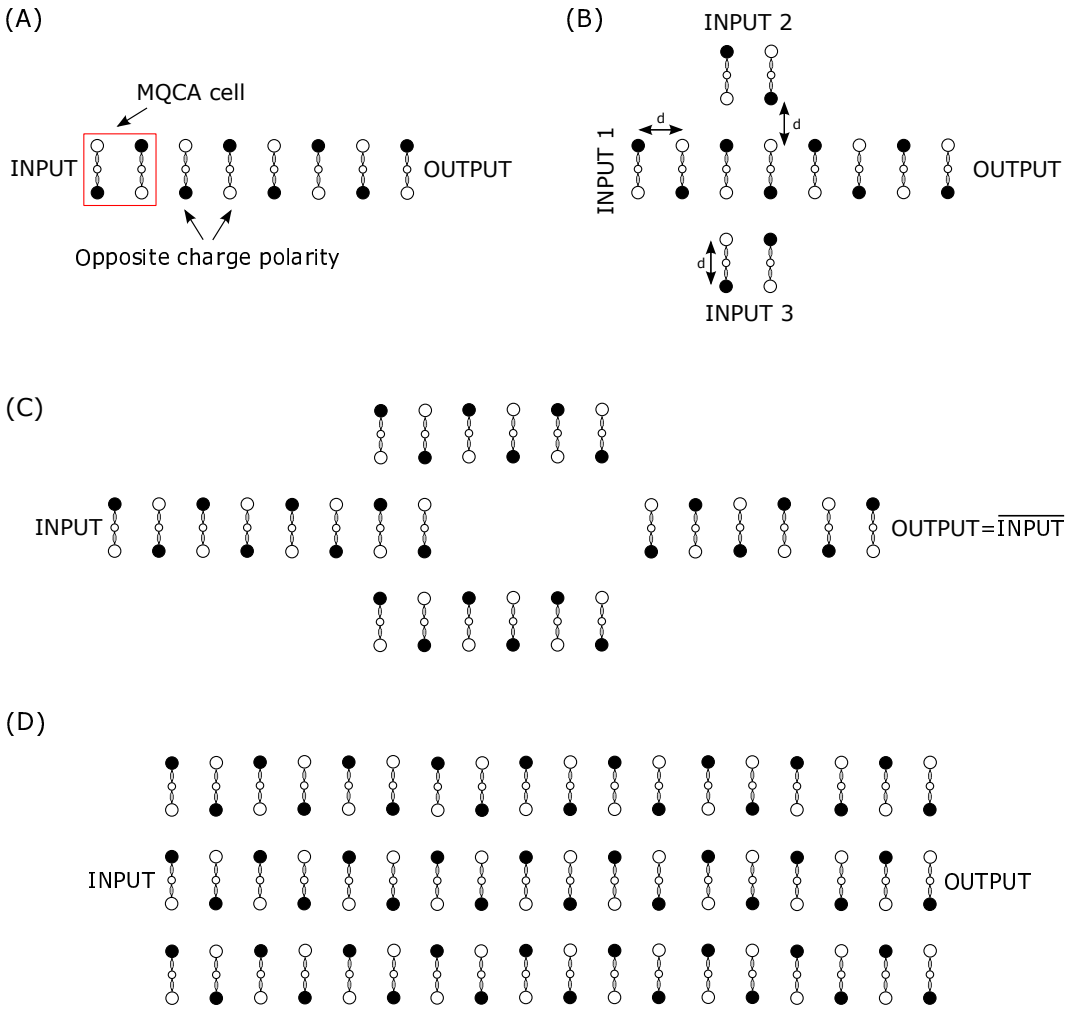

Figure 3.8 Top view of MQCA functional blocks. (A) A MQCA binary wire; (B) A three-input MQCA majority voter; (C) A MQCA inverter; (D) A MQCA wire bus.

3.2.2 Biasing Conditions

Follow the aim of characterizing the functional properties of bis-ferrocene molecule as MQCA devices and further MQCA device performance, it is noteworthy to introduce the *Biasing conditions* which are necessary for the analyzing process. Similar analysis has been done by the authors in [48] for non-thiolated bis-ferrocene molecules. Nevertheless, here the characterized molecule is thiolated and hereinafter the thiolated bis-ferrocene molecule is under focus for analyzing. Considering the thoil as well as the ending group (-SH) together with molecule is a more close-to-reality condition since during computation, molecules are anchored to substrate, hence the existence of those binding elements could be crucial for molecular behavior.

In particular, the relevant biasing condition considered to apply on bis-ferrocene MQCA system here are discussed as follows:

3.2.2.1 Electric Field

The electric field could be applied externally as reference signal to stimulate molecule in terms of changing its charge configuration, i.e., logic state encoding. Depending the field directions, two types of biasing conditions are created: the *Switching Field* [45] and the *Clock Field* [25].

Figure 3.9(A) depicts that the switching field has a direction that is parallel to the dot-axis (*X-axis*). The authors in [54] have demonstrated that using the electric field generated by two electrodes placed near molecule as switching field , the logic state of the input cell or input molecules for MQCA logic blocks can be defined according to requirement. For example, in Figure 3.9(B) a MQCA wire is sketched with oxidized bis-ferrocene molecules aligned and anchored to the substrate (a gold nanowire) through binding elements, whereas a possible write-in system for this wire is realized in principle by adding switching field. This is because following the direction of applied field, the molecules themselves would re-arrange their charge distribution thus encoding logic state “0” or “1”. The corresponding localization of atomic charges for bis-ferrocene molecule is schematically demonstrated in Figure 3.10(a) and Figure 3.10(b). The density of spheres in the figure represents the amount of atomic charge distributed on the molecule. The blue color stands for the largest value charge, whereas the red color represents the lowest value of charge.

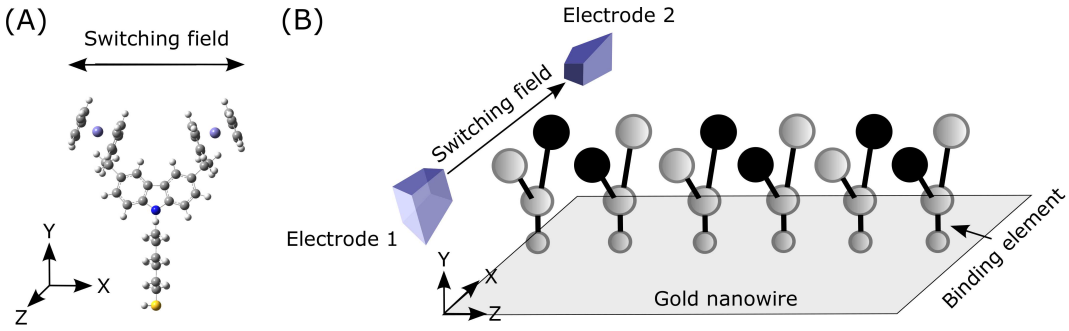

Figure 3.9 MQCA switching field: (A) For single bis-ferrocene molecule; (B) Acting as write-in system for MQCA wire.

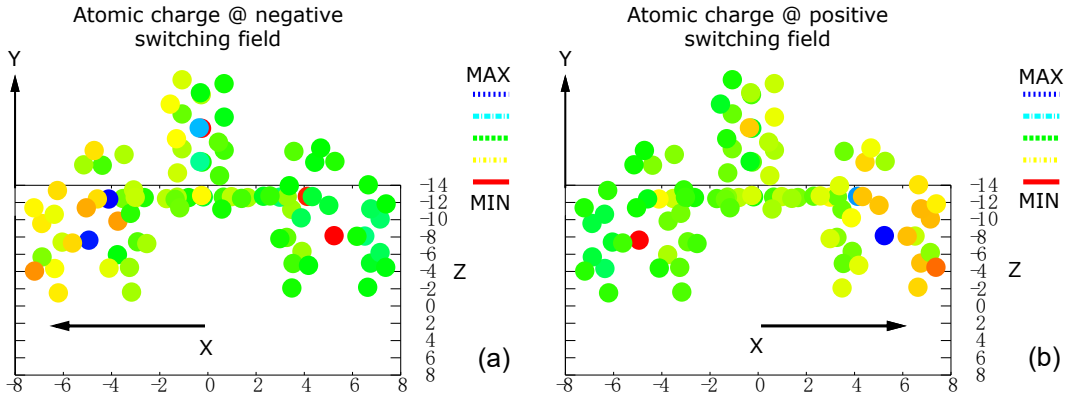

Figure 3.10 Schematic demonstration of atomic charges localized on bis-ferrocene molecule in presence of (a) negative switching field pointing left side of X-axis; (b) positive switching field pointing right side of X-axis.

On the other hand, concerning the clock field it is a reference signal, which is perpendicular to the dot-axis of molecule, applied externally for the sake of accomplishing adiabatic switching in terms of raising or lowering the tunneling barriers during QCA computation (Figure 3.11(A)). For single molecule inside MQCA circuit, schematically placing two metal electrodes on the top/bottom of the bis-ferrocene molecule and applying a potential in between, thus the generated uniform electric field along the vertical *Y-axis* of the molecule is recognized as the clock signal, see Figure 3.11(B). The geometry of the molecule allows the ability of changing tunneling barrier to be realized in terms of different signs and intensities of the applied electric field [53].

In particular, if the clock signal is with negative value (*Release* and *Relax* phase), free charge would be drawn into the lower central *Dot3* keeping the molecule in *NULL* state hence no information is stored in the molecule and no interaction exists

among molecules, as shown in Figure 3.12(a). On the contrary, if the clock signal has a positive value (*Switch* and *Hold* phase), as depicted in Figure 3.12(b), nearly the entire amount of free charge would be pushed to the upper two logic dots (*Dot1* and *Dot2*). At this moment, the charge is able to tunnel through the central *Dot3* via bridging ligands making the molecule activated and ready to be switched to defined logic state, either "0" or "1".

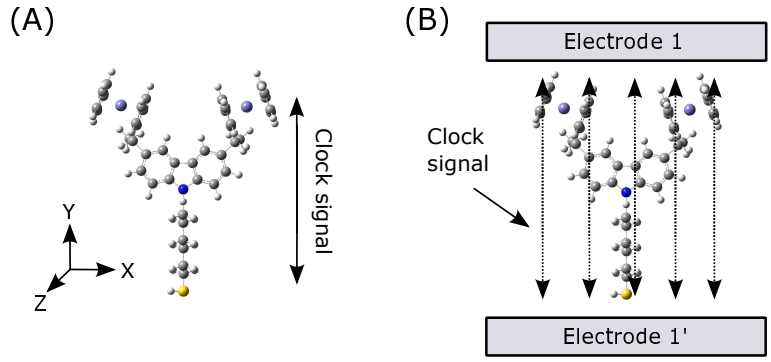

Figure 3.11 MQCA clock field: (A) Clock signal for bis-ferrocene molecule; (B) Tunneling path exists between logic dots and central dot; the clock signal, which is generated between two electrodes thus perpendicular to the logic dots axis, can be used to move charges pushing upwards or pulling downward depending the clock signal pointing direction.

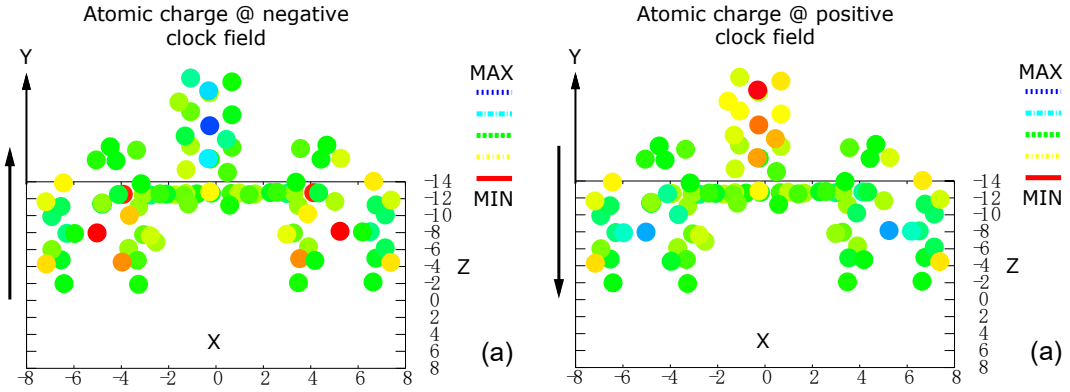

Figure 3.12 Schematic demonstration of atomic charges localized on bis-ferrocene molecule in presence of (a) negative clock field pointing upward; (b) positive switching field pointing downward.

Regarding the clock system for the large MQCA devices, as mentioned in Section 1.4, first the MQCA device should be divided into several clock zones and then multi-phase clock signals are applied to these partitioned zones. For complex circuits like binary wire or majority voter, this could be possibly done placing bis-ferrocene molecules on plane X-Z and between two properly segmented electrodes,

e.g., nanowires. The pattern of the segmented electrodes is the same as the clock zones, see Figure 3.13(A). Then varying in time the values and signs of voltages applied to these segmented electrodes resulting the waveform of multi-phase clock. Figure 3.13(B) demonstrates schematically the similar clock system for a MQCA three-input majority voter.

Each clock zone is the area where computation happens and inside, several bis-ferrocene molecules are located. In order to figure out the information propagation mechanism controlled by the clock, Figure 3.13(C) depicts a multi-phase clock system for bis-ferrocene MQCA wire inherited by [42]. In presence of different clock signal values for each specific clock zone, the molecules on the wire behave correspondingly. Once the input molecule is assigned externally with fixed logic state, the clock signal applied in *zone*1 allows the molecules in the zone to configure their logic states following the input molecule via electrostatic forces. In the meantime, the clock signal in *zone*2 "freezes" the molecules in that zone in *NULL* state isolating them from reacting to the influence of molecules in previous *zone*1. When all molecules in *zone*1 finish their logic states switching, the clock signal then raises and allows them to lock their states thus turning into new inputs for molecules in *zone*2. Therefore, applying the multi-phase clock signal sketched in Figure 1.4(B) to these clock zones while alternating their phases along the molecular QCA wire or other bis-ferrocene MQCA functional blocks, the proper information flow as well as correct QCA computation are created and more important, ensured.

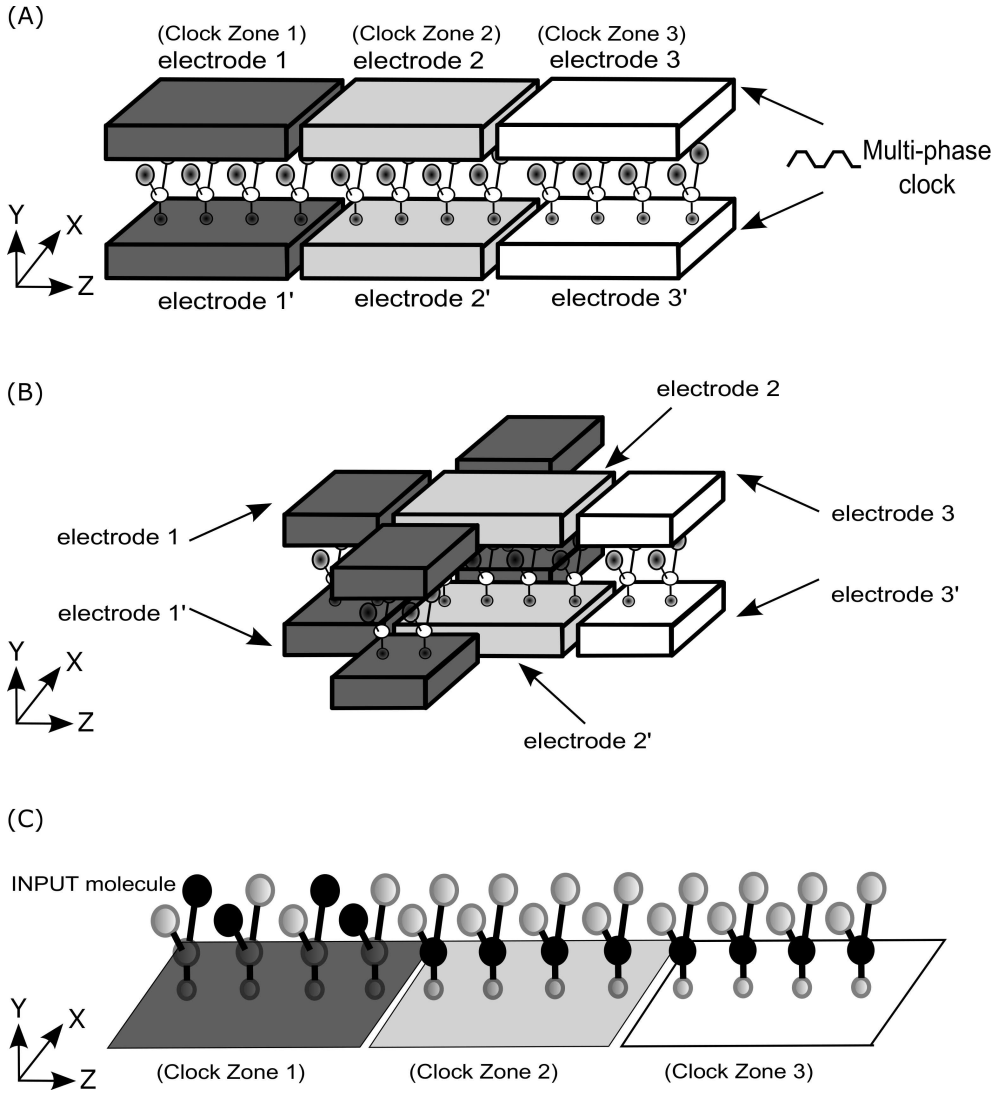

Figure 3.13 Clocked MQCA: schematic implementation of the physical clock system with periodic multi-phase clock signals assigned for (A) A binary MQCA wire; (B) Three-input MQCA majority voter. (C) Molecular performance when different clock zones are applied along the MQCA wire.

3.2.2.2 Point Charges

The point charges are set near the bis-ferrocene molecule during simulations for MQCA device analysis and named the *Polarized Charge Driver (Dr)*. Specifically, the polarized charge driver can be set with two point charges *D1* and *D2* (either in logic state "0" or "1") to simulate the stimuli as an input for MQCA devices, e.g., a wire see Figure 3.14(A). Otherwise, the polarized charge driver can be also set with the values of *Aggregated Charges* from the three dots of a bis-ferrocene molecule *Mol 1* (*Q1*, *Q2* and *Q3*) to approximately mimic its influence to the other molecule *Mol 2* in presence, i.e., the intermolecular Coulomb interaction, during information propagation, as sketched in Figure 3.14(B). About the aggregated charges, it is a figure of merits defined to present temporarily the state of bis-ferrocene molecule, more information will be discussed in Section 4.2.2.

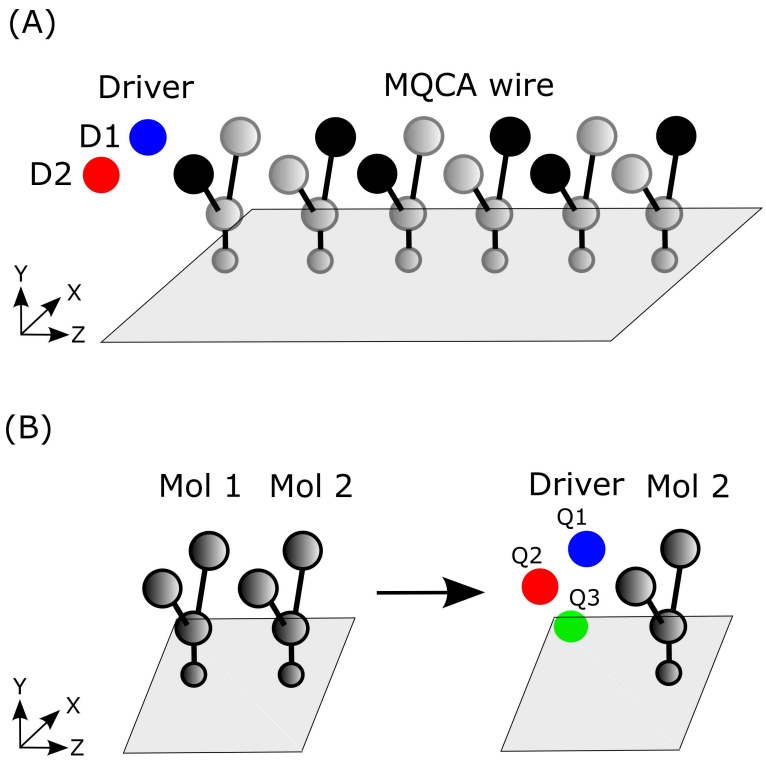

Figure 3.14 Point charges are used as polarized charge driver for (A) Simulating input molecule of MQCA wire; (B) Replacing one the two molecules to simulate their molecular interaction.

Chapter 4

BIS-FERROCENE MOLECULE ANALYSIS AS QCA DEVICE

In the QCA paradigm, the basic nanoblock is a QCA cell, whereas regarding its molecular solution based on bis-ferrocene molecules, the basic unit of interest is a molecule. The performance of bis-ferrocene molecule is thus rather important for the whole MQCA circuit functionality. Therefore, in this chapter a detailed methodological procedure is described with the aim of analyzing a single bis-ferrocene molecular behavior in terms of satisfying QCA computation purpose from an electronic point of view. After that, such methodology is also applied for MQCA cell study in which two bis-ferrocene molecules are located. Furthermore, the achieved results of analysis are reported at the end for a complete and direct demonstration of bis-ferrocene molecular features as QCA devices.

To begin with, the procedure of molecular study in terms of evaluating and simulating all the important parameters necessary for molecular QCA devices is organized in two stages [41]. The scheme in Figure 4.1 illustrate the two stages performed based on the bis-ferrocene molecule itself and at the end, relevant properties for molecule as MQCA devices are provided in terms of defined figures of merits.

In particular, in **Stage I** as being highlighted in Figure 4.2, quantum chemistry ab-initio simulations are carried out in presence of difference biasing conditions which are detailed mentioned in Section 3.2.2 for characterizing single bis-ferrocene molecule functionality. Whereas, the temperature considered inside the simulations is set by default with the value of *300K* (room temperature). On the other hand,

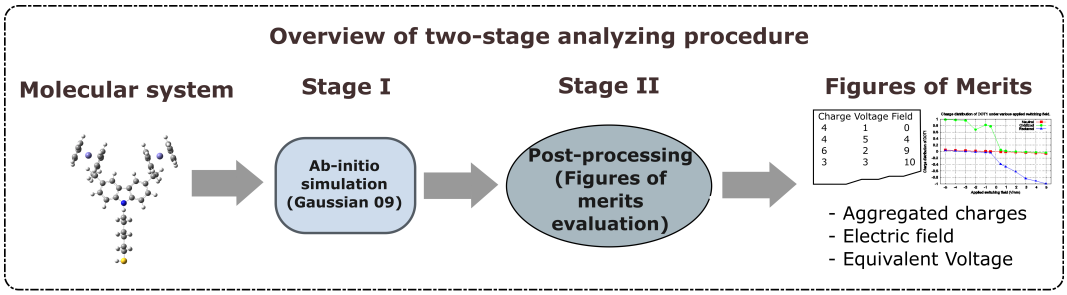

Figure 4.1 An overview of the two-stage analysis procedure for bis-ferrocene molecule: it transfer the molecular system together with its property into device-level figures of merits modeling bis-ferrocene molecule as electronic devices [41].

regarding **Stage II**, starting from ab-initio simulation results which are chemical and physical properties of molecule, new figures of merits are defined through adopting electrostatic equations and models in order to describe bis-ferrocene molecule as well as its potential for building molecular electronic devices.

4.1 Stage I: Ab-Initio Simulations

Quantum chemistry belongs to a branch of chemistry which is specialized to study and explain the behavior of the electrons inside atoms and molecules. Therefore, based on our bis-ferrocene MQCA system, it can be utilized for solving the *Schroedinger Equation* defined as:

$$i\hbar\frac{\partial}{\partial t}\Psi(\overrightarrow{r},t) = \hat{H}(\overrightarrow{r},t) \tag{4.1}$$

where $\Psi(\overrightarrow{r},t)$ is the wave function that describes the probability to find an electron in a specific position $\overrightarrow{r}$ and at a specific time t; $\hbar$ is the reduced Planck constant; $\hat{H}$ is the Hamiltonian related to the energy of the system and defined as the sum of the kinetic energy and the potential energy following the equation

$$\hat{H} = -\frac{\nabla^2}{2m} + V(\overrightarrow{r}). \tag{4.2}$$

The solutions of the Schroedinger equation above describe the chemical and physical properties of our molecular system, including the optimized physical geometrical molecular structure with the minimum total energy taken into considera-

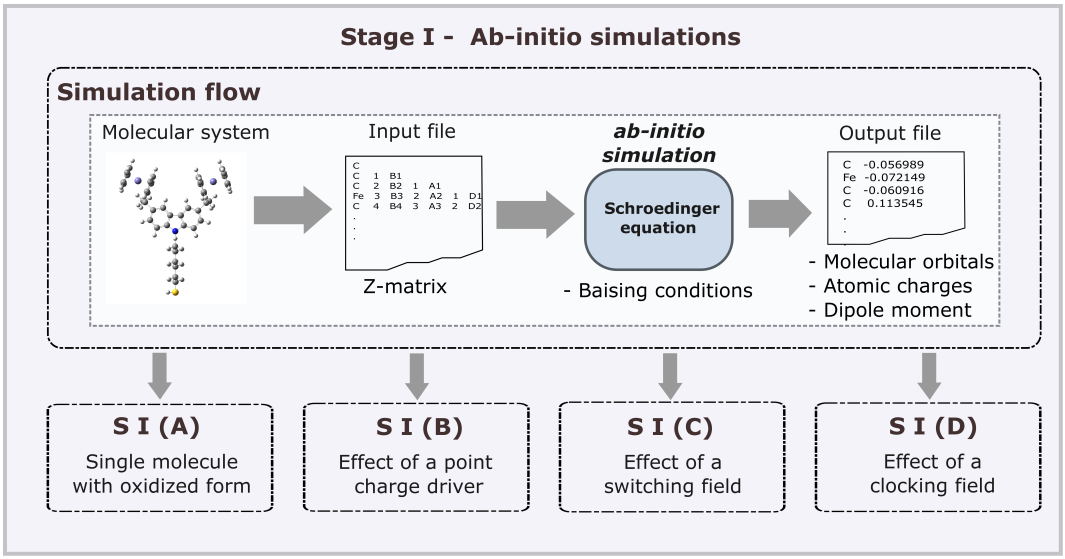

Figure 4.2 The first stage of methodological procedure is in terms of performing ab-initio simulations of oxidized bis-ferrocene molecular system in presence of different biasing conditions, e.g., point charges, electric fields [41].

tion, the interaction energies, the electronic charge distributions, dipoles and higher multi-pole moments, vibrational frequencies, etc. Since the Schroedinger equation could be solved analytically only for hydrogen atom, hence for molecular system with other types of molecules, it is required to bring some approximations. In particular, the computational chemistry provides three classes of approximation methods for achieving that:

- **Semi-empirical methods**: The sets of parameters necessary for solving equations are derived by data obtained from experiments.
- **Ab-initio methods**: These computations focus mainly on the laws of quantum mechanics and a set of physical constants (the speed of light, masses and charges of electrons and nuclei, Plank's constant). These methods base on the theory from the first principle and are highly accurate and, as a consequence, computationally intensive.
- **Density Functional Theory (DFT) methods**: they are similar to ab-initio methods, but they include the effects of *Electron Correlation*, which is the fact that electrons in a molecular system react to one another motion. Ab-initio calculations take into account this issue in an average sense meaning that

each electron sees and reacts to an averaged electron density, whereas DFT methods pay attention to the instantaneous interactions of pairs of electrons with opposite spin.

Each class of approximation is characterized by the combination of theoretical procedure (hereinafter called *method*) and a *basis set*. For example, the well-known *Hartree-Fock (HF)* is a *method* for ab-initio approximation methods and the *B3LYP* is for DFT. Meanwhile, the *basis set* is a mathematical representation of the molecular orbitals within a molecule. The basis set can be interpreted as restricting each electron to a particular region of space. The larger basis sets are, the more accurately approximate molecular orbitals can be introduced. As a consequence of that, these simulations will require correspondingly more computational resources, hence more accurate approximations methods become more computationally expensive.

4.1.1 Ab-initio simulation

With the aim of facilitating scientists to solve the Schroedinger equation in numerous cases of molecular system, many computational chemistry software were developed. Among them the *Gaussian* is the most common and well developed and it becomes popular for analyzing molecules for MQCA purpose [14, 25, 52, 53].

For our simulations in this work, the version of interest here is called *Gaussian 09* since it includes most of the computational methods at all the approximation levels [55]. Our candidate bis-ferrocene molecule have ninety one atoms including two iron atoms, so a quantum chemistry method named *UB3LYP* and a basis set named *LANL2DZ* are used because they are suitable for large molecular systems based on metal ions. Moreover, due to the fact that *Hartree-Fock (HF)* calculations neglect electron correlation while DFT considers both exchange and correlation energies, albeit approximately. Therefore it is common to use the hybrid approach between these two, popular *UB3LYP* scheme is one such possible solution [53].

Figure 4.3 illustrates the *Graphical User Interface* (GUI) of the tool. Through the GUI, a molecular system based on bis-ferrocene molecule could be constructed atom by atom choosing the types of elements, and putting them in the space or connecting them with atoms that have been already existed. Alternatively, the molecular

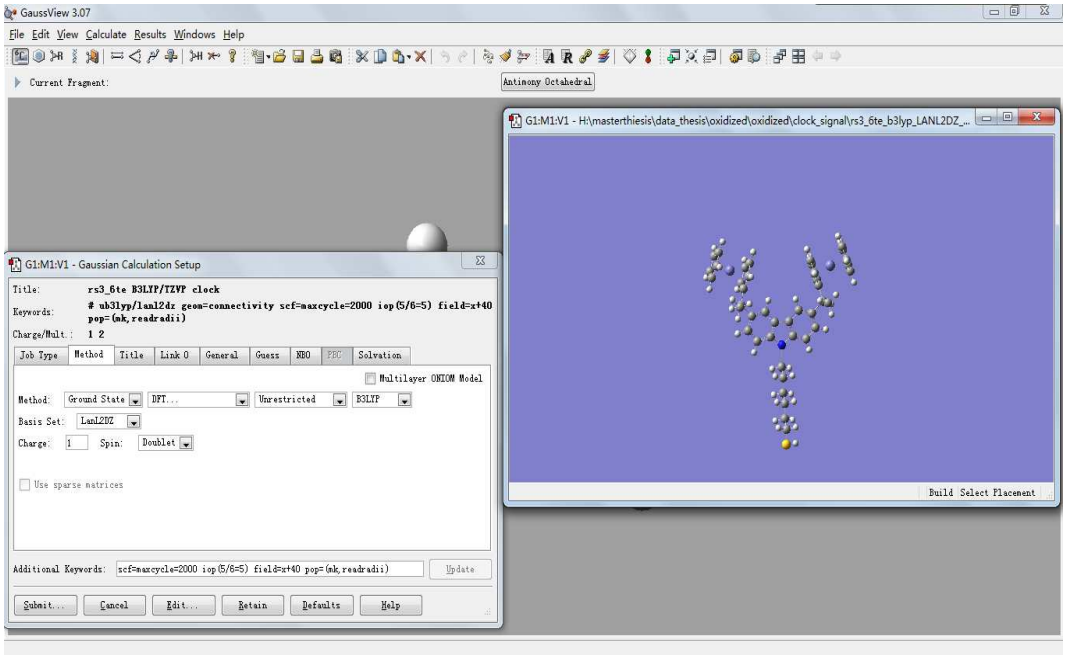

Figure 4.3 Graphical User Interface (GUI) of *Gaussian 09* Viewer Tool.

system can be also described in *Gaussian 09* using a textual file as input. The input file mainly consists of the *Z-matrix* which describes the bis-ferrocene molecular system and a set of commands identifying the purposes of this ab-initio simulation.

4.1.1.1 Z-matrix

In computational chemistry, the *Z-matrix* is the most common way to represent a system built of atoms. Particularly for bis-ferrocene molecule in our work, it records the atomic types, bond lengths, bond angles and dihedral angles between atoms in order to define the *Internal Coordinates* of the molecular system during the whole simulation. Each atom of bis-ferrocene molecule is listed together with another molecule to which it is connected and the length of bond between them. If this atom is also connected with a third atom, then the value of angle between two bonds is also recorded. Apart from that, if a forth atom is connected at the same time, then the generated dihedral angle is written as well, etc. The complete *Z-matrix* for bis-ferrocene molecule is provided in Appendix A, where the connection of the ninety one atoms is explained.

4.1.1.2 Commands

The commands are written in several lines (the route section) at the beginning of the input file. They are necessary to set-up the simulation. In general, at the first row of the input file, starting with the symbol %, the usage of processors is specified. Then the second row defines the associated checkpoint file. The *Gaussian 09* program saves the computed results in a machine readable file, i.e., the checkpoint file. With which it is possible to demonstrate the physical or chemical features of the molecule, like orbitals. The third row is begun with a symbol #, it writes down the instructions that should be followed by the simulation process. The relevant instructions used are explained as follows:

1) Method/Basis Set The quantum chemistry method and proper basis set are defined here. In our simulations, this command has been set to *ub3lyp/lanl2dz*. Nevertheless, they are configurable according to the requirement of the simulation and there are many specified methods and basis sets available in *Gaussian 09*.

2) Molecular Geometry The keyword *Geom* introduces the source of the molecule specification input, options related to coordinate definitions, and geometry related output. By default, it is read from the input stream. *Geom* may be used to specify an alternate input source. It also controls what geometry-related information is printed and use of internal consistency checks on the *Z-matrix*. Whereas in this work, the selected option *connectivity* is adopted. Thus it specifies explicit atom bonding data via an additional input section (terminated via blank line) following the geometry specification or any modification to it. This option requires one line of input per each atom, ordered the same as in the *Z-matrix*.

3) Number Of Cycles For SCF Procedure This command is defined by the keyword *SCF=MaxCycle*, which controls the functioning of the *Self-Consistent Field (SCF)* procedure. In general, options are available for choosing the desired behavior and alternate algorithms according to requirements. For example, it is possible to choose options like *OPTIONS RELATED TO CONVERGENCE AND CUTOFFS*, *INTEGRAL STORAGE OPTIONS*, or *ALGORITHM SELECTION OPTIONS*. Whereas during our simulations based on molecules, the *ALGORITHM SELECTION OPTIONS* specified by $MaxCycle = N$ is used to define the maximum

number (N) of SCF cycles allowed in the simulation, although the convergence may not reached. Nevertheless, if the convergence is achieved before finishing the maximum cycles, the simulation will terminated and record the number of actual execution cycles into the output file, which will be mentioned in Section 4.2.1. The parameter of maximum cycles N is assigned with value of 2000 which is acceptable for bis-ferrocene molecule analysis. If this command is not present, the default number of SCF cycle is 128. However the number of default cycles changes with the algorithm that has been selected for the simulation, e.g., the default number is 512 for *SCF=DM* and *SCF=QC*.

4) Convergence Setting The convergence in the simulation is set with the keyword *IOp*. The syntax is: $IOp(Ov_1/Op_1 = N_1, Ov_2/Op_2 = N_2, ...)$, which sets option number Op_i to the value N_i for every occurrence of overlay Ov_i. In particular, the command $iop(5/6 = m)$ is assigned which configures the convergence of the *Gaussian 09* simulation. The value of m means the accuracy of the convergence expressed as 10^{-m}. If this command is not existed in the command line, it means that the simulation takes the convergence with its default value 10^{-8}. As the convergence increases, the accuracy of the *Gaussian 09* simulation results decreases but saving source consumption in terms of calculation time. Therefore this command is depending the tolerable level of users.

5) Calculation of Atomic Charge The method of calculating the atomic partial charges is defined by the command *pop=(mk, readradii)*. This command chooses the *Merz-Singh-Kollman (MK)* scheme for evaluating the atomic charge distribution around the molecule [56]. In particular, both *Mulliken* population analysis and *ESP* fitting method are embedded inside and both results are provided in the output file of *Gaussian 09* simulation. The command *readradii* read in alternative radii (in Angstroms) for each element for use in fitting potentials in *ESP* method. These are read as pairs of atomic symbol and radius, terminated by a blank line.

6) Point Charge Setting It is feasible to add point charges inside simulation by writing the command *Charge* in the routine section. The coordinates and the point charge values are both necessary and they are defined at the end of the input file (after the *Z-matrix* section).

7) Electric Field Setting *Gaussian 09* offers the possibility to analyze molecular system in presence of the effect of a uniform electric field, simply inserting a keyword with the field value. The syntax for the electric field keyword in *Gaussian 09* is $Field = D \pm N$. The parameter D is the axis direction and the uniform electric field is only allowed along one the three axis of X, Y and Z. The parameter $N * 0.0001$ specifies the magnitude of the field in atomic unit (a.u., $1a.u. = 5.14 \cdot 10^2 V/nm$). For example, an electric field with a modulus of $1.028 V/nm$ and oriented along the positive X-axis could be applied with the following command: *field=x-20*.

8) Molecular Form As discussed in Section 3.1, three forms of bis-ferrocene molecule are available for building MQCA devices. It is also possible to set the form of molecule under analysis in *Gaussian 09* simulation. This could be done inserting in the input file a net charge value of the focused molecule between the routine section of commands and the *Z-matrix* section. For example, the net charge value for neutral, oxidized and reduced form of bis-ferrocene molecule are respectively "0", "+1", "−1".

4.1.2 Biasing Conditions in *Gaussian 09*

Inside the ab-initio simulations performed in this work, besides single bis-ferrocene molecule described by *Z-matrix*, there are also biasing conditions existed with the purpose of characterizing electrostatic properties of the molecule, like molecular orbitals or atomic charges, see Figure 4.2 (bottom). Since the *Gaussian 09* simulation allows uniform electric field and point charges to be inserted in the routine section (Section 4.1.1.2), the biasing conditions are thus possible to be added.

4.1.2.1 S-I A) Oxidized Molecule Simulation

Regarding the type of bis-ferrocene, it is noteworthy to mention that the authors in [53] have demonstrated molecular behavior for all three forms of bis-ferrocene molecule. Due to the optimum performance, hereinafter the oxidized molecule has been of interested and studied throughout this work. Whereas in the *Gaussian 09* simulation, an oxidized molecule can be defined by the *Z-matrix* together with net charge set to "+1".

4.1.2.2 S-I B) Effect Of Point Charge Driver

The MQCA transmits binary information via interactions between molecules, therefore in order to simulate the interaction, we simulate a complete MQCA cell. In stead of two bis-ferrocene molecules inside the cell, one of the molecule is replaced and emulated by an ideal driver with point charges. This driver (*Driver* is located at the distance *d* from the bis-ferrocene molecule (*Molecule*), see Figure 4.4(A). In this way, the interaction between molecules within the cell is approximated as the ideal driver influences the molecule aside, see Section 3.2.2.2. In the case of oxidized molecule, the ideal driver is simulated considering only one positive charge ($+1e$).

In particular, the point charge is located on one the two dots of the driver, depending on its encoded logic state. For logic state "1" of the driver, as sketched in Figure 4.4(B), the resulting charge distribution on the target molecule could be computed by means of ab-initio simulations and is expected to encode the opposite logic state. On the other hand, if the driver is switched to logic state "0", the target molecule should switch as well because of Coulomb forces, see Figure 4.4(C).

For the sake of brevity, the amount of charge mentioned in this work is always referred to the elementary charge (e) as unit of measurement and hereinafter the e will be neglected leaving only the partial numbers.

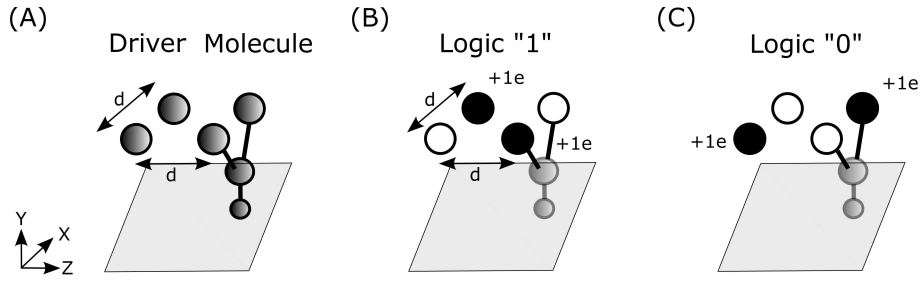

Figure 4.4 Molecular interaction: (A)Driver-Molecule model; (B)Logic state "1" of Driver; (C)Logic state "0" of Driver.

4.1.2.3 S-I C) Effect Of Switching Field

As already demonstrated in Section 3.2.2.1, the switching field is an electric field which is responsible for the write-in system of MQCA device. In principle, the direction of switching field is parallel to the logic dots axis of bis-ferrcene molecule. Once the *Z-matrix* has been read by the *Gaussian 09*, the simulation will automatically convert the structure information into coordinates for all ninety one atoms of the molecule. For single bis-ferrocene molecule, the coordinates generated are symmetric where the logic dots axis is X-axis and the vertical axis of molecule is Y-axis, as shown in Figure 4.5(A). As a consequence of that, during the simulation, the switching field is set to be along X-axis. With the switching field taken into account, the charge localization of molecule could be led in one of the two logic dots hence writing a logic state to the single molecule. For example, Figure 4.5(A) illustrates that with a positive switching field applied, the free positive charge of the oxidized molecule should localize on *Dot2*; while on the contrary, the same charge will move to *Dot1* if a negative switching field is in presence, see Figure 4.5(B).

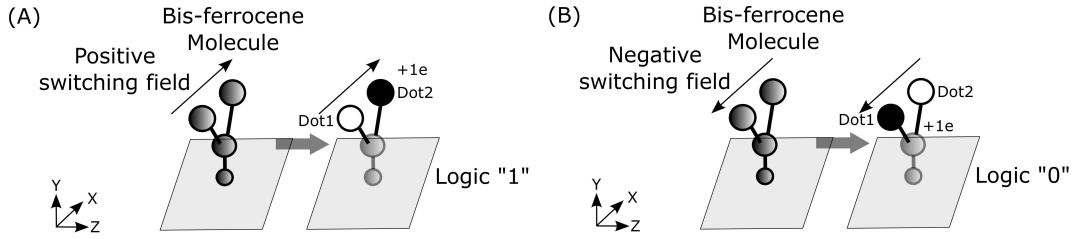

Figure 4.5 Effect of switching field to bis-ferrocene molecule: (A)Logic state “1” encoding; (B)Logic state “0” encoding.

4.1.2.4 S-I D) Effect Of Clock Field

Similar as switching field, the clock field is an electric field applied along the vertical axis of the molecule. Thus inside ab-initio simulation, the clock field is realized setting the electric field along Y-axis, as highlighted in Figure 4.6. Given the explanation from Section 3.2.2.1, it is clear that the clock signal is added with aim of realizing adiabatic switching in MQCA. For a three-dot molecule like bis-ferrocene, the vertical clock signal, depending on its sign, could either push the free positive charge down to central *Dot3* (Figure 4.6(A)) or force the total amount of charge to stay on logic dots for further switching (Figure 4.6(B)). Moreover, simulations could be performed also in presence of both polarized point driver and clock

signal. This means simulating the molecule with simultaneous effects of them giving the possibility to evaluate clock capability of controlling molecular interaction, see Section 4.3.

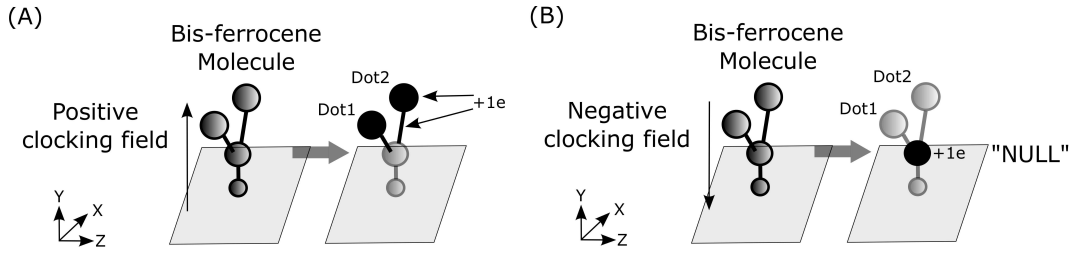

Figure 4.6 Effect of a clock field: (A)Enhancing molecular performance in terms of pushing charge on logic dots for state encoding; (B)Hindering molecular interaction by forcing all charge on central dot of bis-ferrocene molecule (*NULL* state).

4.2 Stage II: Figures of Merits: Post-Processing

Following the aim of characterizing bis-ferrocene molecule as MQCA device, ab-initio simulations have been performed via *Gaussian 09* and as a consequence of that, the these achieved results are computationally tractable and the level of accuracy are high. After that, based on the output files generated from the simulations, the second stage of the procedure in terms of post-processing of data is discussed in this section.

4.2.1 *Gaussian 09* simulation results

The output file given by *Gaussian 09* after the simulation is done contains all information with respect to the requirements defined in the routine section of the input file. However, these achieved results are in terms of physical or chemical properties for the single bis-ferrocene molecule in presence of biasing conditions. An example of generated output file from *Gaussian 09* simulation is provided in Appendix B. In particular, at the beginning of the output file, the *Standard Orientation* is provided. The standard orientation is the internal coordinates (including all X, Y, Z axis) of all atoms generated inside *Gaussian 09* simulation according to the *Z-matrix* of bis-ferrocene molecule. An example of the coordinates is reported in Figure 4.7.

Standard orientation

Center Number	Atomic Number	Atomic Type	Coordinates (Angstroms) X	Y	Z
1	6	0	-4.918827	-6.503165	-0.858753
2	6	0	-3.579317	-6.985817	-0.896848
3	6	0	-3.081190	-7.006256	0.436876
4	6	0	-4.112678	-6.535603	1.299485
5	6	0	-5.248466	-6.225703	0.498685
6	26	0	-3.621776	-5.061555	-0.093920
7	6	0	-3.050836	-3.321389	0.899548
8	6	0	-1.962576	-3.796463	0.105018
9	6	0	-2.416639	-3.822346	-1.249553
10	6	0	-3.763476	-3.365730	-1.289245
11	6	0	-4.158567	-3.058639	0.042877
12	6	0	-0.558257	-4.131058	0.553616
13	6	0	-0.465246	-4.439280	2.058170
14	6	0	0.444124	-3.044541	0.163909
15	6	0	0.139553	-1.691654	0.283352
16	6	0	1.096090	-0.729637	-0.041332
17	6	0	2.373864	-1.140125	-0.491853
18	6	0	2.696541	-2.486842	-0.619626
19	6	0	1.721577	-3.418903	-0.288960
20	6	0	1.100825	0.719432	-0.041284
21	6	0	2.381274	1.121592	-0.491743
22	7	0	3.133515	-0.011731	-0.755438
23	6	0	0.150634	1.687664	0.283527
24	6	0	0.464079	3.038546	0.164253
25	6	0	1.743936	3.404577	-0.288609
26	6	0	2.712770	2.466172	-0.619380
27	6	0	-0.531171	4.131502	0.554190
28	6	0	-0.436340	4.438604	2.058855
29	6	0	-1.937621	3.806277	0.105337
30	6	0	-2.391378	3.835498	-1.249267

Figure 4.7 A section of the standard orientation for single bis-ferrocene molecule which is generated during *Gaussian 09* simulation.

Then, the computation details related to the method and basis set adopted are recorded and the total energy of the system is evaluated after finishing the simulation, see Figure 4.8.

```
Computational details:
SCF Done:  E(UB3LYP) =  -1941.36566574     A.U. after   38 cycles
Convg  =    0.3584D-05             -V/T =  2.0663
<Sx>= 0.0000 <Sy>= 0.0000 <Sz>= 0.5000 <S**2>= 0.7946 S= 0.5221
<L.S>= 0.000000000000E+00
Annihilation of the first spin contaminant:
S**2 before annihilation     0.7946,   after     0.7516
DiagDN has N=   529 LTot=  1619 but NE2=     3 cannot use DSYEVD.
```

Figure 4.8 An example of computation details written in the output file of *Gaussian 09* simulation.

Next, the computation results are provided in terms of physical or chemical properties of simulated bis-ferrocene molecule with biasing conditions recognized as external stimuli. For example, the molecular orbitals and associated dipole moment, iso-potential surfaces data of ground states and atomic charge distribution of the tested molecule. According to MQCA theory, the charge configuration inside molecule is of interest to represent transmitted binary information and in the simulation result section, as mentioned above in Section 4.1.1.2, two schemes are available, i.e., the *Mulliken* analysis and the *ESP* method. For example, Figure 4.9 and Figure 4.10 depict both atomic charge evaluations considering a single bis-ferrocene molecule at equilibrium state (no biasing conditions).

In order to model the MQCA system from an electronic point of view, especially for representing the logic state encoded by molecules during QCA computation, it is still necessary to transforming the directly obtained simulation data into new figures of merits. Figure 4.11 gives an overview of the second stage of our analysis, based on the ab-initio simulation data in different conditions, a post-processing procedure is applied to reckon more useful quantities described as follows.

Mulliken atomic charges:

1	C	-0.200322	31	C	-0.224580	61	H	0.308427
2	C	-0.201614	32	C	-0.252140	62	H	0.291688
3	C	-0.211591	33	C	-0.368658	63	H	0.281498
4	C	-0.199185	34	Fe	-0.179586	64	H	0.291900
5	C	-0.201855	35	C	-0.223774	65	H	0.243097
6	Fe	-0.168201	36	C	-0.219942	66	H	0.228883
7	C	-0.332456	37	C	-0.221778	67	H	0.216883
8	C	0.388949	38	C	-0.235773	68	H	0.213322
9	C	-0.357846	39	C	-0.225678	69	H	0.231524
10	C	-0.195534	40	H	0.200166	70	H	0.252083
11	C	-0.219239	41	H	0.212558	71	H	0.204706
12	C	-0.349551	42	H	0.229651	72	C	-0.239069
13	C	-0.696959	43	H	0.212225	73	C	-0.372657
14	C	0.621231	44	H	0.226271	74	H	0.196167
15	C	-0.549366	45	H	0.202148	75	H	0.195054
16	C	0.142243	46	H	0.212826	76	H	0.221921
17	C	0.106482	47	H	0.281246	77	H	0.220926
18	C	-0.368705	48	H	0.264475	78	C	-0.352511
19	C	-0.487648	49	H	0.248103	79	H	0.192324
20	C	0.147470	50	H	0.244079	80	H	0.189642
21	C	0.105680	51	H	0.276441	81	C	-0.353413
22	N	-0.197145	52	H	0.271017	82	C	-0.356089
23	C	-0.554009	53	H	0.256424	83	H	0.201315
24	C	0.617661	54	H	0.268710	84	H	0.195257
25	C	-0.486259	55	H	0.273640	85	H	0.200263
26	C	-0.369277	56	H	0.298789	86	H	0.223229
27	C	-0.352626	57	H	0.299709	87	C	-0.981499
28	C	-0.725925	58	H	0.298430	88	H	0.264582
29	C	0.409465	59	H	0.295430	89	H	0.291328
30	C	-0.389866	60	H	0.308334	90	S	0.342632
						91	H	0.003820

Figure 4.9 An example of atomic charges using *Mulliken* analysis for bis-ferrocene molecule at equilibrium state.

```
3200 points will be used for fitting atomic charges
Fitting point charges to electrostatic potential
Charges from ESP fit, RMS=0.00240 RRMS=0.03270:
Charge=1.00000 Dipole=-15.1426 -12.7091 -2.3129 Tot=19.9040
ESP fitting atomic charges:
 1  C   -0.037069    32  C   -0.195943    63  H    0.144721
 2  C   -0.101010    33  C   -0.212182    64  H    0.160212
 3  C   -0.063930    34  Fe  -0.014634    65  H    0.170067
 4  C   -0.067803    35  C   -0.101443    66  H    0.152933
 5  C   -0.051660    36  C   -0.083072    67  H    0.207943
 6  Fe  -0.050023    37  C   -0.142138    68  H    0.208446
 7  C   -0.152288    38  C   -0.114262    69  H    0.152902
 8  C    0.136307    39  C   -0.117095    70  H    0.170877
 9  C   -0.159271    40  H    0.086341    71  H    0.079381
10  C   -0.051805    41  H    0.110560    72  C   -0.132684
11  C   -0.140617    42  H    0.134388    73  C    0.091145
12  C    0.001055    43  H    0.103772    74  H    0.114253
13  C   -0.396665    44  H    0.135997    75  H    0.115223
14  C    0.087077    45  H    0.105493    76  H   -0.006244
15  C   -0.216757    46  H    0.127097    77  H    0.012916
16  C   -0.054136    47  H    0.150309    78  C    0.266066
17  C    0.372081    48  H    0.150531    79  H   -0.066195
18  C   -0.349248    49  H    0.131119    80  H   -0.061670
19  C   -0.244224    50  H    0.121329    81  C   -0.021282
20  C   -0.096180    51  H    0.147713    82  C    0.317598
21  C    0.383653    52  H    0.150639    83  H   -0.070466
22  N   -0.475184    53  H    0.160342    84  H   -0.034338
23  C   -0.203991    54  H    0.175759    85  H   -0.101748
24  C    0.119372    55  H    0.160724    86  H   -0.065102
25  C   -0.246416    56  H    0.159376    87  C    0.093035
26  C   -0.355796    57  H    0.168891    88  H   -0.007313
27  C    0.047687    58  H    0.186701    89  H    0.121183
28  C   -0.469712    59  H    0.175919    90  S   -0.603301
29  C    0.095404    60  H    0.156139    91  H    0.321461
30  C   -0.215751    61  H    0.158046
31  C   -0.097226    62  H    0.147693
```

Figure 4.10 An example of atomic charges based on *ESP* fitting method for bis-ferrocene molecule at equilibrium state.

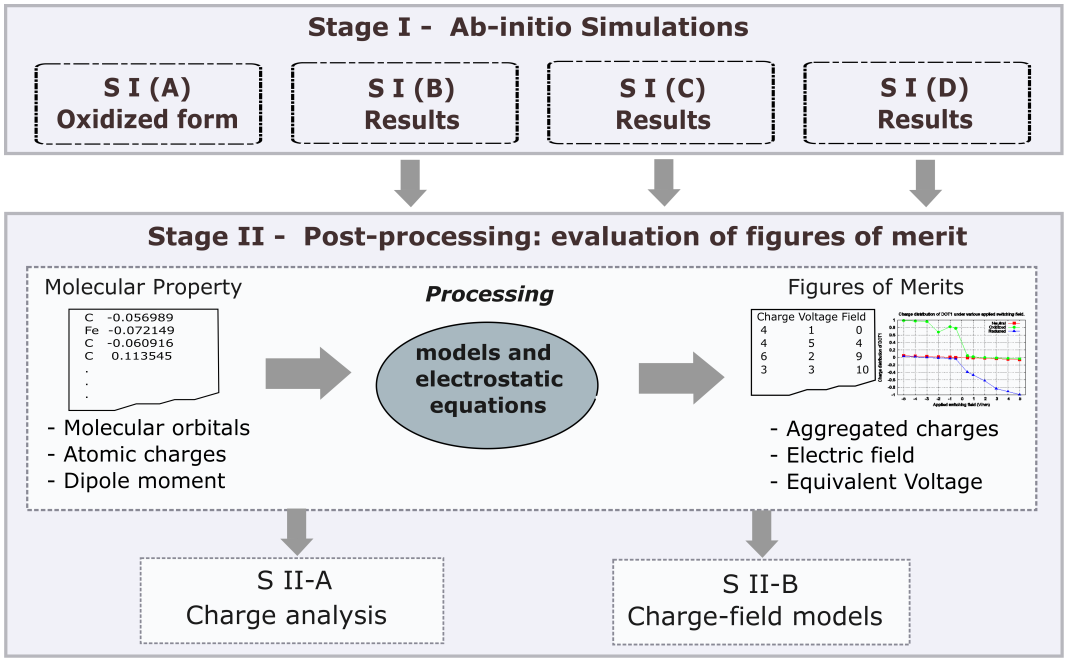

Figure 4.11 The second stage of the methodological procedure describes the path from ab-initio simulations results to device-level figures of merits [41].

4.2.2 S-II A) Charge analysis

In stead of focusing only on the molecular orbitals or iso-potential surfaces (HOMO, LUMO, etc), as mainly done in the chemical approach proposed in literature, a new figure of merits based on atomic charge distribution of molecule is introduced and named *Aggregated Charge*. Whereas the scheme chosen for atomic charge configuration is the *ESP* fitting method which is popular for electrostatic analysis of molecules [56][57].

Based on the given atomic charges of the molecule, no matter which operation condition is taken into account (ground state of biasing), these partial charges are divided into four parts depending on the molecular structure of bis-ferrocene, i.e., the two ferrocenes, the carbazole and the thiol bonding group. Particularly, the aggregated charge of molecule is calculated summing the atomic partial charges of all the atoms which form each redox center as working dots (logic and middle dots). For the sake of simplicity, the atomic charges of carbazole and thiol element are summed together representing the central dot, see Figure 4.12.

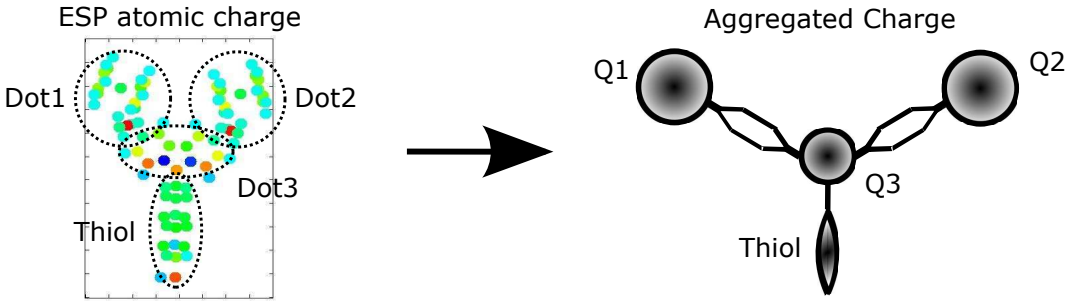

Figure 4.12 The aggregated charge is defined for each dot of bis-ferrocene molecule.

Figure 4.12(A) illustrates that the atoms of bis-ferrocene molecule are represented by small circles filled with different colors according to their values; whereas summing the atoms included in each part of the molecule makes it possible to approximately model the molecule as well as its dots *Dot1*, *Dot2* and *Dot3* with a system of aggregated charges *Q1*, *Q2* and *Q3*, respectively, see Figure 4.12(B). Regarding the accuracy of this modeling, since the atomic partial charge itself is a theoretical approximation for easily demonstrating molecular charge localization instead of an exact physical measurable quantity, so the aggregated charge is introduced which could present the molecular charge localization from a macroscopic point of view and at the same time, it could also be a readable quantity in order to

build the read-out system for further applications [54]. Therefore, this modeling is acceptable in terms of simplifying the molecular system to describe the gross feature of molecular behavior. Hereinafter, when dot charge is referred, it means the reference to the aggregated charges of the corresponding dots.

4.2.3 S-II B) Charge-field models

Once the the aggregated charges of the molecule in different operating conditions (ground state or biasing) are obtained by means of simulations with further summing procedure, it is possible to perform electrostatic analysis in presence of these point charges. For example, the electric field generated by the aggregated charges of molecule at any specific working point can be calculated through mathematical equations developed in *MATLAB/OCTAVE* [58][59].

To be specific, if a point charge $+q_1$ is put at the position (x_0, y_0, z_0), thus the electric field $E(x,y,z)$ can be evaluated via introducing a positive test charge $+q_t$ in position (x,y,z). The distance $\overrightarrow{r_1}$ between q_1 and q_t as well as its modulus r_1 are defined as

$$r_1 = \sqrt[2]{(x-x_0)^2 + (y-y_0)^2 + (z-z_0)^2} \tag{4.3}$$

$$\overrightarrow{r_1} = r_1 \cdot \widehat{r} \tag{4.4}$$

where $\widehat{r}$ is the unit vector of the axis that includes the space point of q_1 and q_t. Applying the Gauss's Law, the Coulomb force $\overrightarrow{F_1}$ applied on the test charge can be calculated as

$$\overrightarrow{F_1} = \frac{1}{4\pi\varepsilon_0} \frac{q_1 \cdot q_t}{r_1^2} \cdot \widehat{r}. \tag{4.5}$$

Then, the electric field generated by q_1 is evaluated at the place of the test charge though equation

$$\overrightarrow{E_1} = \frac{\overrightarrow{F_1}}{q_t} = \frac{1}{4\pi\varepsilon_0} \frac{q_1}{r_1^2} \cdot \widehat{r}. \tag{4.6}$$

By the same logic, considering a system of N point charges, the total force from the system to the test charge is a combination of multiple calculations and written as

$$\overrightarrow{F_{tot}} = \sum_{i=1}^{N} \frac{1}{4\pi\varepsilon_0} \frac{q_i \cdot q_t}{r_i^2} \cdot \widehat{r} \tag{4.7}$$

and the resulting equation for the total electric field becomes

$$E_{tot}(x,y,z) = \frac{\overrightarrow{F_{tot}}}{q_t} = \sum_{i=1}^{N} \frac{1}{4\pi\varepsilon_0} \frac{q_i}{r_i^2} \cdot \widehat{r}. \tag{4.8}$$

In addition, considering a generic test charge placed at a generic point of the space (x,y,z), the three component (E_x, E_y and E_z) of the electric field generated by a system of point charges can be derived as

$$E_x(x,y,z) = \sum_{i=1}^{N} E_{xi}(x,y,z) \tag{4.9}$$

$$E_y(x,y,z) = \sum_{i=1}^{N} E_{yi}(x,y,z) \tag{4.10}$$

$$E_z(x,y,z) = \sum_{i=1}^{N} E_{zi}(x,y,z). \tag{4.11}$$

With this model of analysis, if a system of point charges (*D1* and *D2*) are used as *Driver*, as shown in Figure 4.13(A), the electric field generated by the polarized charge driver can be evaluated at any points in the space all around it. Then such electric field is "measured" by means of putting an virtual bis-ferrocene molecule (*Molecule*) nearby the driver with the distance d in between to form a squared QCA cell. The measurement of the electric field is the so-called *Equivalent-Input-Voltage* (V_{IN}) which is computed by considering the component of the electric field parallel to the dot-axis of molecule and integrating it along the width of the molecule. Similarly, if a system of charges represent the aggregated charges (*D1*, *D2* and *D3*) of a bis-ferrocene molecule (*Mol1*) in a specific condition (ground or biasing), then the

electric field generated by these charges is "measured" as V_{IN} for *Mol2* in the same way, see Figure 4.13(B).

More importantly, this equivalent voltage is recognized as another figure of merits during the analysis. It could describe the influence from the write-in system to the molecules or the interaction existed between two molecules within the cell, depending on whether the equivalent voltage is generated by charges representing a *Driver* or a molecule, respectively.

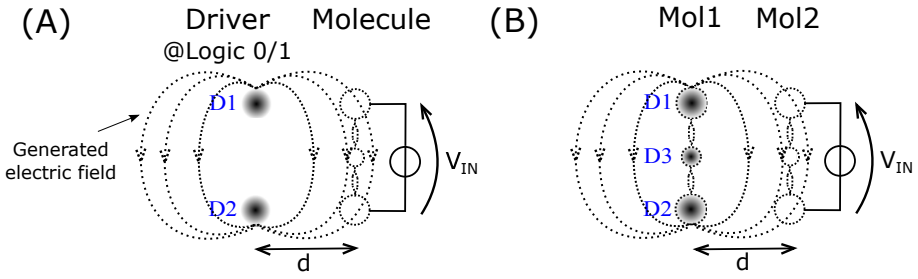

Figure 4.13 (A)Electric field generated by the charge distribution of an ideal driver and a V_{IN} is "measured"; (B))Electric field generated by the aggregated charge distribution of a bis-ferrocene molecule and the corresponding computed V_{IN}.

4.3 Characterization of Molecular Interaction

Since the electrostatic interactions among molecules would eventually determine the binary information propagation among MQCA devices, thus the modeling and evaluation of the molecular interaction are necessary. Therefore, as an application of the analysis procedure with two mentioned stages in Section 4.2 and Section 4.11, here in this section, the electrostatic interaction between two bis-ferrocene molecules is studied.

In particular, regarding the molecule-to-molecule interaction, in the first stage, a set of ab-initio simulations have been performed to simulate a complete QCA cell, as shown in Figure 4.14(A). In stead of two bis-ferrocene molecules, inside the cell for simulation, there is a *Driver* and a bis-ferrocene molecule (*Molecule-Under-Test (MUT)*). This *Driver* is made of a system of point charges which emulates the presence of a proper molecule. In this way, the interaction between two nearby molecule is computed by means of one polarized charge driver influencing another molecule, see Figure 4.14(B).

The distance in between is assigned with d which is a variable can be modified. Whereas concerning the point charges of the driver, their values *D1*, *D2*, *D3* correspond to the aggregated charges of three dots of the a bis-ferrocene molecule depending on the operating condition (ground state or biasing). For example, if during the simulations only a positive clock signal ($+2V/nm$) is present with the oxidized molecule (MUT), the resulting aggregated charges are $+0.482$, $+0.479$ and $+0.039$ for *Dot1*, *Dot2* and *Dot3*, respectively. These values can be found in Section 5.1.4. As is seen that almost the entire positive unit charge $+1.0$ is forced to localize on the two logic dots, while the value of charge left on the central dot is null. Therefore the setting of driver configuration in the simulations is following the obtained results. However, these values *D1* and *D2* of the aggregated charges on two logic dots can be in different conditions describing different states of molecule. In order to consider all possible interactions from the driver to the molecule, the corresponding values of driver charges are set as follow.

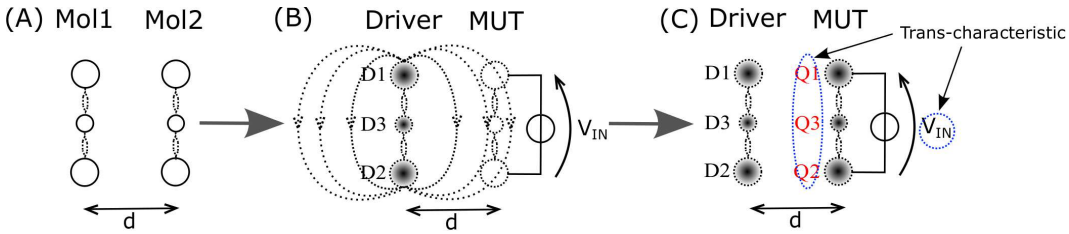

Figure 4.14 (A)Interaction between two bis-ferrocene molecules; (B)Replace one of the two molecule with its aggregated charges $D1$, $D2$ and $D3$ as driver, then the V_{in} is computed at the Molecule-Under-Test (MUT); (C)The MUT re-distributes itself according to the voltage and eventually forms aggregated charge distribution $Q1$, $Q2$ and $Q3$.

In presence of the positive clock, the equilibrium state is firstly considered, in which the two logic dots of the driver have the same values. Namely, the driver values *D1*, *D2* and *D3* are set to $+0.475$, $+0.471$ and $+0.054$. After that, starting from equilibrium state and keeping the charge on *D3* untouched due to existence of clock, driver values *D1* and *D2* are gradually out of balance until those charges are entirely distributed on *D1* or *D2*. Thus encoding logic state logic state "1" or "0", respectively. This unbalance is obtained with a step of 0.1 varying between *D1* and *D2* of the driver. Eventually, the MUT in Figure 4.14(C) will react to all driver conditions listed before in terms of re-arranging its aggregated charge distribution *Q1*, *Q2* and *Q3*, and these reactions are computed through our two-stage methodology procedure in terms of ab-initio simulations combined with post-processing of data.

Meanwhile, following the discussion in Section 4.2.3, the influences of these driver configurations to bis-ferrocene molecule can also be equivalently transformed into the so-called V_{IN} which are applied on the molecule, see Figure 4.14(B). As a consequence of that, by correlating the generated V_{IN} "measured" at the MUT in all conditions of driver configurations to the corresponding obtained aggregated charges, a *Trans-Characteristic* relation (Charge vs. Equivalent Voltage) for bis-ferrocene molecule is thus achieved.

Accordingly, if the equivalent voltage V_{IN} generated from the aggregated charges of one molecule, which is recognized as *Driver*, is "measured" at the other molecular (MUT) nearby is known, then under such effect the MUT starts to re-arrange itself and the resulting system of aggregated charges localized on the MUT is thus calculated applying the proper trans-characteristic. Hence it pictures and further evaluates the influence from one molecule to the other, namely the molecule-to-molecule interaction.

More importantly, during the above procedure for deriving such relationship, the applied clock signal is playing a key role in terms of controlling the amount to total charge on molecule that participates the interaction, so the trans-characteristic is clock-dependent. For different clock signals applied inside the molecular system for simulations, the resulting performance of trans-characteristic for bis-ferrocene molecule varies. Detailed results of this relationship are reported in Section 5.2.

4.4 Bis-Ferrocene MQCA Cell Simulation

Following the similar procedure with two stages in terms of ab-initio simulations and post-processing of simulation data, here in this section a complete MQCA cell with two molecules located together is studied. In addition, as a further possible application of the cell structure, a three-input majority voter based on the MQCA cell is also simulated.

4.4.1 Ab-initio Simulations of MQCA cell

Here the ab-initio simulations in *Gaussian 09* have been performed with two bis-ferrocene molecules aligned together. Regarding the input file of simulations,

by the same logic, the physical structure of these two molecules together has been described through a larger *Z-matrix* and the amount of net charge considered for the total molecular system is thus $+2$ since the two bis-ferrocene molecules should be both in their oxidized form. Whereas the rest of setting in the input file are kept unchanged except the command which defines the *Number Of Cycles For SCF Procedure*, because the presence of two bis-ferrocene molecules together would require much more SCF procedure to achieve the convergence becoming computationally intensive.

On the other hand, concerning the biasing conditions applied, some notifications should be addressed.

4.4.1.1 Point Charge Driver

Similar as single bis-ferrocene molecule analysis, the point charges here can be also added in the simulation to emulate the presence of another cell nearby, i.e., the cell-to-cell interaction. As shown in Figure 4.15(A), the four point charges (*D1*, *D2*, *D3* and *D4*) represents the four logic dots of a virtual driver cell (*INPUT*) and they have a squared shape also. They are placed at distance d away from the bis-ferrocene MQCA cell. Therefore, once these four point charges are assigned with values, they will influence the neighboring MQCA cell and force it to change its logic states. For example, if two point charges located at the diagonal of the driver cell are assigned with positive unit charge $+1$ simultaneously, then the driver cell would encode a logic state "0" or "1". Due to the electrostatic interaction, soon afterwards the MQCA cell will configure its logic state accordingly, see Figure 4.15(B) and (C).

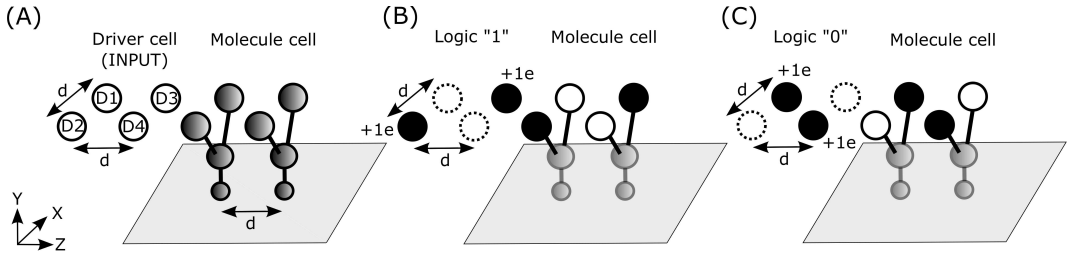

Figure 4.15 (A)Point charge driver (driver cell) for complete MQCA cell; (B)Driver cell is configured into logic state "1" as input; (C)Driver cell is configured into logic state "0" as input.

4.4.1.2 Clock Signal

As mentioned in Section 4.2.1, based on the input *Z-matrix* the *Gaussian 09* generates its internal coordinates as standard orientation for all atoms inside the molecular system. For single bis-ferrocene molecule simulation, the generated coordinates of atoms are turned out to be symmetric with respect to X-Z plane, as sketched in Figure 4.16. The red, green and blue arrows are standing for X-axis, Y-axis and Z-axis, respectively. Thus by definition, the switching field and clock field could be applied uniformly for single molecule case with different directions.

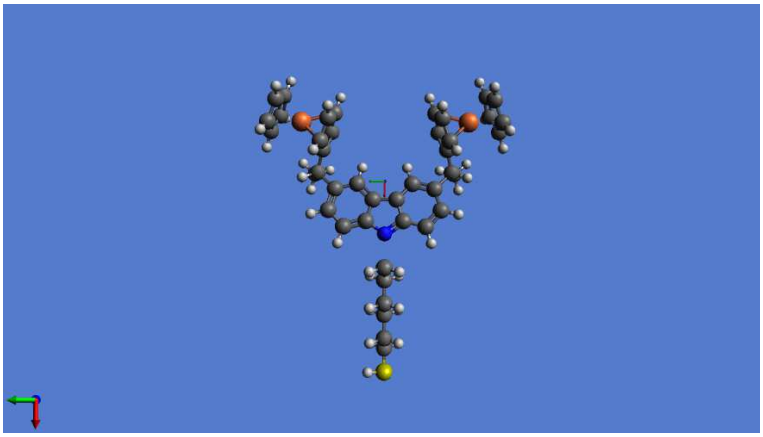

Figure 4.16 The symmetric coordinates generated by the simulation for single bis-ferrocene molecule.

However, regarding the case of two bis-ferrocene molecules, the generated internal coordinates for simulation are no more symmetric with respect to any axis, see Figure 4.17. In this condition, neither the switching field nor the clock field desired for these two molecules system is parallel to any axis. Due to the fact that in the routine section of *Gaussian 09* input file, only electric field parallel to one of the three axes is allowed to apply, so another way of introducing electric field is thus necessary, particularly in the case when clock field is necessary.

Similar as illustrated in Figure 4.18(A), electric field exists inside a capacitor with opposite charges localized on the two metal plates when an external voltage (V_{ap}) is applied, here inside ab-initio simulation two rows point charges are built around the molecules with opposite charge polarities assigned. The generated electric field in between is thus approximately uniform, especially in the space where two molecules are located. Furthermore, the direction of such electric field can be easily modified depending on the positions of those point charges. Figure 4.18(B)

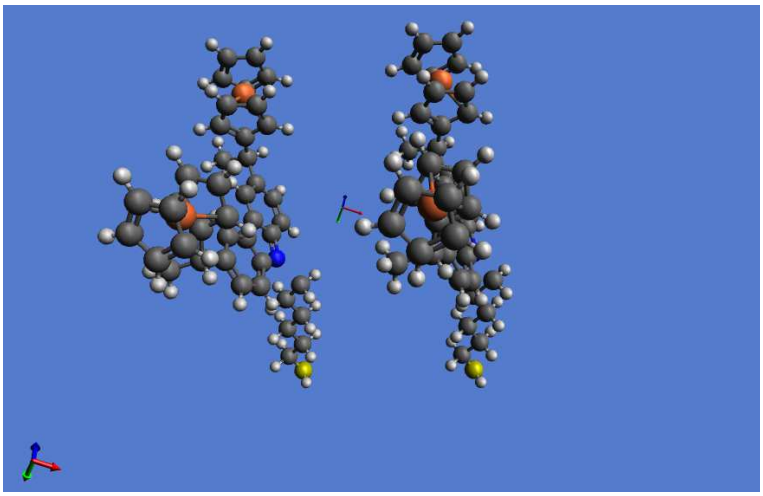

Figure 4.17 The asymmetric coordinates generated by the simulation for two bis-ferrocene molecules aligned together as a MQCA cell.

depicts the implemented clock system in ab-initio simulation for two bis-ferrocene molecules with two rows of point charges distributed above/below bis-ferrocene molecules, therefore the generated electric field is parallel to the vertical axis of molecule and recognized as clock field. In particular, if the positive charges are placed above while negative charges locate below, a negative clock signal is provided point downwards; whereas if the polarities of charges are swapped, a positive clock signal is hence generated pointing upwards.

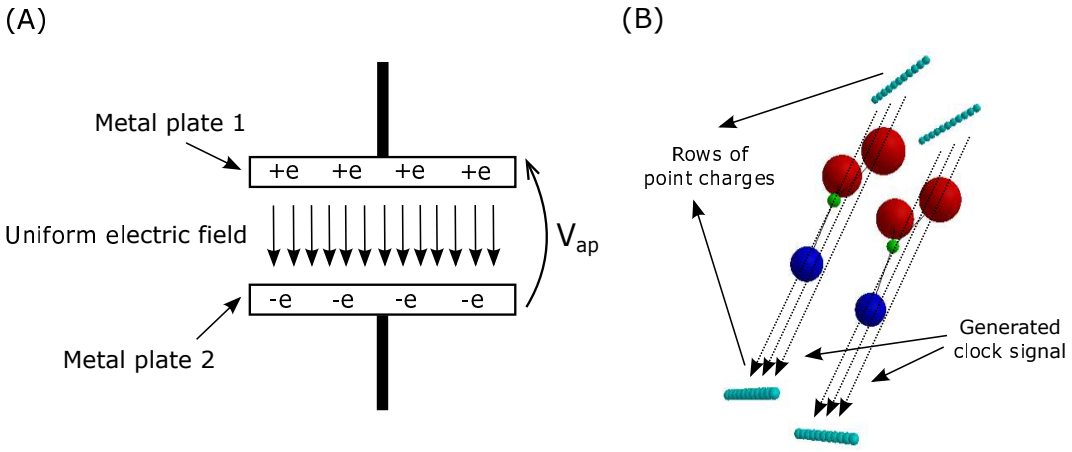

Figure 4.18 (A)Uniform electric field exists between two metal plates of a capacitor when voltage is applied; (B)In ab-initio simulations, the clock signal for MQCA cell is realized placing rows of point charges around molecules.

Videlicet, now the biasing conditions for cell simulations are in terms of defining point charges with different purposes inside the input file. An example of complete *Gaussian 09* input file for two bis-ferrocene molecules simulation is illustrated in Appendix C.

In addition, in order to quantify the value of the clock field generated by the system of point charges, the generated electric field is "measured" along the height of the molecule (vertical axis), thus resulting an equivalent voltage V_{eq}. Then this V_{eq} is divided by the height of the molecule with value of $1.8nm$ and hence the equivalent clock field is obtained. Hereinafter, this equivalent clock field based on point charge system is adopted for the MQCA cell simulations and the accuracy of this approximation is acceptable in terms of giving a general review of clock system for controlling MQCA cell behavior.

In the end, combining the polarized point charge driver together with the equivalent clock system, the cell response is emulated and detailed results after post-processing of simulation data are reported in Section 5.3.

4.4.2 Three-Input Majority Voter

Similarly as the configuration of *Gaussian 09* input file for the MQCA cell in Section 4.4.1, here the MQCA cell in terms of two molecules are equipped with three polarized point charge driver cells as *INPUT*, hence a simple three-input majority voter is demonstrated, see Figure 4.19(A). The MQCA cell re-configures the aggregated charge distribution for both molecules according to the majority logic state that encoded by these driver cells. For example, as schematically highlighted in Figure 4.19(B), with three input cells assigned to logic state "0", "0" and "0", the MQCA cell in the middle eventually encodes the expected logic state "0". During ab-initio simulations, the majority voter is simulated with all eight possible configurations of three input driver cells, obtained results are recorded in Section 5.3.5.

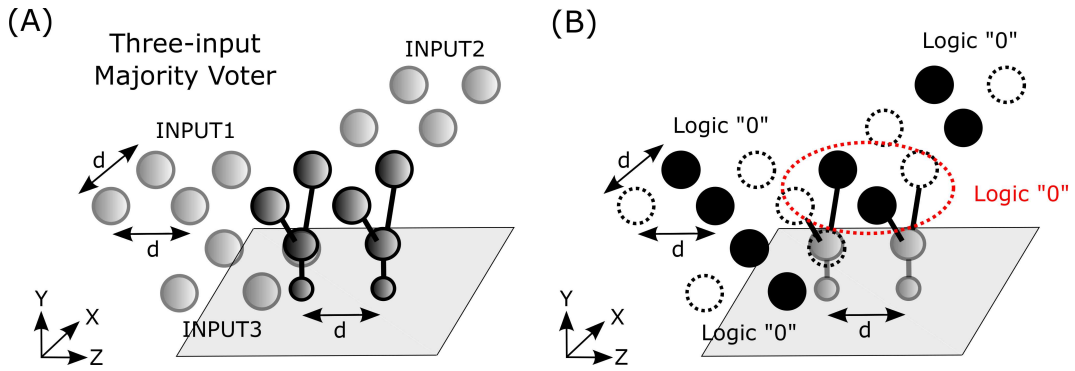

Figure 4.19 A simple three-input structure: (A)Schematic view of majority voter structure based on a complete MQCA cell; (B)With three input driver cells set to logic state “0”, the middle cell of the majority voter should encode the expected logic state “0” following its functionality.

Chapter 5

Molecule Characterization Results

In this chapter, we have provided results about the characterization of oxidized bis-ferrocene molecules based on different externally applied biasing conditions, e.g., electric field, point charges. Moreover, such characterization includes both single molecule behavior as half MQCA cell and a complete MQCA cell performance with two molecules placed together.

5.1 Biasing Condition

As for single oxidized bis-ferrocene molecule, firstly the equilibrium state of the molecule is demonstrated; then the polarized charge driver is added to verify the molecular interaction; at last, the external electric field is considered to simulate the presence of both switching field and clock field for the single molecule. The results discussed here are in terms of aggregated charge distribution of bis-ferrocene molecule, including its two logic dots (*Dot1* and *Dot2*) and the central *Dot3*.

5.1.1 Ground Stage: Equilibrium

At the equilibrium state of oxidized molecule, no biasing condition is considered, the ab-initio simulation computes the ground stage of the molecule minimizing the total energy and the result of aggregated charge distribution is shown in Table 5.1.

Oxidized Molecule	Molecule Dots		
Equilibrium state	Dot1	Dot2	Dot3
Aggregated charge	+0.370	+0.352	+0.278

Table 5.1 Bis-ferrocene molecule: aggregated charges at equilibrium.

5.1.2 Effect of Point Charge Driver

The polarized charge drivers emulate the presence of bis-ferrrocene molecule. Setting the driver with point charges makes it possible to compute the molecular interaction from one to the other. Figure 5.1 illustrates the aggregated charge distribution on bis-ferrocene molecule in presence with polarized charge driver configured into two different logic states. Consequently, the bis-ferrocene molecule re-arranges its aggregated charges with respect to the driver and due to the lack of clock signal, the total amount of charge on logic dots is not ideal ($+1e$).

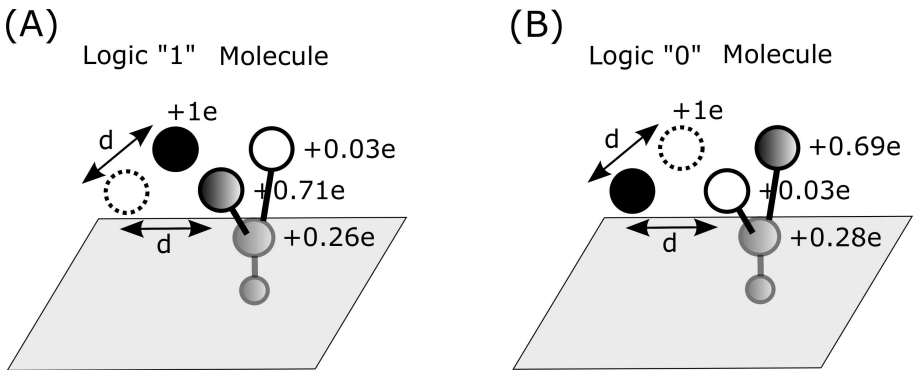

Figure 5.1 Bis-ferrocene molecule together with polarized charge driver ($d = 1.0nm$): (A)Driver is configured into logic state “1”; (B)Driver is configured into logic state “0”.

5.1.3 Effect of Switching Field

The switching field is responsible for writing a defined logic state to bis-ferrocene molecule by means of pushing charge on one of the two logic dots, depending on its direction. Quantitative results are recorded in Table 5.2. Whereas Figure 5.2 highlights also the MQCA bi-stable properties of the bis-ferrocene molecule in terms of its suitability if a write-in system based on electric field.

Oxidized Molecule	Molecule Dots		
Switching field	Dot1	Dot2	Dot3
+5.0 V/nm	-0.034	+0.995	+0.039
+4.0 V/nm	-0.023	+0.977	+0.046
+3.0 V/nm	-0.013	+0.968	+0.045
+2.0 V/nm	-0.001	0.933	+0.068
+1.0 V/nm	+0.020	+0.820	+0.160
+0.5 V/nm	+0.050	+0.680	+0.270
-0.5 V/nm	+0.780	+0.030	+0.190
-1.0 V/nm	+0.820	+0.020	+0.160
-2.0 V/nm	+0.880	+0.003	+0.117
-3.0 V/nm	+0.960	-0.013	+0.053
-4.0 V/nm	+0.975	-0.024	+0.049
-5.0 V/nm	+0.988	-0.035	+0.047

Table 5.2 Aggregated charge distribution of oxidized bis-ferrocene molecule as function of the switching field.

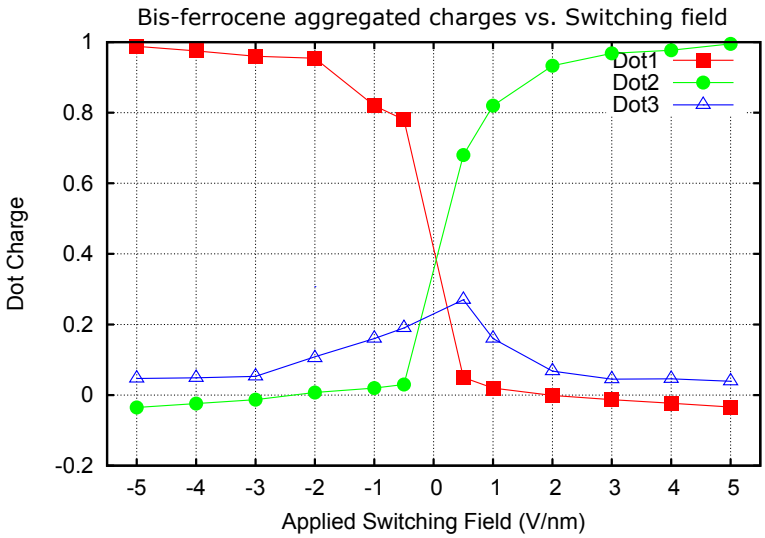

Figure 5.2 Oxidized bis-ferrocene molecule: aggregated dot charges as function of the switching field.

5.1.4 Effect of Clock Field

When the clock field is externally applied, the charge on molecule will be pulled up to logic dots or pushed down to central dot depending its sign. During the ab-initio simulations, several values of clock intensities have been considered to verify the clock functionality, quantitative results are written in Table 5.3. As expected, the positive clock field forces the major charge on logic dots of molecule, whereas with negative applied, the charge is hidden in the central dot leaving less charge for participating interaction. This proves the sensitivity of bis-ferrocene molecule with respect to the presence of clock field.

Oxidized Molecule	Molecule Dots		
Clock field	Dot1	Dot2	Dot3
+2.0 V/nm	+0.475	+0.471	+0.054
+1.0 V/nm	+0.464	+0.447	+0.089
0.0 V/nm	+0.370	+0.352	+0.278
-1.0 V/nm	+0.110	+0.109	+0.781
-2.0 V/nm	+0.027	+0.026	+0.947

Table 5.3 Aggregated charge distribution of oxidized bis-ferrocene molecule as function of the clock field.

5.2 Trans-Characteristic Relation

5.2.1 Molecular Interaction Modeling

For the sake of modeling molecular interaction and further computation, as discussed in Section 4.3, the trans-characteristic relation of bis-ferrocene molecule is introduced considering both clock field and polarized point charge driver in presence with bis-ferrocene molecule. It reflects the ability of molecule moving its charge distribution according to the influence from other molecule (driver) in terms of a generated equivalent input voltage V_{IN}.

Figure 5.3 depicts an example of the obtained trans-characteristic of bis-ferrocene molecule. The clock field considered is $+2V/nm$. In particular, since the sign of the equivalent input voltage V_{IN} represents the polarity of the driver, therefore with pos-

itive input voltage, the major charge is located on *Dot2*; otherwise the major charge moves to *Dot1*. Regarding the sign of input voltage and charge movement, see Figure 4.14. The quantitative results are recorded in Table 5.4 for complementary understanding.

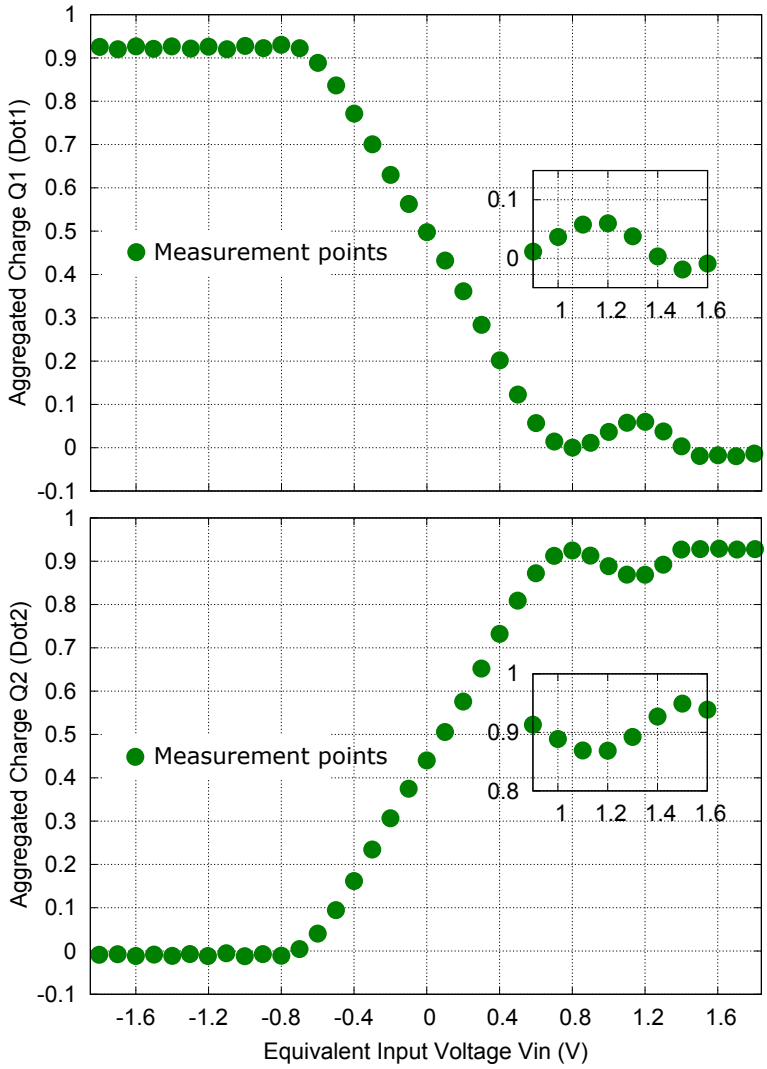

Figure 5.3 Tran-characteristic of an oxidized bis-ferrocene molecule in presence of $+2V/nm$ as clock signal.

Trans-characteristic @ CK=$+2V/nm$			
Oxidized Molecule	Molecule Dots		
Equivalent V_{IN}	Q1(Dot1)	Q2(Dot2)	Q3(Dot3)
+1.9889 V	+0.003	+0.927	+0.070
+1.8526 V	+0.003	+0.927	+0.070
+1.7889 V	+0.003	+0.927	+0.070
+1.6526 V	+0.003	+0.927	+0.070
+1.5889 V	+0.003	+0.927	+0.070
+1.4526 V	+0.043	+0.887	+0.070
+1.3889 V	+0.073	+0.857	+0.070
+1.2526 V	+0.093	+0.837	+0.070
+1.0889 V	+0.107	+0.818	+0.075
+0.9252 V	+0.075	+0.852	+0.073
+0.7615 V	+0.047	+0.877	+0.076
+0.5978 V	+0.023	+0.905	+0.072
+0.5160 V	+0.110	+0.822	+0.068
+0.4378 V	+0.195	+0.739	+0.066
+0.3523 V	+0.253	+0.683	+0.064
+0.2704 V	+0.310	+0.627	+0.063
+0.1886 V	+0.365	+0.572	+0.063
+0.1067 V	+0.422	+0.514	+0.064
+0.0249 V	+0.479	+0.459	+0.062
-0.0570 V	+0.534	+0.404	+0.062
-0.1388 V	+0.588	+0.349	+0.063
-0.2206 V	+0.644	+0.293	+0.063
-0.3025 V	+0.700	+0.235	+0.065
-0.3877 V	+0.758	+0.176	+0.066
-0.5482 V	+0.881	+0.048	+0.071
-0.7117 V	+0.922	+0.004	+0.074
-0.8754 V	+0.924	+0.003	+0.073
-1.0391 V	+0.927	+0.002	+0.071
-1.2028 V	+0.929	+0.000	+0.071
-1.3391 V	+0.927	+0.002	+0.071
-1.4328 V	+0.929	+0.000	+0.071
-1.5391 V	+0.927	+0.002	+0.071
-1.6028 V	+0.929	+0.000	+0.071
-1.7391 V	+0.927	+0.002	+0.071
-1.8328 V	+0.929	+0.000	+0.071

Table 5.4 Trans-characteristic of bis-ferrocene molecule: aggregated dot charges (Q) vs. applied input voltage (V_{IN}).

The trans-characteristic of single molecule performance could be approximately divided into two regions:

- *Quasi-linear region*: Examining the obtained trans-characteristic curve, when the applied equivalent input voltage $|V_{IN}| < 0.65V$, the aggregated dot charges of the two logic dots on molecule exhibit a quasi-linear tendency of change. The charge moves from one logic dot to another depending on the value and sign of V_{IN}. However, the total amount of charge available on molecule is kept constant (i.e., $+1.0e$).
- *Saturation region*: If the magnitude of the applied voltage generated by the driver is increasing, according to electrostatic repulsion, the unit positive charge tends to concentrate almost on one of its two logic dots of bis-ferrocene molecule. As a consequence of that, with further increasing intensity of V_{IN}, the aggregated dot charges for logic dots begin to saturate neglecting some existing fluctuations.

5.2.2 Clock-dependent Relation

It is noteworthy that the pictured trans-characteristic which describes the reaction from one molecule to the other is clock-dependent, since the intensity of applied clock signal determines the amount of charge available on logic dots for molecular interaction. Therefore, in Figure 5.4 multiple trans-characteristics curves are plotted together for comparison ($-2V/nm$, $0V/nm$ and $+2V/nm$). Besides some fluctuations of these curves, it can be seen that if the clock field increases, the amount of charge involved inside molecular interaction increases proportionally, thus more evident charge separation is observed on two logic dots when input voltage is applied. For example, if the negative clock ($-2V/nm$) is considered, the charge left on the two logic dots is null as expected, thus the interaction phenomena is hardly observed. On the contrary, if the clock field arises, the charge separation on molecule due to electrostatic interaction is better.

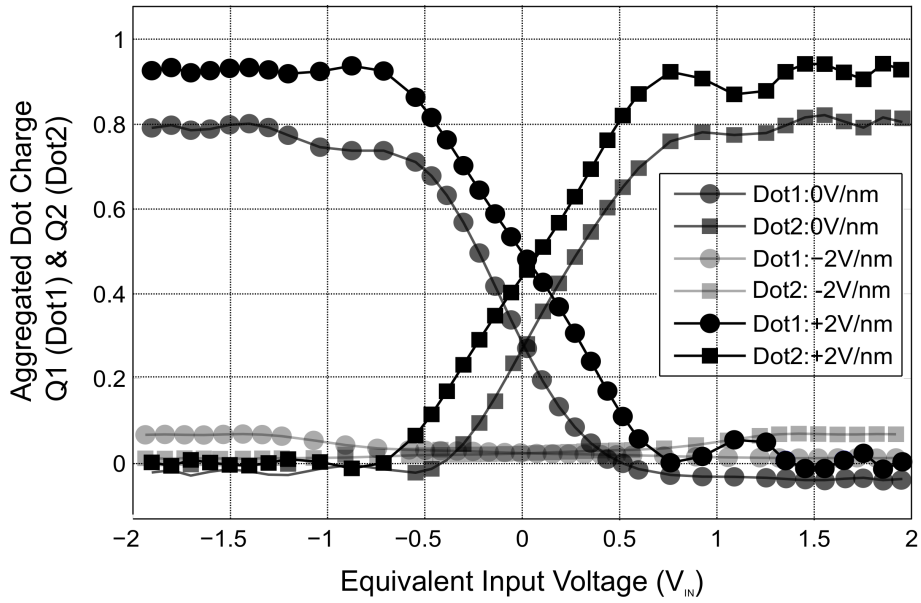

Figure 5.4 Tran-characteristics of different clock field applied.

5.3 MQCA Cell Response

Here the *Gaussian 09* simulations of a complete MQCA cell with two oxidized bis-ferrocene molecules are executed. Similar as single molecule analysis, results regarding the cell both at equilibrium ground state and in presence with biasing conditions are discussed as follows.

5.3.1 Ground State: Equilibrium

For equilibrium state, no biasing condition is taken into account, the results terms of aggregated dot charges of these two molecules are recorded in Table 5.5.

MQCA cell	Molecule1 Dots			Molecule2 Dots		
Equilibrium state	Dot1	Dot2	Dot3	Dot1	Dot2	Dot3
Agg. Charge	+0.421	+0.409	+0.170	+0.379	+0.379	+0.242
Total charge	+1.000			+1.000		

Table 5.5 MQCA cell: two bis-ferrocene molecules at equilibrium.

5.3.2 Effect of Clock System

Simulations have also been performed taking into account clock field. As mentioned in Section 4.4.1, here the clock signal is implemented with rows of point charges that equivalent to externally applied electric field. Furthermore, the polarity of rows of charges determines the sign of the clock signal. For example, with positive point charges on the rows above MQCA cell and negative point charges located below MQCA cell, an equivalent negative clock signal is generated, whereas if the polarity is swapped, a positive clock signal is thus created.

In Table 5.6, results of MQCA cell in presence of this point charge based clock system are provided. With above mention positive clock system, by the same logic as single bis-ferrocene molecule case, almost all the charge is localized on logic dots (for both molecules), e.g., for *Molecule1*, aggregated charges of two logic dots are generated with values of $+0.498$ and $+0.490$, while the charge left on central dot is 0.012. Such values for *Molecule2* are $+0.497$, $+0.498$ and $+0.005$. The aggregated charges on logic dots of molecules are turned out to be balanced since no other biasing condition is applied for configuring the logic state of molecule.

On the other hand, if negative clock system is introduced, the charge moves from logic dots to central dot prohibiting the interaction among molecules. These obtained results prove the functionality of this clock system in terms of satisfying the purpose of enhancing or hindering molecular interaction is MQCA.

MQCA cell	Molecule1 Dots			Molecule2 Dots		
Positive Clock	Dot1	Dot2	Dot3	Dot1	Dot2	Dot3
Agg. Charge	+0.498	+0.490	0.012	+0.497	+0.498	0.005
Total charge	+1.000			+1.000		
Negative Clock	Dot1	Dot2	Dot3	Dot1	Dot2	Dot3
Agg. Charge	+0.089	+0.090	+0.821	+0.068	+0.070	+0.862
Total charge	+1.000			+1.000		

Table 5.6 MQCA cell: two bis-ferrocene molecules in presence of point charge based clock system.

5.3.3 Cell-to-Cell Response: *d=1.0 nm*

As mentioned in Section 4.4.1, we have also examined the complete response with respect to another driving cell based on point charges, see Figure 4.15. In this condition, simulations have been performed considering the existence of different clock system together with both logic states of driver cell. The distance between two bis-ferrocene molecules inside the cell is 1.0*nm*. Quantitative results in terms of aggregated dot charges for two molecules are recorded in Table 5.7.

In general, with the presence of driver cell, the MQCA cell re-configures the aggregated dot charges for both molecules thus encoding the same logic state as driver cell. This can be observed in the Table 5.7 for both logic states. Moreover, the clock functionality in terms of controlling interaction between molecules is also highlighted. For example, the negative clock system considered, two molecules are both in *NULL* state and no interacting phenomena happens. Whereas if positive clock system is applied, the molecular interaction results an evident charge separation between the two logic dots of bis-ferrocene molecule (both molecules) for representing proper logic state.

Cell-to-cell response @ Logic state "0", $d = 1.0nm$								
Driver cell		Agg.	Negative clock		No clock		Positive clock	
D1 D2	D3 D4	Q	Mol 1	Mol 2	Mol 1	Mol 2	Mol 1	Mol 2
1.0	0.0	Q1	0.098	0.063	0.709	0.237	0.782	0.403
0.0	1.0	Q2	0.089	0.070	0.102	0.517	0.186	0.587
-	-	Q3	0.813	0.867	0.189	0.246	0.032	0.010
Cell-to-cell response @ Logic state "1", $d = 1.0nm$								
Driver cell		Agg.	Negative clock		No clock		Positive clock	
D1 D2	D3 D4	Q	Mol 1	Mol 2	Mol 1	Mol 2	Mol 1	Mol 2
0.0	1.0	Q1	0.082	0.062	0.114	0.512	0.222	0.593
1.0	0.0	Q2	0.102	0.073	0.699	0.241	0.747	0.378
-	-	Q3	0.816	0.865	0.187	0.247	0.031	0.029

Table 5.7 Cell-to-cell response in MQCA with $d = 1.0nm$.

5.3.4 Cell-to-Cell Response: *d=0.8 nm*

However, with standard 1.0*nm* of distance between two molecules (square shape cell), the separation between aggregated dot charges of logic dots on second molecule in the cell is small ($\simeq 0.2$) making it difficult to read-out the information carried by MQCA. As a solution of that, the inter-molecule distance d could be theoretically shrank, e.g., to 0.8*nm*, which could lead to a stronger electrostatic interaction favoring information propagation. Similar ab-initio simulations have been carried out for shorter distance between molecules localized in the cell with clock system and driver cell as biasing conditions. Quantitative results in terms of aggregated dot charges for two molecules in these conditions are presented in Table 5.8 (equilibrium ground state), Table 5.9 (clock response) and Table 5.10 (cell-to-cell response).

These generated results suggest in evident that with a shorter inter-molecule distance $d = 0.8nm$, the MQCA complete cell still hold a balanced aggregated charge distribution with respect to clock system if no external driver cell is present. On the contrary, if a driver cell is introduced, it is necessary to mention that the driver cell should possess the same shape of the cell and the distance between two cells is also 0.8*nm*. As a consequence of that, the electrostatic interaction between molecules and driver is much stronger hence leading to a more evident charge separation between logic dots on molecules, see Table 5.10.

MQCA cell	Molecule1 Dots			Molecule2 Dots		
Equilibrium state	Dot1	Dot2	Dot3	Dot1	Dot2	Dot3
Agg. Charge	+0.441	+0.323	+0.236	+0.320	+0.402	+0.278
Total charge	+1.000			+1.000		

Table 5.8 MQCA cell: two bis-ferrocene molecules at equilibrium with $d = 0.8nm$.

5.3.5 Three-Input Majority Voter Response

As an application of MQCA cell, a simple three-input majority has been demonstrated assigning three driver cells near the MQCA cell with point charges, see Figure 4.19(A). The distance d between nearby cell is 1.0*nm*. Then the two bis-ferrocene molecules configure their aggregated charges with respect to the present driver cells. In Figure 5.5, the aggregated dot charges for two molecules are shown

MQCA cell	Molecule1 Dots			Molecule2 Dots		
Positive Clock	Dot1	Dot2	Dot3	Dot1	Dot2	Dot3
Agg. Charge	+0.491	+0.483	0.026	+0.481	+0.500	0.019
Total charge	+1.000			+1.000		
Negative Clock	Dot1	Dot2	Dot3	Dot1	Dot2	Dot3
Agg. Charge	+0.059	+0.047	+0.894	+0.058	+0.062	+0.880
Total charge	+1.000			+1.000		

Table 5.9 MQCA cell: two bis-ferrocene molecules in presence of point charge based clock system with $d = 0.8nm$.

Cell-to-cell response @ Logic state "0", $d = 0.8nm$								
Driver cell		Agg.	Negative clock		No clock		Positive clock	
D1 D2	D3 D4	Q	Mol 1	Mol 2	Mol 1	Mol 2	Mol 1	Mol 2
1.0	0.0	Q1	0.036	0.056	0.717	0.197	0.904	0.127
0.0	1.0	Q2	0.053	0.069	0.053	0.543	0.043	0.827
-	-	Q3	0.911	0.875	0.230	0.260	0.053	0.046
Cell-to-cell response @ Logic state "1", $d = 0.8nm$								
Driver cell		Agg.	Negative clock		No clock		Positive clock	
D1 D2	D3 D4	Q	Mol 1	Mol 2	Mol 1	Mol 2	Mol 1	Mol 2
0.0	1.0	Q1	0.027	0.054	0.019	0.624	0.019	0.843
1.0	0.0	Q2	0.078	0.070	0.790	0.085	0.949	0.132
-	-	Q3	0.895	0.876	0.191	0.291	0.032	0.025

Table 5.10 Cell-to-cell response in MQCA with $d = 0.8nm$.

without clock system taken into account. The three inputs are all configured into logic state "0", whereas the MQCA cell localized in the middle of them encodes the same logic state as expected, although the charge separation between two logic dots for each molecule is not ideal ($+1.0e$).

After that, if an enhancing clock (positive clock) system is added during simulation, more charge is available on logic dots which could lead to more distinct encoding of logic state, see Figure 5.6.

On the other hand, when a prohibiting clock (negative clock) system is concerned inside simulation, most of the charge move to central dots leaving the molecules in *NULL* state, therefore the molecular interaction is hardly observed, see the aggregated dot charges recorded in Figure 5.7.

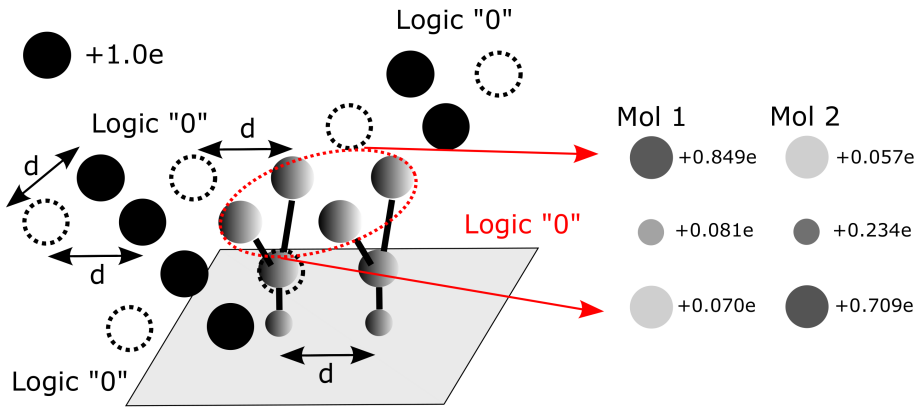

Figure 5.5 Aggregated dot charges of simple majority voter with “000” as three inputs.

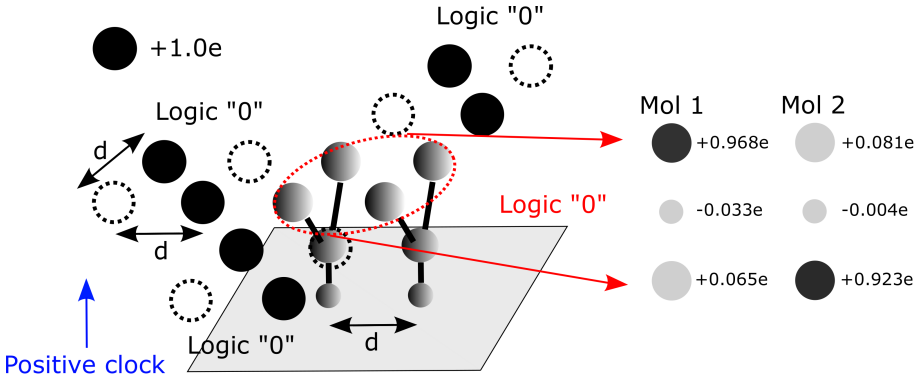

Figure 5.6 Aggregated dot charges of simple majority voter in presence of positive clock (enhancing clock) and “000” as three inputs.

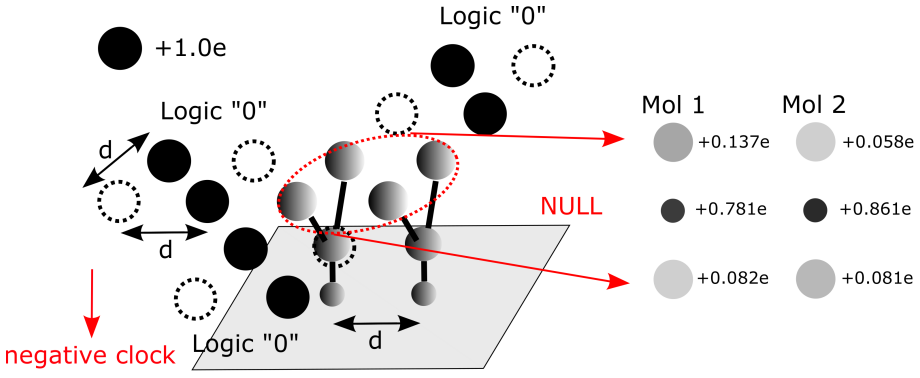

Figure 5.7 Aggregated dot charges of simple majority voter in presence of negative clock (prohibiting clock) and “000” as three inputs.

With the aim of completely verifying the majority voter performance, Table 5.11 records quantitative results in terms of aggregated dot charges for all possible inputs for the simple majority voter based on MQCA cell. In the meantime, the influence

from different clock systems to the majority voter behavior has been also considered during simulation and corresponding results are listed in Table 5.12 and Table 5.13.

Inputs	"0" "0" "0"		Inputs	"0" "0" "1"	
Molecule Dots	Mol 1	Mol 2	Molecule Dots	Mol 1	Mol 2
Q1(Dot1)	+0.849	+0.057	Q1(Dot1)	+0.802	+0.039
Q2(Dot2)	+0.070	+0.709	Q2(Dot2)	+0.079	+0.710
Q3(Dot3)	+0.081	+0.234	Q3(Dot3)	+0.119	+0.251
Inputs	"0" "1" "0"		Inputs	"0" "1" "1"	
Molecule Dots	Mol 1	Mol 2	Molecule Dots	Mol 1	Mol 2
Q1(Dot1)	+0.799	+0.037	Q1(Dot1)	+0.229	+0.697
Q2(Dot2)	+0.078	+0.713	Q2(Dot2)	+0.574	+0.070
Q3(Dot3)	+0.123	+0.250	Q3(Dot3)	+0.197	+0.233
Inputs	"1" "0" "0"		Inputs	"1" "0" "1"	
Molecule Dots	Mol 1	Mol 2	Molecule Dots	Mol 1	Mol 2
Q1(Dot1)	+0.586	+0.061	Q1(Dot1)	+0.137	+0.550
Q2(Dot2)	+0.212	+0.707	Q2(Dot2)	+0.741	+0.198
Q3(Dot3)	+0.202	+0.232	Q3(Dot3)	+0.122	+0.252
Inputs	"1" "1" "0"		Inputs	"1" "1" "1"	
Molecule Dots	Mol 1	Mol 2	Molecule Dots	Mol 1	Mol 2
Q1(Dot1)	+0.143	+0.551	Q1(Dot1)	+0.063	+0.706
Q2(Dot2)	+0.728	+0.191	Q2(Dot2)	+0.832	+0.066
Q3(Dot3)	+0.129	+0.258	Q3(Dot3)	+0.105	+0.228

Table 5.11 Simple three-input MQCA majority voter behavior.

In summary, regarding above listed results of bis-ferrocene molecule characterization, including both single molecule performance and the complete MQCA cell analysis, some comments are necessary to be stated: (i)the bis-ferrocene molecule as a real system, especially in its oxidized form, is proved to be a good candidate for building MQCA circuits and it has been already bonded to a gold substrate [48]; (ii)the bi-stable condition of charge localization in presence of driver or driver cell allows molecule to encode proper digital logic states while transmitting binary information; (iii)the bis-ferrocene molecule is also sensitive with respect to the introduced electric field, both for switching field and clock field. Moreover, the molecule also responses properly to the clock system which are implemented based on point charges with opposite polarities, thus it is possible to achieve adiabatic switching in terms of controlling (enhancing or hindering) interaction between nearby molecules.

Inputs	“0” “0” “0”		Inputs	“0” “0” “1”	
Molecule Dots	Mol 1	Mol 2	Molecule Dots	Mol 1	Mol 2
Q1(Dot1)	+0.968	+0.081	Q1(Dot1)	+0.817	+0.392
Q2(Dot2)	+0.065	+0.923	Q2(Dot2)	+0.190	+0.602
Q3(Dot3)	-0.033	-0.004	Q3(Dot3)	-0.007	+0.006
Inputs	“0” “1” “0”		Inputs	“0” “1” “1”	
Molecule Dots	Mol 1	Mol 2	Molecule Dots	Mol 1	Mol 2
Q1(Dot1)	+0.815	+0.389	Q1(Dot1)	+0.407	+0.792
Q2(Dot2)	+0.193	+0.617	Q2(Dot2)	+0.650	+0.199
Q3(Dot3)	-0.008	-0.006	Q3(Dot3)	-0.057	+0.009
Inputs	“1” “0” “0”		Inputs	“1” “0” “1”	
Molecule Dots	Mol 1	Mol 2	Molecule Dots	Mol 1	Mol 2
Q1(Dot1)	+0.657	+0.196	Q1(Dot1)	+0.201	+0.621
Q2(Dot2)	+0.383	+0.808	Q2(Dot2)	+0.809	+0.379
Q3(Dot3)	-0.040	-0.004	Q3(Dot3)	-0.010	+0.000
Inputs	“1” “1” “0”		Inputs	“1” “1” “1”	
Molecule Dots	Mol 1	Mol 2	Molecule Dots	Mol 1	Mol 2
Q1(Dot1)	+0.199	+0.618	Q1(Dot1)	+0.057	+0.923
Q2(Dot2)	+0.813	+0.380	Q2(Dot2)	+0.974	+0.083
Q3(Dot3)	-0.012	+0.002	Q3(Dot3)	-0.031	-0.006

Table 5.12 Simple three-input MQCA majority voter behavior in presence of a positive clock system (enhancing clock).

Inputs	“0” “0” “0”		Inputs	“0” “0” “1”	
Molecule Dots	Mol 1	Mol 2	Molecule Dots	Mol 1	Mol 2
Q1(Dot1)	+0.137	+0.058	Q1(Dot1)	+0.111	+0.063
Q2(Dot2)	+0.082	+0.081	Q2(Dot2)	+0.099	+0.075
Q3(Dot3)	+0.781	+0.861	Q3(Dot3)	+0.790	+0.862
Inputs	“0” “1” “0”		Inputs	“0” “1” “1”	
Molecule Dots	Mol 1	Mol 2	Molecule Dots	Mol 1	Mol 2
Q1(Dot1)	+0.107	+0.067	Q1(Dot1)	+0.089	+0.056
Q2(Dot2)	+0.102	+0.058	Q2(Dot2)	+0.092	+0.084
Q3(Dot3)	+0.791	+0.875	Q3(Dot3)	+0.819	+0.860
Inputs	“1” “0” “0”		Inputs	“1” “0” “1”	
Molecule Dots	Mol 1	Mol 2	Molecule Dots	Mol 1	Mol 2
Q1(Dot1)	+0.086	+0.077	Q1(Dot1)	+0.097	+0.065
Q2(Dot2)	+0.095	+0.065	Q2(Dot2)	+0.105	+0.071
Q3(Dot3)	+0.819	+0.858	Q3(Dot3)	+0.798	+0.864
Inputs	“1” “1” “0”		Inputs	“1” “1” “1”	
Molecule Dots	Mol 1	Mol 2	Molecule Dots	Mol 1	Mol 2
Q1(Dot1)	+0.093	+0.067	Q1(Dot1)	+0.076	+0.073
Q2(Dot2)	+0.108	+0.060	Q2(Dot2)	+0.134	+0.067
Q3(Dot3)	+0.799	+0.873	Q3(Dot3)	+0.790	+0.860

Table 5.13 Simple three-input MQCA majority voter behavior in presence of a negative clock system (prohibiting clock).

Chapter 6

MQCA Binary Wire Analysis

As mentioned in Chapter 3, in MQCA the logic circuits are possible to be implemented arranging molecules according to specific designed patterns. The most fundamental functional logic block of MQCA is the binary wire. It could be realized juxtaposing a group of bis-ferrocene molecules together with identical distance in between. Then the binary information is thus propagated by means of electrostatic interaction existed among molecules along the wire.

In this chapter, several methods have been performed with the aim of demonstrating the information propagated along the wire in terms of computing the aggregated charge distribution of each molecule and therefore the functionality of MQCA wire is verified. In particular, these proposed methods discussed here include direct ab-initio simulations of MQCA wire with post-processing of simulation data, iterative simulation of interaction between every two nearby molecules on wire and eventually, an effective algorithm that alternatively models molecular interaction on wire. The relevant generated results describing MQCA wire performance are also presented here.

6.1 Ab-Initio Simulations Of Wire

First of all, the method based on ab-initio simulations and post-processing of data is turned out to be functional and efficient for MQCA analysis in cases like single bis-ferrocene molecule characterization and MQCA cell response study. Therefore, it is worthy to adopt similar procedure also for MQCA binary wire analysis.

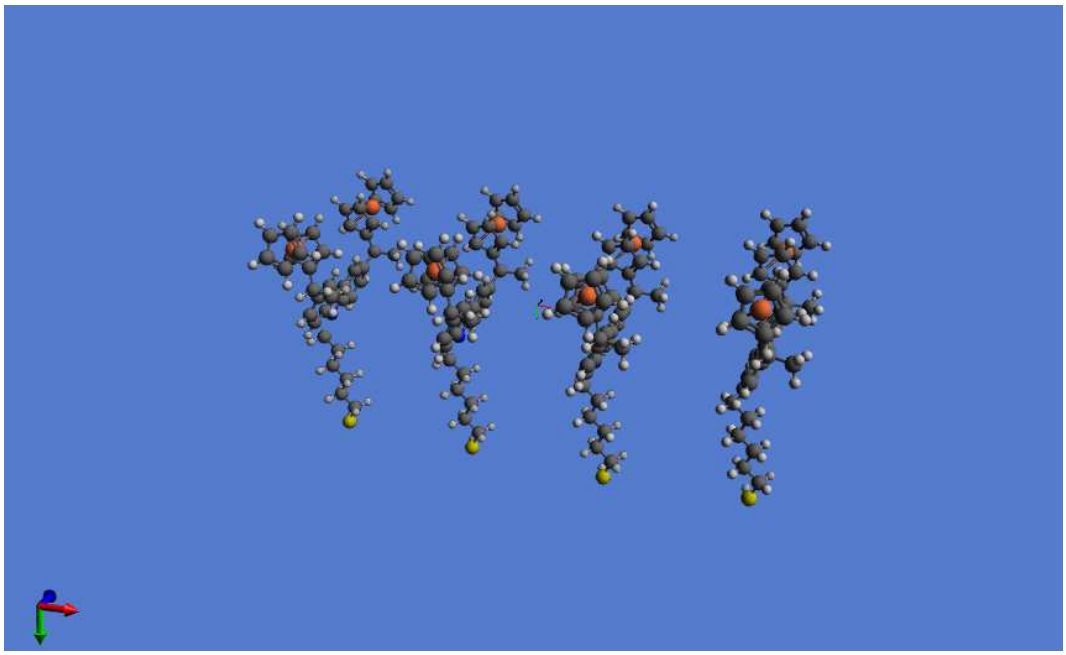

Figure 6.1 A MQCA wire with four bis-ferrocene molecules aligned together.

6.1.1 Four-Molecule Wire

As a first trial of molecular wire study, a MQCA wire with four oxidized bis-ferrocene molecules has been of interested for ab-initio simulation, see Figure 6.1. In the *Gaussian 09* input file of simulation, the Z-matrix contains structural information about four bis-ferrocene molecules, the distance d between nearby molecules is identical. By the same logic, the aggregated dot charges of all four molecules are obtained via post-processing of simulation data, quantitative results in terms of aggregated dot charges on wire in both cases like equilibrium ground state and influenced by driver cell placed aside are respectively listed in Table 6.1 (equilibrium), Table 6.2 (logic "0" of driver cell) and Table 6.3 (logic "1" of driver cell).

Four-molecule wire charge distribution				
Molecule Dots	Mol 1	Mol 2	Mol 3	Mol 4
Q1(Dot1)	+0.666	+0.190	+0.127	+0.653
Q2(Dot2)	+0.675	+0.111	+0.209	+0.599
Q3(Dot3)	+0.116	+0.239	+0.234	+0.181
Total charge	+1.457	+0.540	+0.570	+1.433

Table 6.1 Four-molecule MQCA wire: aggregated charges at equilibrium.

Four-molecule wire charge distribution				
Molecule Dots	Mol 1	Mol 2	Mol 3	Mol 4
Q1(Dot1)	+0.688	+0.212	+0.129	+0.752
Q2(Dot2)	+0.082	+0.393	+0.159	+0.706
Q3(Dot3)	+0.226	+0.221	+0.241	+0.190
Total charge	+0.996	+0.826	+0.529	+1.648

Table 6.2 Four-molecule MQCA wire: aggregated charges with driver cell configured in logic state "0".

Four-molecule wire charge distribution				
Molecule Dots	Mol 1	Mol 2	Mol 3	Mol 4
Q1(Dot1)	+0.082	+0.495	+0.081	+0.753
Q2(Dot2)	+0.702	+0.099	+0.249	+0.685
Q3(Dot3)	+0.212	+0.211	+0.228	+0.172
Total charge	+0.996	+0.805	+0.558	+1.640

Table 6.3 Four-molecule MQCA wire: aggregated charges with driver cell configured in logic state "1".

There results in Table 6.1 represent the equilibrium ground state of the four bis-ferrocene molecules located on wire. Since no other biasing conditions like clock system or driver cell are in presence, molecular interaction is weak and no clear information is propagated along the wire. On the other hand, it can be noticed that the last row of the table highlights the sum of total charge for each molecule which should be ideally $+1.0e$. As mentioned at the beginning in Section 1.3, the charge movement in QCA should be within a cell instead of outside. As for MQCA, a single molecule represents half of cell thus the charge is expected to move inside the molecule through tunneling path between redox centers (dots) of molecule. Whereas for four-molecule wire simulation, the resulting total charge of each molecule is not $+1.0e$ suggesting that the charge moves from one molecule to the other and this violates the general QCA working principle. This is due to that the ab-initio simulations allow us to solve the molecular structure (e.g., a wire) as a whole system in numerous biasing conditions, rather than optimizing separately the components.

Meanwhile, even though the results in Table 6.2 and Table 6.3 illustrate the interaction among molecules along wire with driver cell in presence, the movement of

charge from one molecule to another still exists which sabotages the quality of binary information propagation at the end of wire, namely the aggregated dot charges of the last molecule (*Mol 4*) on wire are almost balanced between two logic dots.

Apart from that, as the number of molecules increases, the simulation calculation becomes much more computationally intensive which is not affordable for further MQCA complex circuits analysis. In addition, as mentioned in Section 1.4, the MQCA device should be divided into several clock zones and then multi-phase clock signals are applied to these partitioned zones for guaranteeing proper information propagation. Although in the case of four-molecule wire, the generated standard orientation, i.e., coordinates of atoms, is symmetric for all molecules allowing an application of electric field as clock signal, the assignment of multiple values of electric field at the same time inside *Gaussian 09* is not allowed. Consequently, the direct use of ab-initio simulations for evaluating MQCA performance is thus discarded.

6.1.2 Iterative Method Of Simulation

As the second trial for molecular wire study, here an iterative method is introduced for modeling molecular interaction and further computing the charge distribution in a MQCA wire. In specific, this trial is based on the characterization result of single bis-ferrocene molecule and the MQCA wire made of bis-ferrocene molecules is emulated by means of iterative steps of ab-initio simulations [60].

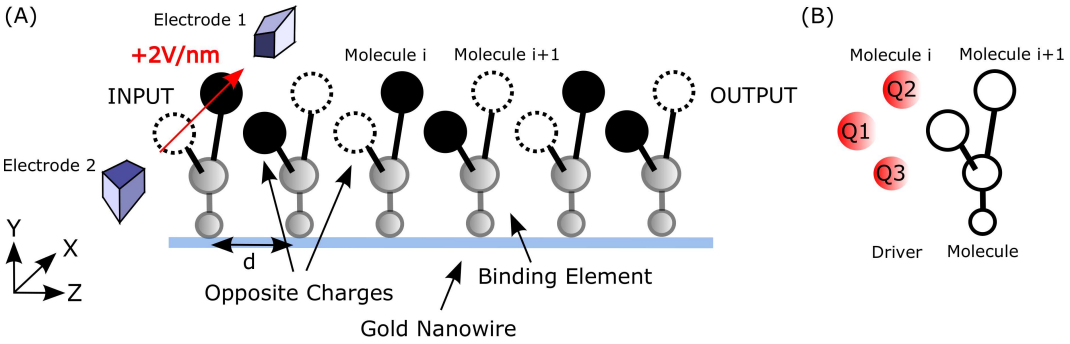

Figure 6.2 Implementing a MQCA wire by means of iterative method of ab-initio simulations and post-processing of data based on bis-ferrocene molecules.

In particular, see Figure 6.2(A), a logic state of the first molecule on the wire is written applying the switching field with values of $+2.0V/nm$ between two elec-

trodes along the ferrocene axis. Then the re-arranged aggregated dot charges of this molecule are thus formed and computed via ab-initio simulation, which are -0.001, $+0.933$ and $+0.068$ for the two logic dots ($Dot1$ and $Dot2$) and central dot $Dot3$, respectively (see Section 5.1.3). Next, we take the charge configuration of this molecule as stimulus for the successive molecule located nearby to model the interaction between them. So the second bis-ferrocene molecule is simulated in presence of a driver with aggregated charges from the first molecule.

From a generic point of view, as depicted in Figure 6.2(B), once the aggregated dot charge distribution of $Moli$ is evaluated as a response of the previous molecule $Moli-1$, then the $Moli$ with its charges $Q1$, $Q2$ and $Q3$ is recognized as the driver system of the neighboring molecule $Moli+1$ in the next step of simulation. By iterating this method of simulation for calculating interactions among all molecules on the wire from the first one ($INPUT$) to the end ($OUTPUT$), it is possible to determine the information propagated through the wire.

Eight-molecule wire @ Logic state "1" ($d = 1.0nm$)				
Molecule Dots	Mol 1	Mol 2	Mol 3	Mol 4
Q1(Dot1)	-0.001	+0.773	+0.066	+0.648
Q2(Dot2)	+0.933	+0.006	+0.622	+0.050
Q3(Dot3)	+0.068	+0.221	+0.312	+0.302
Molecule Dots	Mol 5	Mol 6	Mol 7	Mol 8
Q1(Dot1)	+0.110	+0.560	+0.174	+0.418
Q2(Dot2)	+0.543	+0.108	+0.455	+0.218
Q3(Dot3)	+0.347	+0.332	+0.371	+0.364
Eight-molecule wire @ Logic state "0" ($d = 1.0nm$)				
Molecule Dots	Mol 1	Mol 2	Mol 3	Mol 4
Q1(Dot1)	+0.880	+0.028	+0.653	+0.123
Q2(Dot2)	+0.003	+0.732	+0.047	+0.523
Q3(Dot3)	+0.117	+0.240	+0.300	+0.354
Molecule Dots	Mol 5	Mol 6	Mol 7	Mol 8
Q1(Dot1)	+0.514	+0.208	+0.423	+0.286
Q2(Dot2)	+0.142	+0.417	+0.214	+0.336
Q3(Dot3)	+0.344	+0.375	+0.363	+0.378

Table 6.4 Aggregated charge distribution of eight-molecule MQCA wire ($d = 1.0nm$).

Table 6.4 and Table 6.5 present the results about a eight-molecule wire obtained using the iterative method. During our simulations, both logic states have been

Eight-molecule wire @ Logic state "1" ($d = 0.8nm$)				
Molecule Dots	Mol 1	Mol 2	Mol 3	Mol 4
Q1(Dot1)	-0.001	+0.811	+0.016	+0.784
Q2(Dot2)	+0.933	+0.001	+0.793	+0.019
Q3(Dot3)	+0.068	+0.188	+0.191	+0.197
Molecule Dots	Mol 5	Mol 6	Mol 7	Mol 8
Q1(Dot1)	+0.015	+0.783	+0.013	+0.734
Q2(Dot2)	+0.797	+0.021	+0.805	+0.009
Q3(Dot3)	+0.188	+0.196	+0.182	+0.257
Eight-molecule wire @ Logic state "0" ($d = 0.8nm$)				
Molecule Dots	Mol 1	Mol 2	Mol 3	Mol 4
Q1(Dot1)	+0.880	+0.012	+0.782	+0.014
Q2(Dot2)	+0.003	+0.801	+0.023	+0.801
Q3(Dot3)	+0.117	+0.187	+0.195	+0.185
Molecule Dots	Mol 5	Mol 6	Mol 7	Mol 8
Q1(Dot1)	+0.783	+0.014	+0.781	+0.072
Q2(Dot2)	+0.020	+0.800	+0.023	+0.610
Q3(Dot3)	+0.197	+0.186	+0.196	+0.318

Table 6.5 Aggregated charge distribution of eight-molecule MQCA wire ($d = 0.8nm$).

assigned to the first molecule $Mol1$ as input and also two values of inter-molecule distance d ($1.0nm$ and $0.8nm$) have been taken into consideration for comparison. Moreover, the clock field can be also added during each step of simulation for a complementary analysis.

Based on the values recorded in Table 6.4, it can be summarized that with positive switching field $+2.0V/nm$ assigned, first molecule $Mol1$ is forced with aggregated dot charges of -0.001, $+0.933$ and $+0.068$, then the second molecule $Mol2$ re-arrange itself with charge distribution of $+0.773$, $+0.006$ and 0.221. Therefore, these two molecules represent a MQCA cell with logic state "1" encoded. After that, this encoded logic information is thus propagated along the wire. However, such information is degraded heavily during transmission, the charge difference between two logic dots is hardly recognized as logic state when reaching the last cell that contains $Mol7$ and $Mol8$. These discussions are also valid for logic state "0" propagated along the wire when negative switching field $-2.0V/nm$ is applied as write-in system.

Then again, with a shorter distance between two molecules on wire, as stated by the values in Table 6.5, the molecular interaction is more stronger and the binary information encoded is thus well preserved and delivered throughout the whole wire.

Figure 6.3 and Figure 6.4 depict the same results as the Table 6.4 and Table 6.5 for a more directive observation concerning the quality of wire behavior. It clearly sketches both the information degradation with distance of 1.0*nm* and the preserved logic states inside wire with distance of 0.8*nm*.

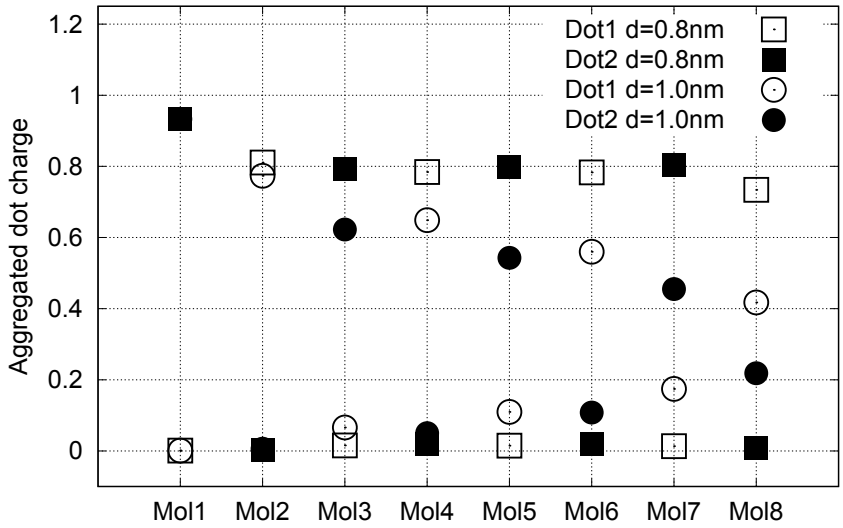

Figure 6.3 Aggregated charge distribution along eight-molecule wire (1.0*nm* and 0.8*nm*) with logic state "0" propagated.

Concerning the above mentioned iterative method, the generated results are notable because they reveal the strength of the logic signals in MQCA wire. Nevertheless, due to the reality that inside QCA devices implemented with molecules, electrostatic interactions are existed not only between neighboring molecules, but indeed a molecule should response to all molecules around. Meanwhile, the molecular interaction considered here is unidirectional, i.e., from the *INPUT* to the *OUTPUT* of the wire. Actually, such interaction should multi-directional, namely once a molecule re-arranges itself with respect to the rest of molecules, then the newly formed aggregated charges would on its turn influence back to other molecules. Hence an alternative method for wire analysis has to be brought into focus.

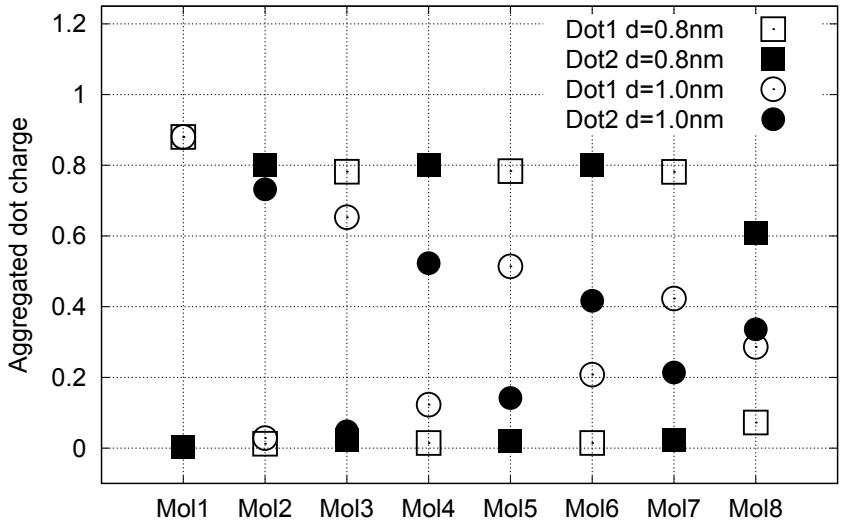

Figure 6.4 Aggregated charge distribution along eight-molecule wire (1.0*nm* and 0.8*nm*) with logic state "1" propagated.

6.2 Alternative Method For MQCA Wire Analysis

There has been extensive research for exploiting the performance of MQCA structures, as a matter of fact that previous approaches are either non dedicated to actual real molecular systems, like in the case of adopting *QCADesigner* [61][62][63], or based on theoretical analysis. Particularly, the only available source comes from quantum chemistry, in which the results are based on the solution of Shrodingher's equation. But this kind of information which can be achieved, though very accurate, is far from what is necessary to determine, i.e., the proper behavior of a MQCA from an electronic point of view [64]. Therefore, following the desire of overcoming the lack of tools suitable for this purpose, we have proposed an alternative method to evaluate the molecular interactions which facilitates the eventual demonstration of MQCA as electronic device. This method is based on an effective algorithm which renders a more close-to-reality way of modeling and computing electrostatic interactions among all molecules since such interactions determine the digital information transferred throughout the whole MQCA device.

6.2.1 Modeling Of Molecular Interaction On Wire

During the operation of MQCA devices, according to QCA principle, the electrostatic interactions among molecules (or cells) eventually determine their charge configurations used for encoding binary logic states which carry information, therefore it is extremely important to model and even further evaluate such interactions existed inside MQCA in a more close-to-reality way. Meanwhile, the interactions among molecules that are of interest are electrostatic, whereas questions about the speed of molecular switching response are not currently addressed during molecular interaction modeling and further computation.

As mentioned in Section 6.1.2, the interaction exists between any two molecules located on the wire, not necessarily nearby. In addition, in the case of a MQCA wire with molecules aligned together, the molecular interaction is also bi-directional, once the aggregated charges of a specific molecule on wire are known, this molecule will act as a driver with charges to influence not only the successive molecules located after it in terms of forwarding the information, but also affect backward its previous molecules as a feedback. In fact, the molecules interact with each other should be in terms of superposing these forward and backward effects together until reaching the final steady state in which further generated influence, either forward or backward, to each molecule on wire could be negligible.

Concerning the modeling of molecular interactions, as mentioned in Section 4.3, when one molecule influence another (e.g., MUT) as a driver, the electric field generated by the aggregated charges of the driver is computed and furthermore an equivalent input voltage is evaluated to "measure" the intensity of such electric field at the place where locates the target molecule (MUT) under effect. After that, the target molecule will configure its charge distribution according to the obtained trans-characteristic. In this way, the molecule-to-molecule response is thus modeled and calculated.

Since the study of a MQCA wire behavior requires the superposition of both forward and backward effects for determining the propagated information, numerous applications of trans-characteristic would be needed to present the molecular interactions. In order to realize and further facilitate the computation procedure of MQCA wire, an algorithm is hence proposed, see the following Section 6.2.2.

6.2.2 Algorithm

Based on the way for modeling interaction between two molecules and the superposition theorem, we proposed and developed an algorithm to evaluate aggregated dot charges of all molecules distributed along wire, this allows the demonstration of MQCA wire behavior and to foresee the information propagation at the same time.

In general, this novel algorithm relies on the single bis-ferrocene molecule characterization, i.e., the trans-characteristic obtained from ab-initio simulations and post-processing of simulation data; and on models of describing and calculating electrostatic interactions among all molecules. As an example of a MQCA wire, the algorithm iteratively models and computes all possible bi-directional molecular interactions in a self-consistent way. After that, the algorithm superposes all considered effects and outputs the final aggregated charge distribution of the wire thus demonstrating its performance concerning the ability of transmitting information.

In particular, the algorithm is divided mainly in three stages. Together with the flow chart in Figure 6.5, the proposed algorithm for wire application is thoroughly described as follows.

6.2.2.1 I) Initialization Stage

The algorithm begins with the preliminary definitions of physical parameters that render fundamental biasing conditions and structural information of the MQCA wire layout. They are recognized as inputs of the proposed algorithm. As illustrated in the *Initialization* stage in Figure 6.5 (top dashed rectangular box), these parameters are listed:

- **Molecule number**: the total number of molecules localized along MQCA wire, denoted as *MolNum*;
- **Inter-molecule distance**: the distance between two consecutive molecules placed on wire, denoted as d, see Figure 6.6;
- **Molecule position**: inside the algorithm, we approximate the molecule position with coordinates of its three redox centers, thus exact coordinates of X,Y,Z axes for these redox centers that form the bis-ferrocene molecule are recorded;

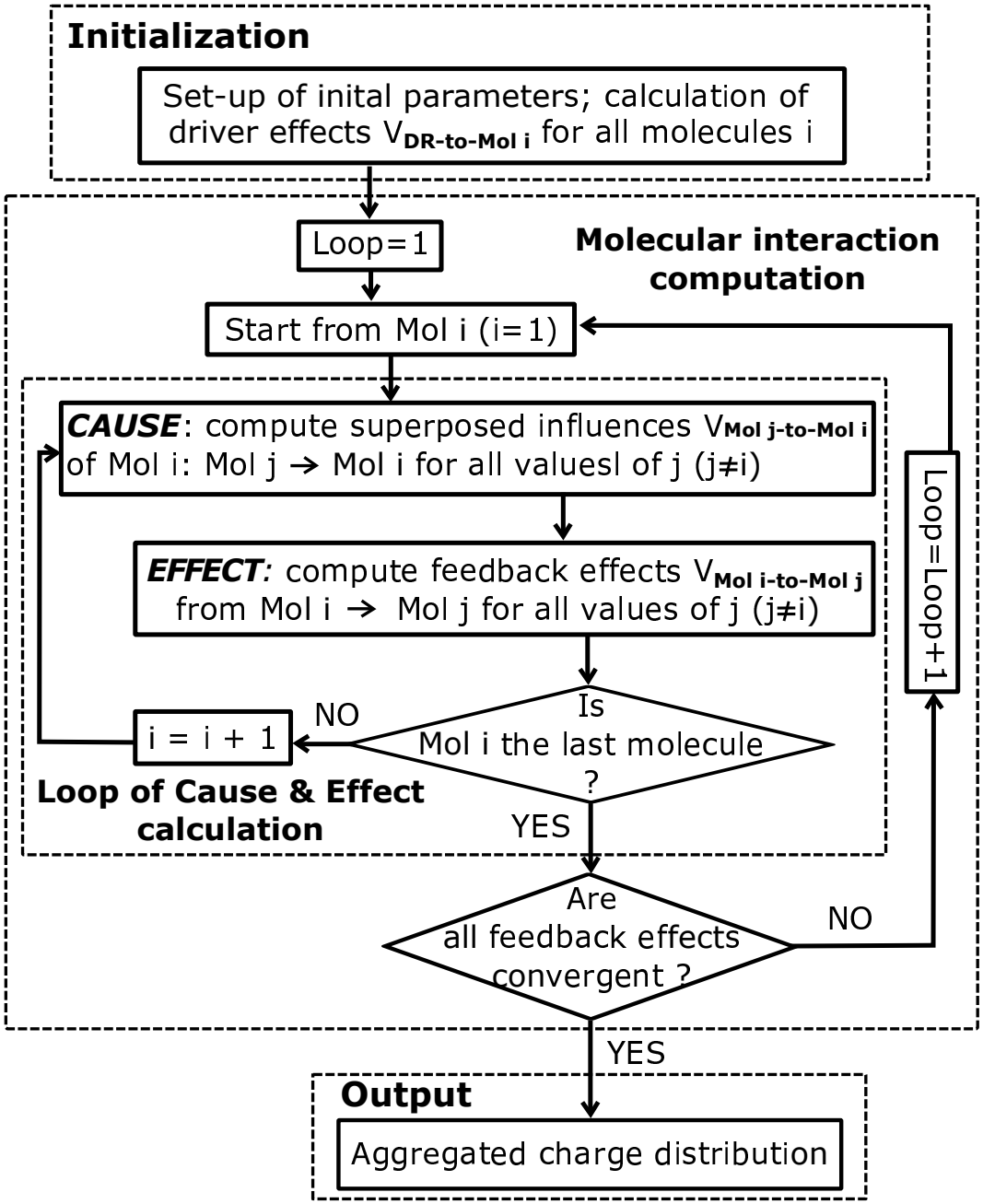

Figure 6.5 Flowchart of the proposed novel algorithm for evaluating molecular interactions along the molecular wire.

- **Ground state charge distribution**: the algorithm considers the balanced aggregated charge distribution of each molecule in equilibrium ground state as a starting point for calculation, such values are achieved via ab-initio simulations of single molecule and post-processing of data;

- ***INPUT* cell as driver**: Set-up of logic states for *INPUT* cell as driver for the MQCA wire, as depicted in Figure 6.6. The algorithm defines this *INPUT* cell with two positive unit charges (black spheres) located on one of the two diagonals;

- **Clock assignment**: here a uniform clock field (e.g., $+2V/nm$ or $-2V/nm$) is applied for each molecule on wire, thus its corresponding trans-characteristic of bis-ferrocene molecule is also integrated inside the algorithm.

Then, the initial interactions from the *INPUT* cell to all the molecules are computed and saved in terms of a series of equivalent voltages, named as $V_{IN-to-Moli}$, where *i*=1,2,...,*MolNum*. These voltages are calculated by means of integrating the electric field, which is generated by the *INPUT* cell based on its charge configuration, along the logic dot axis for each molecule *Molecule i*.

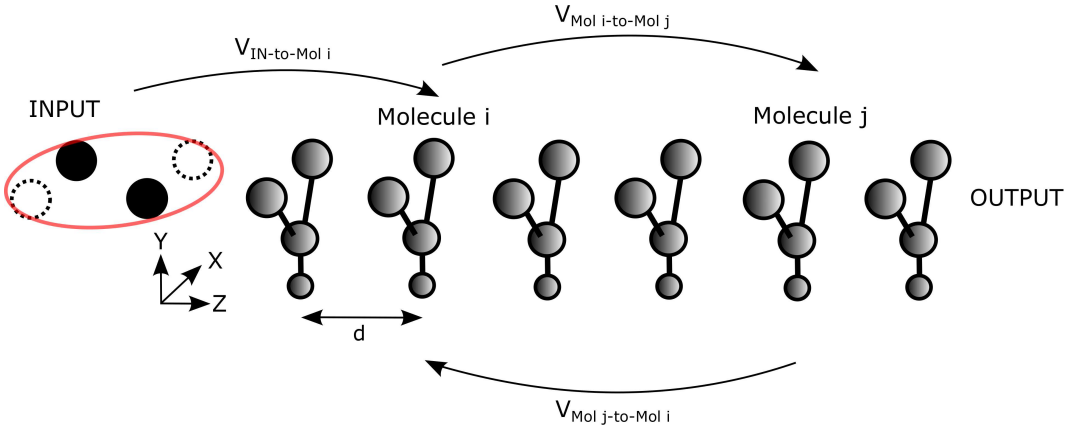

Figure 6.6 Algorithm for MQCA wire calculation.

6.2.2.2 II) Interaction Computation Stage

After the initializing part, inside the interaction computation stage, the modeling and further computation of interactions existed among molecules are discussed, as indicated in Figure 6.5(middle dashed rectangular box). Based on the previous saved influences provided by *INPUT* cell, starting from the first molecule on wire, every bis-ferrocene molecule *Molecule i* will be affected by all the other molecules *Molecule j* except itself. To be specific, the aggregated charge distributed on *Molecule j* influences *Molecule i* by means of generating an equivalent voltage

$V_{Mol\,j-to-Moli}$, as shown in Figure 6.6. These effects for all values of j ($j \neq i$) are accumulated and called the ***Cause*** influence. As a consequence of that, *Molecule i* would re-arrange itself in terms of forming a new aggregated charge distribution once the sum of *Cause* influence is obtained adopting the trans-characteristic.

Meanwhile, as a feedback the *Molecule i*, together with its re-located aggregated charges, will on its turn influence back to those exact molecules *Molecule j*, see Figure 6.6. Such feedback effects $V_{Moli-to-Mol\,j}$ are named the ***Effect*** influence, where *j*=1,2,...,*MolNum* ($j \neq i$). Then they are stored and later they will be recognized as *Cause* influence again for *Molecule j*. In this way, these molecules continue to interact with each other in terms of a combination between the *Cause* and *Effect* influences and such procedure is performed for every *Molecule i*, where i=1,2,...,*MolNum*, following a random sequence, e.g., their molecular positions located along the wire. When reaching the last molecule ($i = MolNum$) on wire, the first loop ($Loop1 = 1$) of interaction computation is finished. Nevertheless, this computation would be carried out back-and-forth in a self-consistent way for several loops, until the generated feedback effects in the current loop for all molecules reach the convergence, which implies further change of *Effect* influence among molecules is negligible thus ending the whole stage of molecular interaction calculation.

Regarding the trans-characteristic embedded in the algorithm, it depends on the clock assignment in the initializing stage. For example, if the clock with value of $+2V/nm$ is chosen, the corresponding trans-characteristic is thus called by the algorithm, see Figure 6.7 (green spheres). Only aggregated charges for logic dots ($Dot1$ and $Dot2$) are shown since positive clock pushes almost all the charge upwards to logic dots leaving null in the central dot. However, these measured points are discrete, whereas during molecular interaction calculation, the summed *Cause* influence for any molecule could be a voltage value located between two nearby measured points. Therefore we came up a solution by means of fitting these measured points from simulations with high-order (23^{th}) of polynomials. This would allow us to obtain polynomial equations which represents analytically the trans-characteristic of bis-ferrocene molecule, as depicted in Figure 6.7 (red curves). This analytic equation is hence stored inside the algorithm.

In this way, for any *Cause* influence during calculation assigned to molecule, the fitting trans-characteristic is capable of computing its aggregated charges for further calculation about generated *Effect* influence to other molecules inside the algorithm.

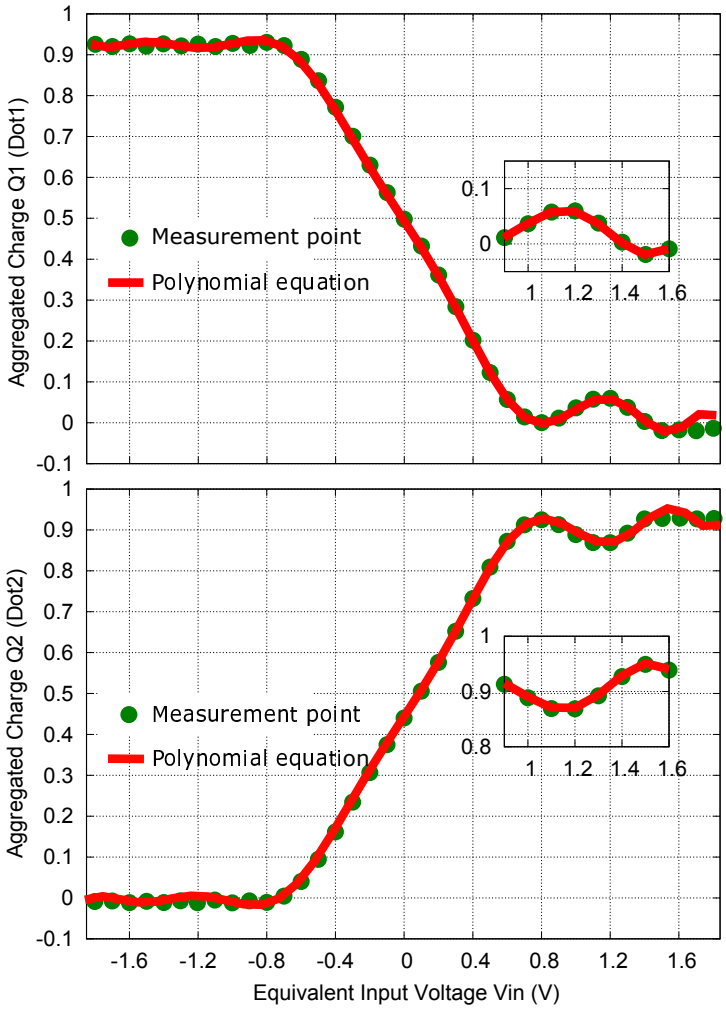

Figure 6.7 Trans-characteristic adopted inside algorithm: the real measurements points (green spheres) are fitting approximately into high-order polynomial equation (red curves), both for *Dot*1 (top) and *Dot*2 (bottom).

Furthermore, this fitting procedure should be performed multiple times with respect to the trans-characteristics obtained from different assigned clock signals.

6.2.2.3 III) Output Stage

At last, regarding the final output stage of the algorithm, as depicted in Figure 6.5(bottom dashed rectangular box), once the molecular interaction reaches the convergence, the algorithm superposes all counted and computed *Cause* & *Effect* influences in every loop including the initial interactions from the *INPUT* cell for every

molecule on wire, and eventually outputs the aggregated dot charges distributed along the MQCA wire applying again the trans-characteristic. By examining the charge distribution, it is possible to verify the ability of MQCA wire to forward binary information as well as the quality of information propagation.

A pseudo code of the proposed algorithm implementation is reported as follows. At the beginning two lines (L.1-L.2), the first initializing stage is described; then from L.3 to L.19, the stage of interaction computation is performed; in the end, the last two lines of code (L.20-L.21) state the final stage where aggregated charge distribution of molecular wire is output.

Algorithm 1 Modeling and computing molecular interaction along MQCA wire

1: Initialing MQCA device layout;
2: Compute *INPUT* effects $V_{IN-to-Moli}$ from *INPUT* cell to all molecules (*Molecule i*);
3: **procedure** EVALUATE ***Cause*** AND ***Effect*** INFLUENCES
4: *Loop=1*;
5: *NotConvergent = Ture*;
6: **while** *(NotConvergent)*
7: **for** *Mol i = 1:MolNum*
8: Compute $\sum_{j=1}^{j=MolNum;j\neq i} V_{Mol\,j-to-Moli}$ (***Cause***);
9: **for** *Mol j = 1:MolNum*
10: Compute ***Effect*** effects: $V_{Moli-to-Mol\,j}(j \neq i)$;
11: **end**;
12: **end**;
13: Store computed ***Effect*** influences of each molecule in current loop of calculation;
14: **if** *ConvergenceIsReached = Ture*
15: *NotConvergent = False*;
16: **else**
17: *Loop=Loop+1*;
18: **end**;
19: **end**;
20: Superposing all counted and computed interactions in terms of ***Cause & Effect*** effects for every molecule;
21: Output eventual aggregated charge distribution for all molecules distributed on wire;

In order to better understanding the working principle of the proposed algorithm, a wire consists of four bis-ferrocene molecules is being analyzed using the

algorithm as an example. Figure 6.8(A) highlights the physical layout of the wire structure with an *INPUT* cell as driver. The logic state encoded by the *INPUT* cell will be the binary information that propagates through the whole wire. The inter-molecule distance is denoted as d. Whereas in Fig 6.8(B), the detailed evaluation scheme of modeled molecular interactions in terms of *Cause* & *Effect* influences is illustrated.

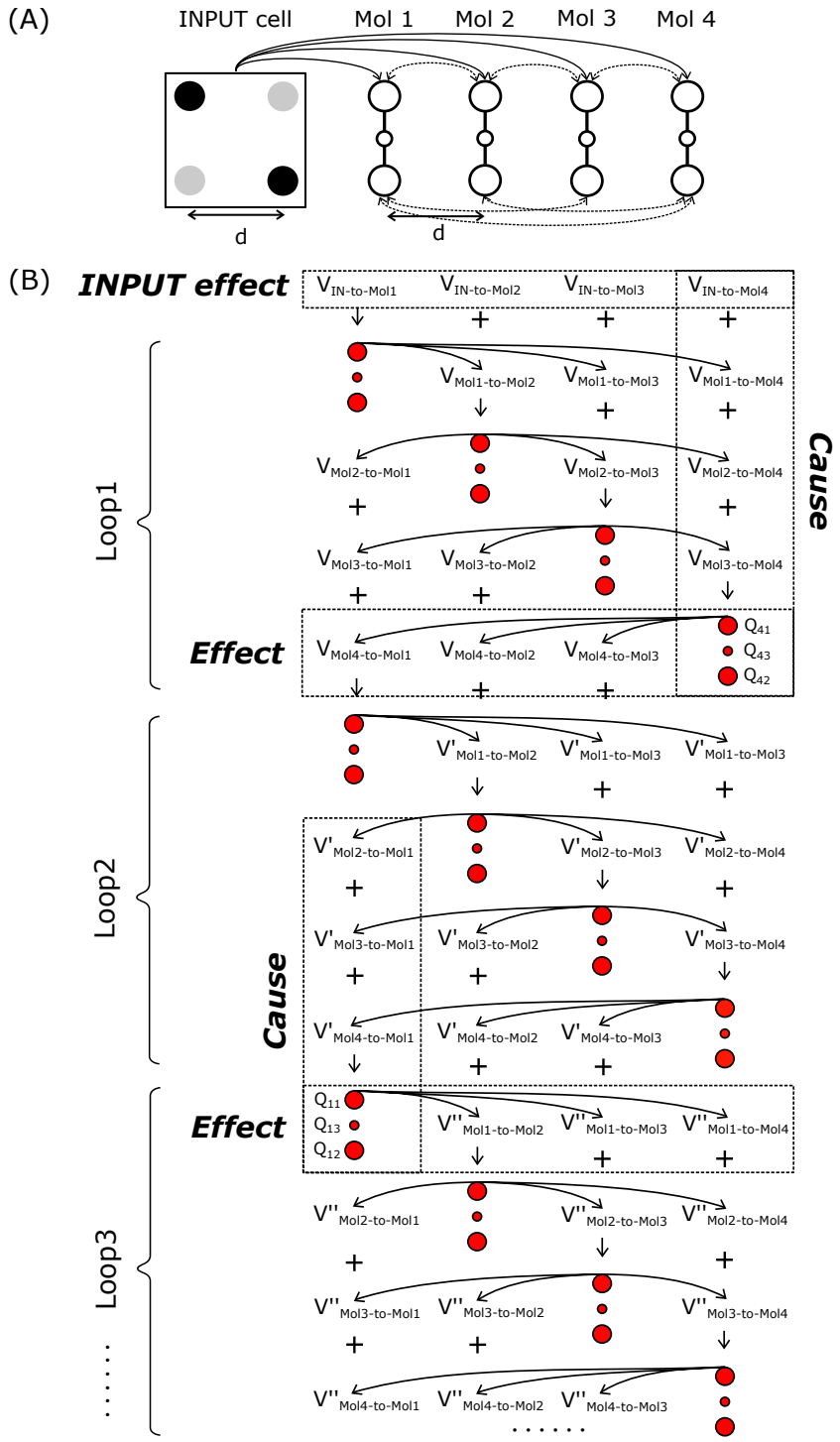

Figure 6.8 A MQCA wire example: (A)Physical layout of the MQCA wire with *INPUT* cell; (B)Detailed modeling and calculation of molecular interactions.

To begin with, the *INPUT* effects are computed after the *Initialization Stage*. Whereas in the first loop of molecular interaction calculation, starting from *Mol1*, its *INPUT* effect $V_{IN-to-Mol1}$ is recognized as the *Cause* influence. Then *Mol1* allocates its aggregated charges and generates its *Effect* influences as feedback to other molecules ($V_{Mol1-to-Moli}$, where i=2,3,4). Next, the *Mol2* takes the superposition between its *INPUT* effect $V_{IN-to-Mol2}$ and the *Effect* influence from *Mol1* $V_{Mol1-to-Mol2}$ as its current *Cause* influence and generates its own *Effect* influences $V_{Mol2-to-Moli}$, where i=1,3,4.

By the same logic, the *Mol3* summarizes its *INPUT* effect $V_{IN-to-Mol3}$ together with *Effect* influences $V_{Mol1-to-Mol3}$ and $V_{Mol2-to-Mol3}$ as *Cause* influence. As a consequence, *Mol3* then provides the generated *Effect* influences $V_{Mol3-to-Moli}$, where i=1,2,4, to the molecules left on wire. Similar procedure is also applied for *Mol4* thence ending the first loop (Loop 1) of molecular interaction calculation.

If calculated interactions in the first loop for each molecule do not reach the convergence, a second loop (Loop 2) is thereby needed. Based on the results in terms of aggregated charge distribution of each molecule in previous loop, the *Cause* & *Effect* procedure of computation in the new loop is performed following the same description in the second stage of the algorithm. Moreover, in Figure 6.8(B), the *INPUT* effects and some calculations of *Cause* & *Effect* influences are highlighted in dashed boxes, e.g., *Mol4* in *Loop 1* and *Mol1* in *Loop 3*, for a more comprehensive explanation of the molecular interaction evaluation given the algorithm. The algorithm will continuously check whether the convergence is reached at the end of each loop for all molecules; if so, the evaluation procedure will be terminated and final aggregated charge distribution along wire is provided.

6.2.3 Multi-phase Clock Assignment

As discussed in Section 1.4, in order to guarantee correct QCA information propagated along the circuits, adiabatic switching is used which technologically implying the partition of molecular QCA circuits into individual clock zones. Whereas for each clock zone, a multi-phase clock signal is assigned, thus the QCA behavior could be controlled to produce a flow of information.

To be specific, Fig 6.9(A) depict schematic implementation of the physical clock system for a binary molecular wire. There are three pairs of electrodes equally

aligned together along z-axis representing the three clock zones. Then the time-varying voltages are externally applied between each pair of electrodes, where a number of bis-ferrocene molecules are located inside, hence the electric field generated between these pairs of electrodes is recognized as the multi-phase clock. It is assumed that inside each clock zone, the clock signal is uniform for every molecule at the same time instant.

Similar as Figure 1.5 in Section 1.4, Figure 6.9(B) highlights the periodic four-phase clock signals generated by the voltages on the electrodes for all the three clock zones. Each clock signal has a phase shift of $\pi/2$ or 1/4 of the signal period T. The shape of the four-phase signal should not have a typical square-wave clocking signal avoiding abrupt change of values. Instead it is a trapezoidal function which linearly increases and decreases to slowly and smoothly control the change of logic states encoded by these molecules. Again, here we ignore the speed of of MQCA cell switching response assuming that the cell changes slowly enough with respect to the charge tunneling time between logic dots and central dots on bis-ferrocene molecule. Hence according to quasi-adiabatic switching, the MQCA cells will always stay close to its ground state consuming little energy [37].

With this physical system considered, the clock assigned is no more static and uniform throughout the whole wire. Instead, the clock field should cause individual molecules in each zone to periodically raise and lower their tunneling barriers thus transitioning among four phases thus forwarding digital information. As a consequence of that, the multi-phase clock is considered inside the proposed algorithm for molecular interaction calculation along wire, see the pseudo code listed below.

From a methodological point of view, inside the algorithm, the linearly increasing and decreasing tendency of the trapezoidal clock signal is approximated using staircase function, as sketched in Figure 6.9(C). The duration of each segment of the staircase signal is assumed to be long enough satisfying the adiabatic switching with little energy loss. Therefore, different from Section 6.2.2, here at the end of initializing stage of the algorithm, a clock matrix with dimension $MolNum \times ClockNum$ is assigned to the algorithm, see L.3, where the *ClockNum* represent the total number of segments for clock signal with respect to the change of time. Hence, this matrix records the multi-phase periodic clock signal for every molecule located inside the clock zones of the wire.

Algorithm 2 Modelling and computing cloked molecular interaction along MQCA wire

Initializing molecular QCA device layout;
Compute *INPUT* effects $V_{IN-to-Moli}$ from *INPUT* cell to all molecules *Molecule i*;
Creating matrix $CK_{MolNum \times CycleNum}$ for arranging clock assignment;
procedure EVALUATE ***Cause*** AND ***Effect*** INFLUENCES FOLLOWING THE ASSIGNED CLOCK MATRIX
  for *ClockCycle = 1:CycleNum*
   Loop=1;
   NotConvergent = Ture;
   while *(NotConvergent)*
    for *Mol i = 1:MolNum*
      Compute $\sum_{j=1}^{j=MolNum; j \neq i} V_{Mol\,j-to-Moli}$ (***Cause***);
      for *Mol j = 1:MolNum*
        Compute ***Effect*** effects: $V_{Moli-to-Mol\,j}(j \neq i)$;
      end;
    end;
    Store computed ***Effect*** influences of each molecule in current loop of calculation during assigned clock cycle;
    if *ConvergenceIsReached = Ture*
      NotConvergent = False;
    else
      Loop=Loop+1;
    end;
   end;
  end;
Superposing all counted and computed ***Cause & Effect*** effects for every molecule during each assigned clock cycle;
Output eventual aggregated charge distribution for all molecules along wire inside the whole period of the clock matrix;

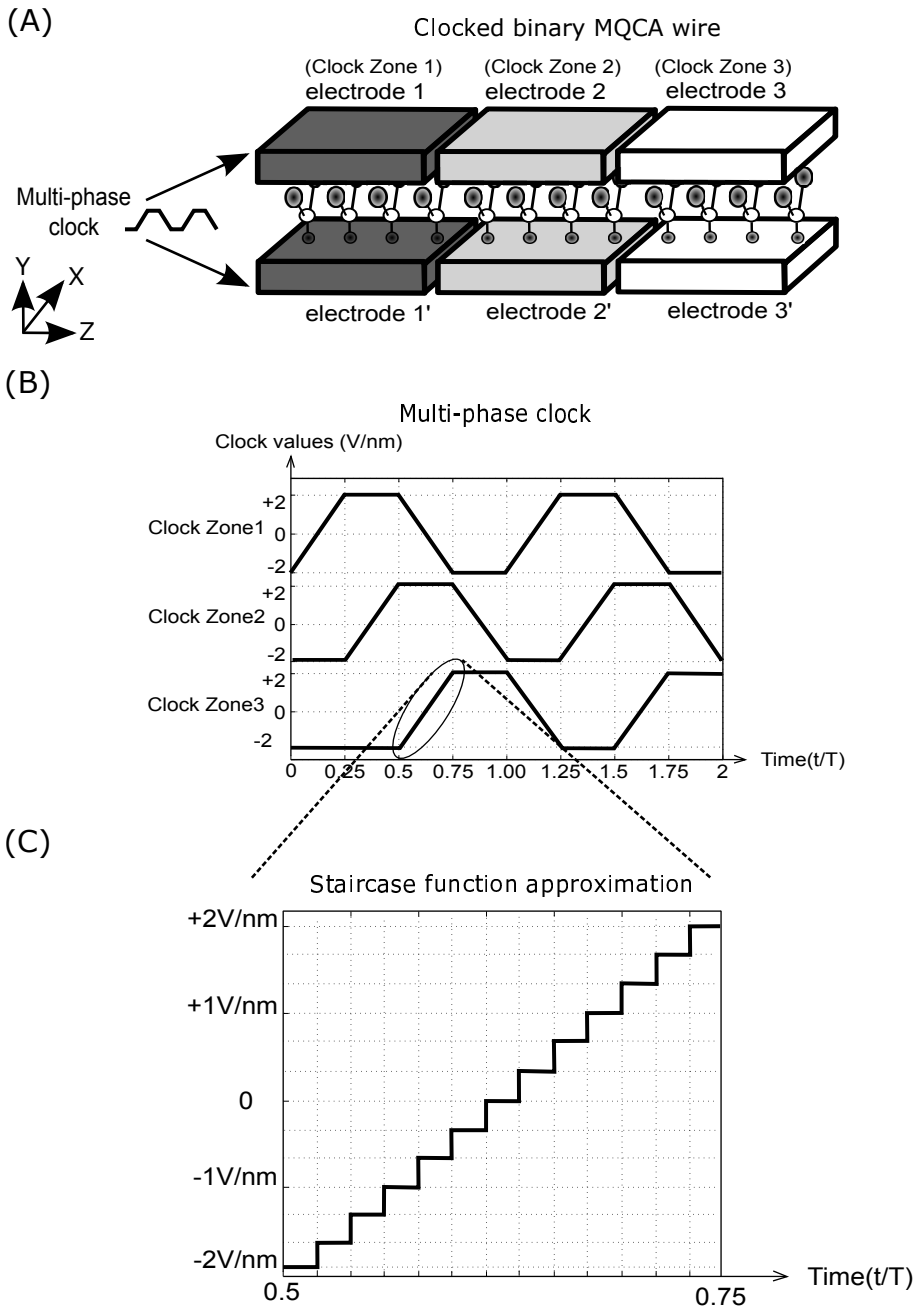

Figure 6.9 Clock zones and clock signals assignment: (A)Schematic implementation of the physical clock system for binary MQCA wire, external potentials are applied between the pairs of electrodes; (B)Periodic clock signals are applied for each clock zone; (C)Staircase function is considered during the algorithm for approximating the linearly increasing or decreasing clock signal.

Then inside the stage of interaction computation, an extra cycle is added considering the multi-phase clock, see L.5. Namely, concerning values of clock signal dis-

tributed along the wire for first time instant ($ClockCycle = 1$), once the calculation of molecular interaction for all molecules reaches convergence, instead of jumping the last stage and outputting final data as before, the algorithm will repeat this stage of interaction computation following the clock values of the next time instant ($ClockCycle = 2$) assigned in the clock matrix. This time the calculation is similar but the starting point of each molecule is no more at equilibrium but the state with aggregated charges obtained from the precedent clock. Since the molecules will re-distribute their aggregated charges with respect to the new clock signals applied, thus previous convergent situation is broken. Consequently, the newly generated *Effect* influences from one molecule to the others would be re-calculated and a new convergent status along the wire is expected. Finally, iterating the calculation of molecular interaction following the sequence of clock values recorded in the matrix, the clocked MQCA wire performance is thereby described.

It is worthy underlying that, with different clock values, the molecules interact with each other following different trans-characteristics. Following the procedure discussed in Section 4.3, we pictured the trans-characteristics corresponded to clock values from $-2V/nm$ to $+2V/nm$ with a step of $0.25V/nm$. However, more values for clock segment, more accurate the calculation of interaction it is. Therefore, if clock values assigned inside the matrix during computation is not existed, the previous stored trans-characteristic curves are useless and the algorithm adopts another method called *Bi-linear Interpolation* to define the new trans-characteristic curve automatically.

In general, during the molecular interaction calculation, if a molecule is given a *Cause* influence in terms of a voltage V_{IN} and currently it localizes inside a clock zone with value of CLK and its aggregated dot charges are needed to be calculated, e.g., $Q2$ ($Dot2$), as shown in Figure 6.10 with the black sphere in the middle. Since the corresponded trans-characteristic does not exist, the algorithm would immediately search for four points around the desired dot charge. More specific, the *Bi-linear Interpolation* method will do the linear research to find two trans-characteristic curves with clock values close to CLK in terms of $CLK_j < CLK < CLK_{j+1}$; then the method does the linear research again to look for two existing input voltages around V_{IN} on the trans-characteristic curves in terms of $V_{IN_i} < V_{IN} < V_{IN_i+1}$. In this way, the four points are found with values of $Q_{i,j}$, $Q_{i,j+1}$, $Q_{i+1,j}$ and $Q_{i+1,j+1}$, whereas the desired aggregated dot charge is approxi-

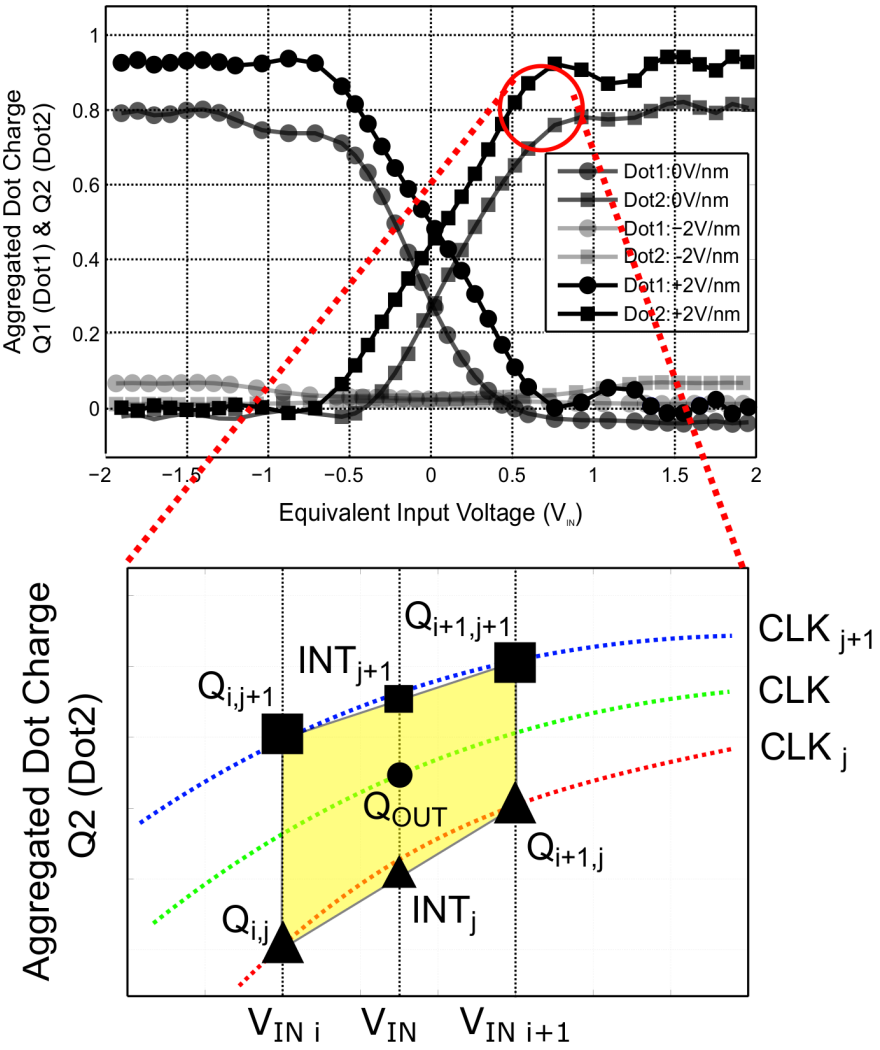

Figure 6.10 Bi-linear interpolation representation for non-existing trans-characteristic curve.

mated to be geographical middle point of the polygon interpolated from these four values, see Figure 6.10. The equations used for bi-linear interpolation are:

$$INT_j + 1 = \frac{V_{IN_i+1} - V_{IN}}{V_{IN_i+1} - V_{IN_i}} \cdot Q_{i+1,j+1} + \frac{V_{IN} - V_{IN_i}}{V_{IN_i+1} - V_{IN_i}} \cdot Q_{i,j+1} \tag{6.1}$$

$$INT_j = \frac{V_{IN_i+1} - V_{IN}}{V_{IN_i+1} - V_{IN_i}} \cdot Q_{i+1,j} + \frac{V_{IN} - V_{IN_i}}{V_{IN_i+1} - V_{IN_i}} \cdot Q_{i,j} \tag{6.2}$$

$$OUTPUT = \frac{CLK_{j+1} - CLK}{CLK_{j+1} - CLK_j} \cdot INT_j + 1 + \frac{CLK - CLK_j}{CLK_{j+1} - CLK_j} \cdot INT_j \qquad (6.3)$$

By the same logic, the aggregated charges, for both logic dots and central dot (including the carbazole and the binding thiol), of molecule with any values of clock and input influence can be derived through the bi-linear interpolation from existing trans-characteristic curves. Figure 6.11, Figure 6.12, Figure 6.13 and Figure 6.14 show that the bi-linear interpolation method has been performed for each dot on molecule, the range of clock is $[-2V, +2V]$ and the input influence V_{IN} of molecule belongs to $[-1.8V, +1.8V]$. The interpolation step used for clock is $0.05V/nm$ and it is more accurate than results from ab-initio simulations which is $0.25V/nm$. Figure 6.11 and Figure 6.12 represent the two logic dots and it can be seen that their behavior is complementary.

In this way, we have obtained a two-dimensional trans-characteristic plane, namely during the molecular interaction computation, once the clock value and the *Cause* influence in terms of equivalent input voltage are known for any molecule, the resulting aggregated dot charges of this molecule is thereby derived. This *Bi-linear Interpolation* method is also more accurate and less computationally intensive than polynomial fitting in the case of trans-characteristic for known clock value, where the only variable is V_{IN}. Meanwhile, outside the polynomial fitting range, the fitted behavior of trans-characteristic is unpredictable, so hereinafter the algorithm embeds the bi-linear interpolation method for evaluating molecular interaction.

In the end, the proposed algorithm has taken into account the multi-phase clock signals applied to multiple clock zones on MQCA wire, therefore the obtained results allow us to foresee the guided information propagation. The Validation of the algorithm and some applications are discussed in the following.

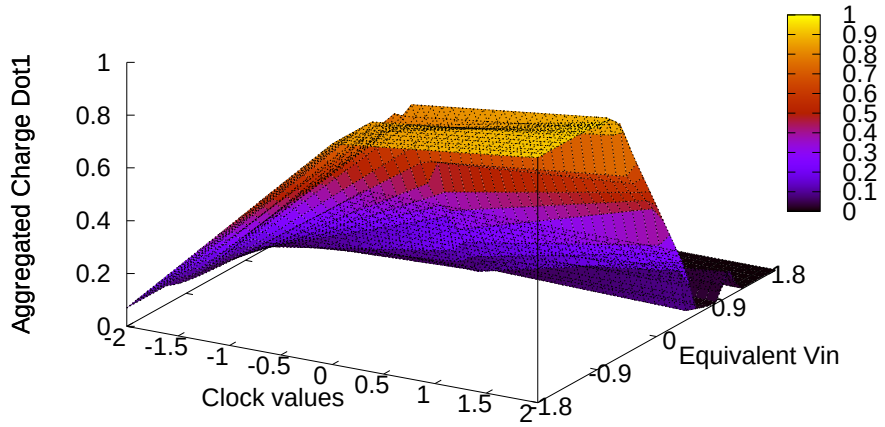

Figure 6.11 Bi-linear interpolation representation for *Dot*1.

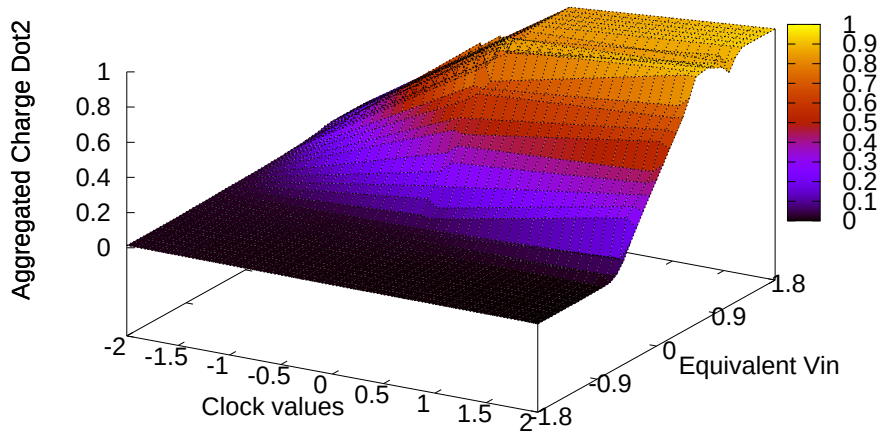

Figure 6.12 Bi-linear interpolation representation for *Dot*2.

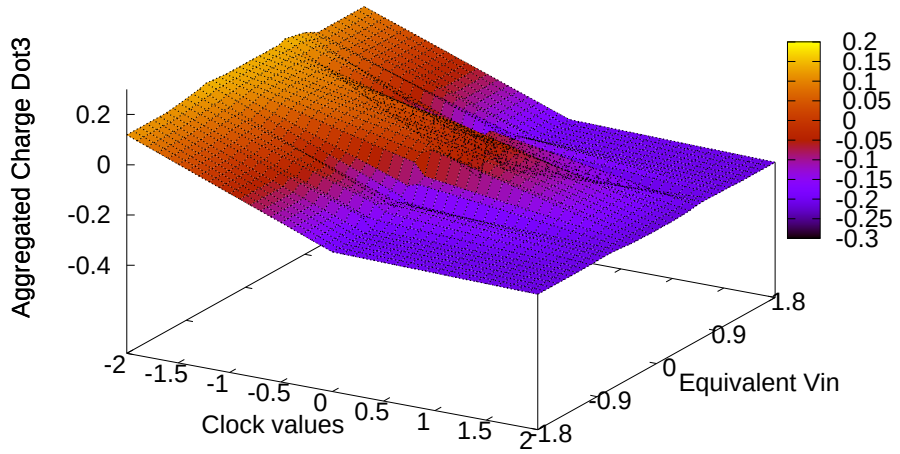

Figure 6.13 Bi-linear interpolation representation for carbazole.

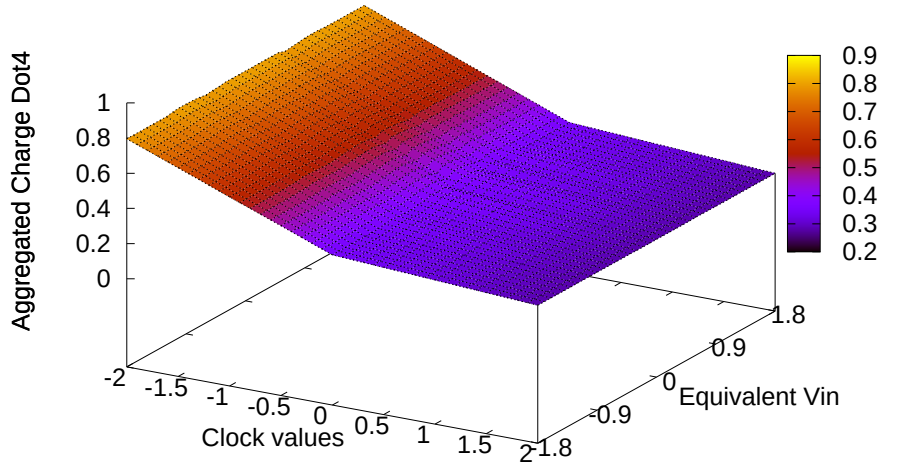

Figure 6.14 Bi-linear interpolation representation for binding thiol.

6.3 Validation Of Algorithm

To begin with, the algorithm has been validated by means of comparing results provided by the algorithm to those ones obtained from ab-initio simulations and post-processing of data. The case under focus is the molecular cell which consists of two bis-ferrocene molecules.

6.3.1 Cell-to-Cell Response

Concerning the MQCA cell, the cell-to-cell response is analyzed through algorithm. In specific, during the initializing stage, the layout is set to two molecules ($Mol1$ and $Mol2$) with a distance d located in between. Regarding biasing conditions, an *INPUT* cell has been place near the MQCA cell as driver and enhancing clock field $+2V/nm$ is also assigned. Therefore, the algorithm outputs the eventual aggregated dot charges of both molecules. Meanwhile, ab-initio simulations and post-processing of data are also performed for the same structure. However, during simulations the enhancing clock is implemented in terms of polarized point charges, see Section 4.4.1. The comparison is illustrated in Table 6.6.

Inside the complete MQCA cell, according to electrostatic repulsion, the two molecules will distribute their aggregated dot charges thus encoding the same binary information carried by the *INPUT* cell. As reported in the Table 6.6(i)(ii), with distance of $1.0nm$, the logic state of the cell is characterized by the six aggregated dot charges which is desirable for QCA operation, although the aggregated charge difference between two logic dots of the *Mol 2* may not be sufficient enough for further read-out of such logic state. However, if a shorter inter-molecule distance $d = 0.8nm$ is assigned, the stronger Coulomb interaction between two molecules leads to a better results in terms of more explicit charge separation between two logic dots. This is true for both logic states of *INPUT* cell (Table 6.6(iii)(iv)). More importantly, the results from the algorithm and ab-initio simulations coincide for both logic states and distances between molecules validating the functional performance of the algorithm. Figure 6.15 also proves this conclusion from a graphical point of view, the aggregated charge for logic dots are represented by the spheres with different patterns and the radius of the sphere is proportional to the exact charge value.

(i) Results based on $d = 1.0nm$, Logic "0" of *INPUT*						
Aggregated Dot Charge	*INPUT* cell Configuration		Algorithm		Ab-initio	
			Mol 1	Mol 2	Mol 1	Mol 2
Q1	+1.000	0.000	+0.781	+0.361	+0.782	+0.403
Q2	0.000	+1.000	+0.152	+0.577	+0.186	+0.587
Q3	-	-	+0.067	+0.062	+0.032	+0.010
(ii) Results based on $d = 1.0nm$, Logic "1" of *INPUT*						
Aggregated Dot Charge	*INPUT* cell Configuration		Algorithm		Ab-initio	
			Mol 1	Mol 2	Mol 1	Mol 2
Q1	0.000	+1.000	+0.185	+0.611	+0.222	+0.593
Q2	+1.000	0.000	+0.749	+0.326	+0.747	+0.378
Q3	-	-	+0.066	+0.063	+0.031	+0.029
(iii) Results based on $d = 0.8nm$, Logic "0" of *INPUT*						
Aggregated Dot Charge	*INPUT* cell Configuration		Algorithm		Ab-initio	
			Mol 1	Mol 2	Mol 1	Mol 2
Q1	+1.000	0.000	+0.916	+0.082	+0.904	+0.127
Q2	0.000	+1.000	+0.014	+0.849	+0.043	+0.827
Q3	-	-	+0.070	+0.069	+0.053	+0.046
(iv) Results based on $d = 0.8nm$, Logic "1" of *INPUT*						
Aggregated Dot Charge	*INPUT* cell Configuration		Algorithm		Ab-initio	
			Mol 1	Mol 2	Mol 1	Mol 2
Q1	0.000	+1.000	+0.093	+0.875	+0.019	+0.843
Q2	+1.000	0.000	+0.832	+0.045	+0.949	+0.132
Q3	-	-	+0.075	+0.080	+0.032	+0.025

Table 6.6 Cell-to-cell response: comparison between aggregate charges from algorithm and ab-initio simulations.

6.3.2 Algorithm Performance

As a glimpse of the algorithm performance, the proposed algorithm is implemented in *MATLAB* with *Windows* environment. The complete version in terms of functional codes for layout design and performance computation are recoded in Appendix D. Based on Intel(R)Core(TM) i5 CPU@2.27GHz and 4.00GB of RAM, the usage of time of the algorithm for the above validation procedure is approximately in the range of seconds. This is acceptable for us at this point for clocked MQCA wire analysis compared to intensive ab-initio simulations.

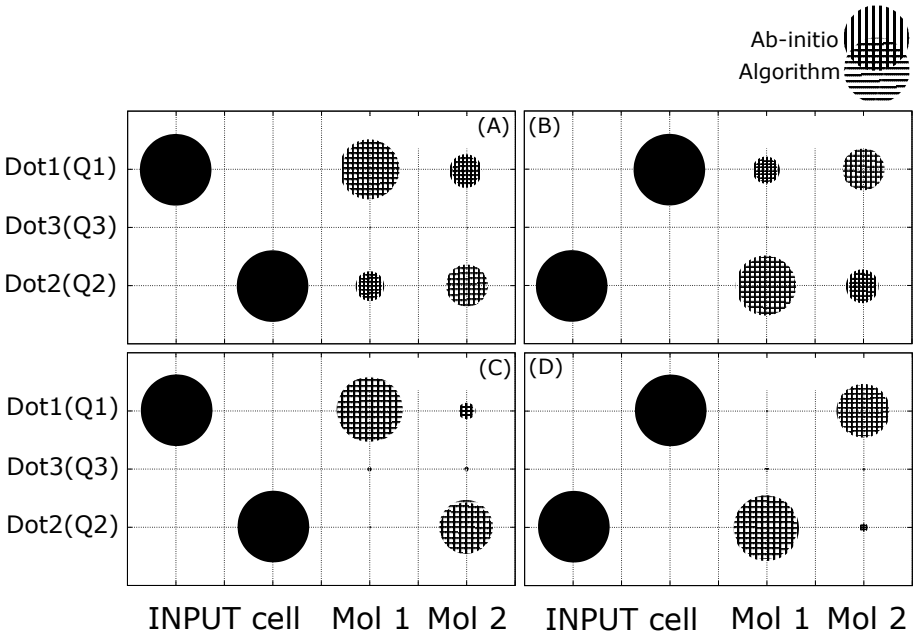

Figure 6.15 Comparison of results for complete MQCA cell: (A)Logic 0 of *INPUT* cell and with distance of 1.0*nm*; (B)Logic 1 of *INPUT* cell and with distance of 1.0*nm*; (C)Logic 0 of *INPUT* cell and with distance of 0.8*nm*; (D)Logic 1 of *INPUT* cell and with distance of 0.8*nm*.

6.4 Wire Results

Following the aim of this chapter at the beginning, a MQCA wire consists of eight bis-ferrocene molecules is analyzed adopting the implemented algorithm. Similarly, the layout of the wire is defined at the beginning stage of the algorithm. These eight molecules are aligned together with identical distance *d* in between. Figure 6.16 sketches the MQCA wire layout generated inside algorithm together with *INPUT* cell.

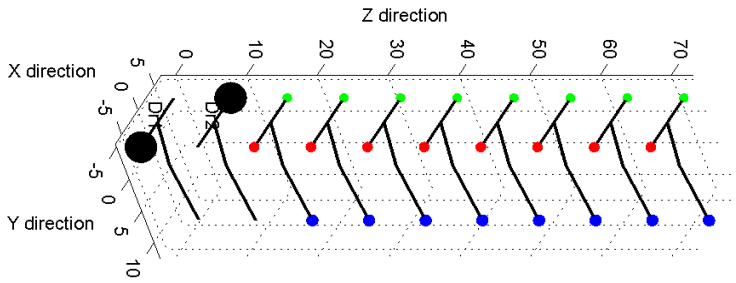

Figure 6.16 MQCA wire layout generated inside the algorithm.

6.4.1 Equilibrium Ground State

At the beginning without *INPUT* cell assigned near the wire, the molecules on wire are with balanced aggregated dot charges. These charges are set in the initializing stage of the algorithm and they are the same for all molecules. However, the set of initial balanced charge for molecule depends on the clock value considered for operation. Figure 6.17 depicts initial balanced dot charges on wire taking into account the presence of both enhancing clock ($+2V/nm$) and prohibiting clock ($-2V/nm$). By the same logic, the spheres represent the obtained aggregated dot charges, whereas their radius is proportional to the exact charge value. In order to highlight the charge distribution, the aggregated charges for logic dots are colored in red ($Dot1$) and green ($Dot2$) while those for central dots ($Dot3$) are painted in blue.

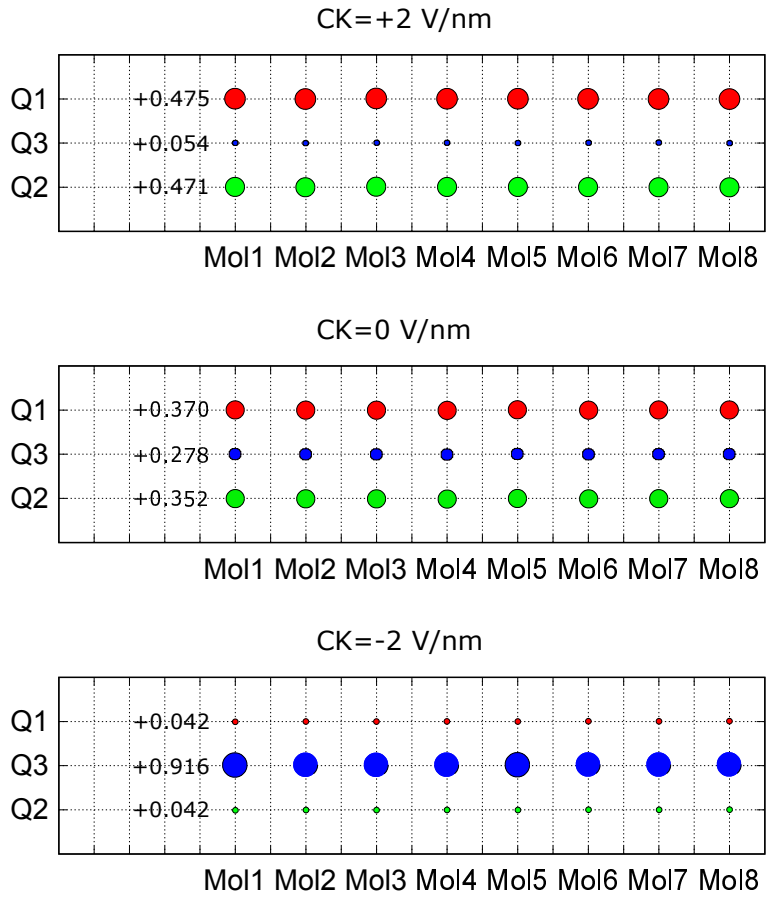

Figure 6.17 Balanced equilibrium charge distribution on MQCA wire for cases of enhancing clock ($+2V/nm$), zero clock and prohibiting clock ($-2V/nm$) inside the algorithm.

6.4.2 Logic Information Propagation

After that, the *INPUT* cell which carries digital information (for both logic states) is assigned for MQCA wire thus allowing us to explore the ability of MQCA wire to forward information. Particularly, here two inter-molecule distances are considered with values of $d = 1.0nm$ and $d = 0.8nm$. It is necessary to mention that the shrinkage of molecule distance is hypothetical with the aim of foreseeing how molecular wire behaves with shorter distance in between, whereas the experimental procedure of manipulating molecule deposition is out of the purpose for this work.

Achieved quantitative results in terms of aggregated charges for molecules along wire are recorded in tables from Table 6.7 to Table 6.12 for cases like enhancing clock ($+2V/nm$), zero clock and prohibiting clock ($-2V/nm$) applied to wires with these two distances, respectively. In the meantime, these values are also sketched correspondingly in figures from Figure 6.18 to Figure 6.23 for more directive observation of MQCA wire performance (top view).

6.4.2.1 *1.0nm* Wire with Enhancing Clock ($+2V/nm$)

Logic "0" Propagated along 1.0*nm* Wire				
Agg. Charge	Mol 1	Mol 2	Mol 3	Mol 4
Q1	0.845	0.268	0.622	0.433
Q2	0.086	0.668	0.315	0.505
Q3	0.069	0.064	0.063	0.062
Agg. Charge	Mol 5	Mol 6	Mol 7	Mol 8
Q1	0.530	0.482	0.505	0.495
Q2	0.408	0.456	0.433	0.443
Q3	0.062	0.063	0.062	0.062
Logic "1" Propagated along 1.0*nm* Wire				
Agg. Charge	Mol 1	Mol 2	Mol 3	Mol 4
Q1	0.103	0.742	0.361	0.569
Q2	0.828	0.192	0.577	0.369
Q3	0.069	0.066	0.062	0.062
Agg. Charge	Mol 5	Mol 6	Mol 7	Mol 8
Q1	0.463	0.515	0.490	0.501
Q2	0.475	0.423	0.448	0.437
Q3	0.061	0.062	0.062	0.062

Table 6.7 Aggregated dot charges on wire (1.0*nm*) with $+2V/nm$ of clock.

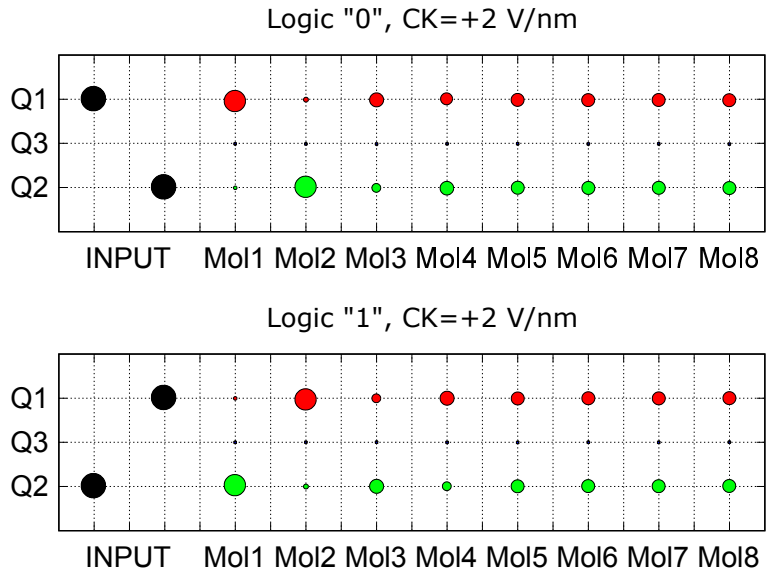

Figure 6.18 Aggregated dot charges on wire (1.0*nm*) with $+2V/nm$ of clock.

6.4.2.2 *1.0 nm* Wire with Zero Clock ($0V/nm$)

Logic "0" Propagated along 1.0*nm* Wire				
Agg. Charge	Mol 1	Mol 2	Mol 3	Mol 4
Q1	0.757	0.063	0.644	0.111
Q2	0.005	0.630	0.053	0.540
Q3	0.238	0.307	0.303	0.349
Agg. Charge	Mol 5	Mol 6	Mol 7	Mol 8
Q1	0.554	0.182	0.468	0.265
Q2	0.112	0.458	0.178	0.357
Q3	0.332	0.360	0.354	0.378
Logic "1" Propagated along 1.0*nm* Wire				
Agg. Charge	Mol 1	Mol 2	Mol 3	Mol 4
Q1	0.034	0.692	0.086	0.597
Q2	0.710	0.026	0.582	0.082
Q3	0.256	0.282	0.332	0.321
Agg. Charge	Mol 5	Mol 6	Mol 7	Mol 8
Q1	0.143	0.507	0.208	0.394
Q2	0.494	0.147	0.416	0.239
Q3	0.363	0.346	0.376	0.367

Table 6.8 Aggregated dot charges on wire (1.0*nm*) with zero clock.

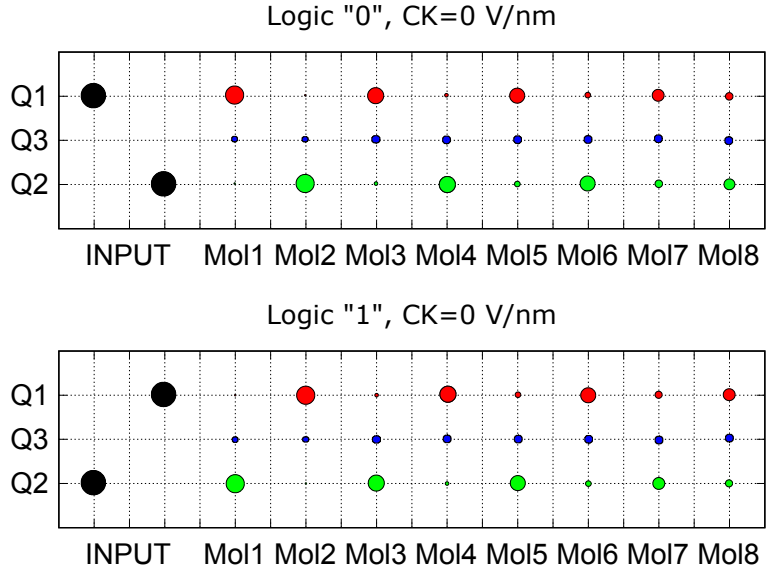

Figure 6.19 Aggregated dot charges on wire (1.0*nm*) with zero clock.

6.4.2.3 *1.0 nm* Wire with Inhibiting Clock ($-2V/nm$)

Logic "0" Propagated along 1.0*nm* Wire				
Agg. Charge	Mol 1	Mol 2	Mol 3	Mol 4
Q1	0.032	0.028	0.027	0.027
Q2	0.023	0.025	0.025	0.025
Q3	0.945	0.947	0.948	0.948
Agg. Charge	Mol 5	Mol 6	Mol 7	Mol 8
Q1	0.027	0.027	0.027	0.027
Q2	0.025	0.025	0.025	0.025
Q3	0.948	0.948	0.948	0.948
Logic "1" Propagated along 1.0*nm* Wire				
Agg. Charge	Mol 1	Mol 2	Mol 3	Mol 4
Q1	0.024	0.026	0.027	0.027
Q2	0.031	0.026	0.025	0.025
Q3	0.946	0.948	0.948	0.948
Agg. Charge	Mol 5	Mol 6	Mol 7	Mol 8
Q1	0.027	0.027	0.027	0.027
Q2	0.025	0.025	0.025	0.025
Q3	0.948	0.948	0.948	0.948

Table 6.9 Aggregated dot charges on wire (1.0*nm*) with $-2V/nm$ of clock.

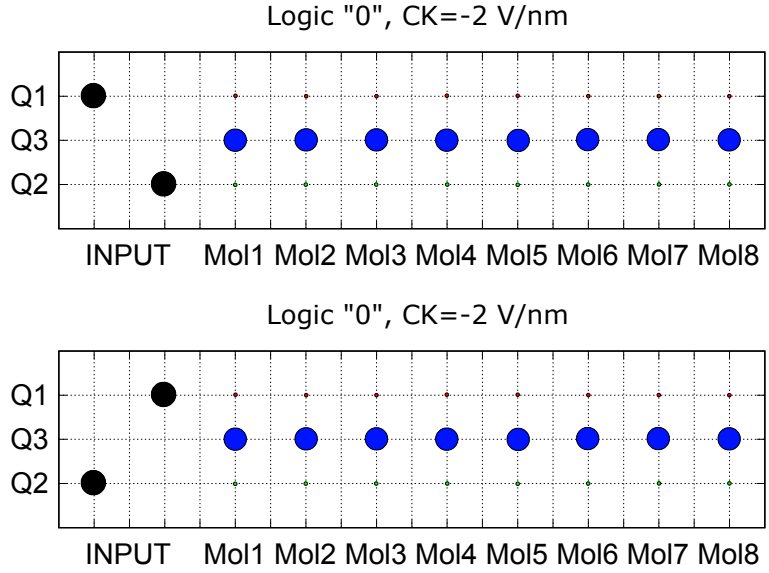

Figure 6.20 Aggregated dot charges on wire (1.0*nm*) with $-2V/nm$ of clock.

6.4.2.4 *0.8 nm* Wire with Enhancing Clock ($+2V/nm$)

Logic "0" Propagated along 0.8*nm* Wire				
Agg. Charge	Mol 1	Mol 2	Mol 3	Mol 4
Q1	0.921	0.029	0.921	0.029
Q2	0.008	0.896	0.007	0.896
Q3	0.071	0.075	0.072	0.075
Agg. Charge	Mol 5	Mol 6	Mol 7	Mol 8
Q1	0.920	0.033	0.922	0.129
Q2	0.009	0.892	0.006	0.803
Q3	0.071	0.075	0.072	0.068
Logic "1" Propagated along 0.8*nm* Wire				
Agg. Charge	Mol 1	Mol 2	Mol 3	Mol 4
Q1	0.044	0.923	0.030	0.921
Q2	0.882	0.005	0.895	0.008
Q3	0.074	0.072	0.075	0.071
Agg. Charge	Mol 5	Mol 6	Mol 7	Mol 8
Q1	0.033	0.920	0.039	0.871
Q2	0.892	0.009	0.887	0.059
Q3	0.075	0.071	0.074	0.070

Table 6.10 Aggregated dot charges on wire (0.8*nm*) with $+2V/nm$ of clock.

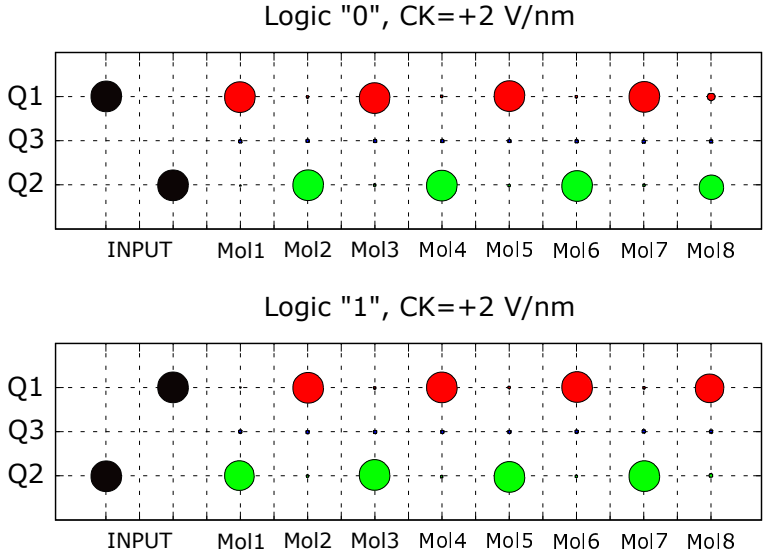

Figure 6.21 Aggregated dot charges on wire (0.8*nm*) with $+2V/nm$ of clock.

6.4.2.5 *0.8 nm* Wire with Zero Clock ($0V/nm$)

Logic "0" Propagated along 0.8*nm* Wire				
Agg. Charge	Mol 1	Mol 2	Mol 3	Mol 4
Q1	0.789	0.015	0.784	0.015
Q2	0.014	0.798	0.020	0.797
Q3	0.197	0.187	0.196	0.188
Agg. Charge	Mol 5	Mol 6	Mol 7	Mol 8
Q1	0.784	0.015	0.781	0.073
Q2	0.020	0.799	0.023	0.607
Q3	0.196	0.186	0.196	0.320
Logic "1" Propagated along 0.8*nm* Wire				
Agg. Charge	Mol 1	Mol 2	Mol 3	Mol 4
Q1	0.013	0.783	0.015	0.783
Q2	0.807	0.021	0.798	0.020
Q3	0.180	0.196	0.187	0.197
Agg. Charge	Mol 5	Mol 6	Mol 7	Mol 8
Q1	0.015	0.783	0.013	0.734
Q2	0.798	0.021	0.805	0.010
Q3	0.187	0.196	0.182	0.256

Table 6.11 Aggregated dot charges on wire (0.8*nm*) with zero clock.

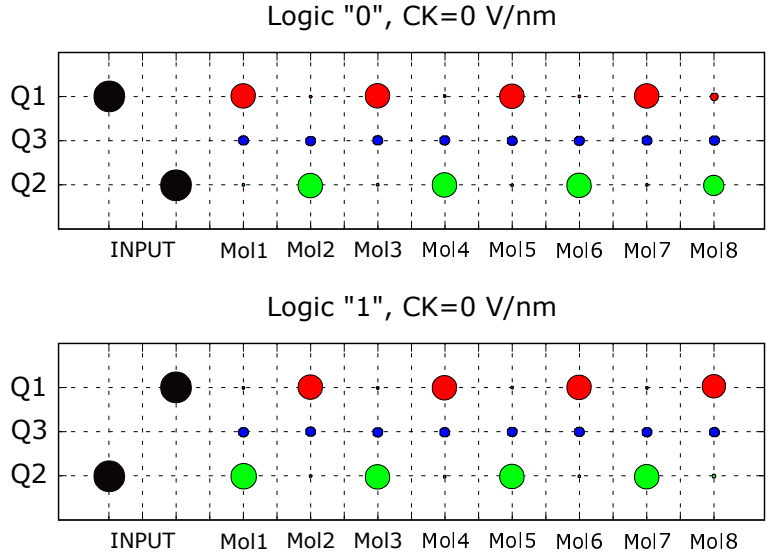

Figure 6.22 Aggregated dot charges on wire (0.8*nm*) with zero clock.

6.4.2.6 *0.8 nm* Wire with Inhibiting Clock ($-2V/nm$)

Logic "0" Propagated along 0.8*nm* Wire				
Agg. Charge	Mol 1	Mol 2	Mol 3	Mol 4
Q1	0.034	0.028	0.027	0.027
Q2	0.021	0.024	0.025	0.025
Q3	0.945	0.948	0.948	0.948
Agg. Charge	Mol 5	Mol 6	Mol 7	Mol 8
Q1	0.027	0.027	0.027	0.027
Q2	0.025	0.025	0.025	0.025
Q3	0.948	0.948	0.948	0.948
Logic "1" Propagated along 0.8*nm* Wire				
Agg. Charge	Mol 1	Mol 2	Mol 3	Mol 4
Q1	0.022	0.026	0.027	0.027
Q2	0.034	0.026	0.026	0.025
Q3	0.944	0.948	0.947	0.948
Agg. Charge	Mol 5	Mol 6	Mol 7	Mol 8
Q1	0.027	0.027	0.027	0.027
Q2	0.025	0.025	0.025	0.025
Q3	0.948	0.948	0.948	0.948

Table 6.12 Aggregated dot charges on wire (0.8*nm*) with $-2V/nm$ of clock.

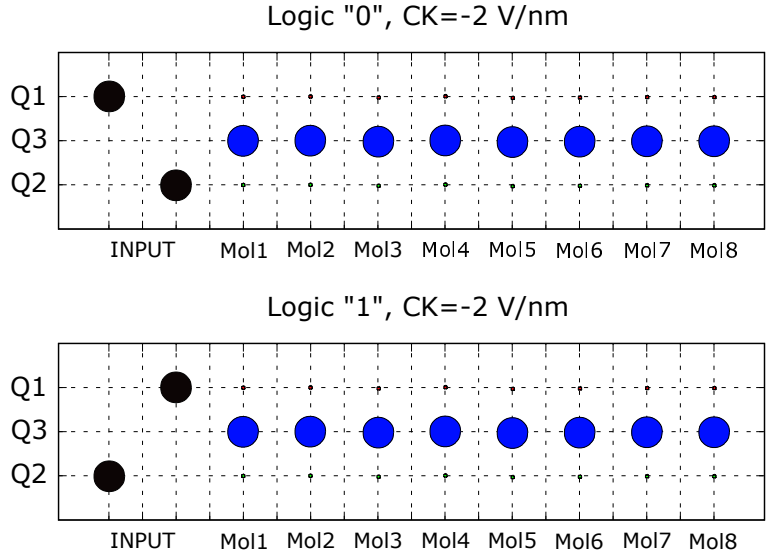

Figure 6.23 Aggregated dot charges on wire (0.8*nm*) with $-2V/nm$ of clock.

Judging from the obtained results, it can be summarized that with 1.0*nm* of inter-molecule distance, the results in terms of aggregated charges on wire demonstrate a evident degradation of binary information along the molecular wire and only first few molecules can be recognized as encoding properly the logic state carried by the *INPUT* cell regardless of the presence of enhancing clock field, see Figure 6.18 and Figure 6.19. Whereas successive molecules localized at the end of the wire are barely influenced and the information is thus lost. Those less distinguished charge differences between logic dots also make read-out of logic states more difficult.

On the other hand, with 0.8*nm* as distance after shrinkage, in the same conditions the electrostatic interaction is much stronger leading to more explicitly charge separation on logic dots of molecules. Moreover, the applied enhancing clock field favors such separation of charge. As a consequence of that, the binary information is hence preserved and transmitted properly to the end of the wire, as shown in Figure 6.21 and Figure 6.22.

However, if the prohibiting clock is applied to the wire, the results obtained from the algorithm calculation illustrate that all the molecules on wire are forced into *NULL* state and no molecular switching is noticed even though there exists the *INPUT* cell carrying information, see Figure 6.20 and Figure 6.23.

6.4.3 Clocked Binary Wire

The results analyzed in Section 6.4.2 corresponds to uniform clock field applied to MQCA wire. Whereas in this section, a clocked MQCA wire is described inside the algorithm and its performance in presence of multi-phase clock signals applied to clock zones distributed on wire is demonstrated in terms of obtained results. The layout of the clocked wire and corresponding multi-phase clock signal applied for each clock zone is depicted following the discussion in Section 6.2.3, see Figure 6.24.

In particular, as illustrated in Figure 6.24, the MQCA wire of interest consists of twelve bis-ferrocene molecules equally aligned together. The *INPUT* cell is placed aside and this wire is partitioned into three clock zones, i.e., four molecules in each zone. Within each clock zone, a multi-phase clock signal is applied and there is a phase shift in terms of 1/4 of the signal period T between nearby clock zones. This clock is approximated with a stair-case function during the molecular interaction

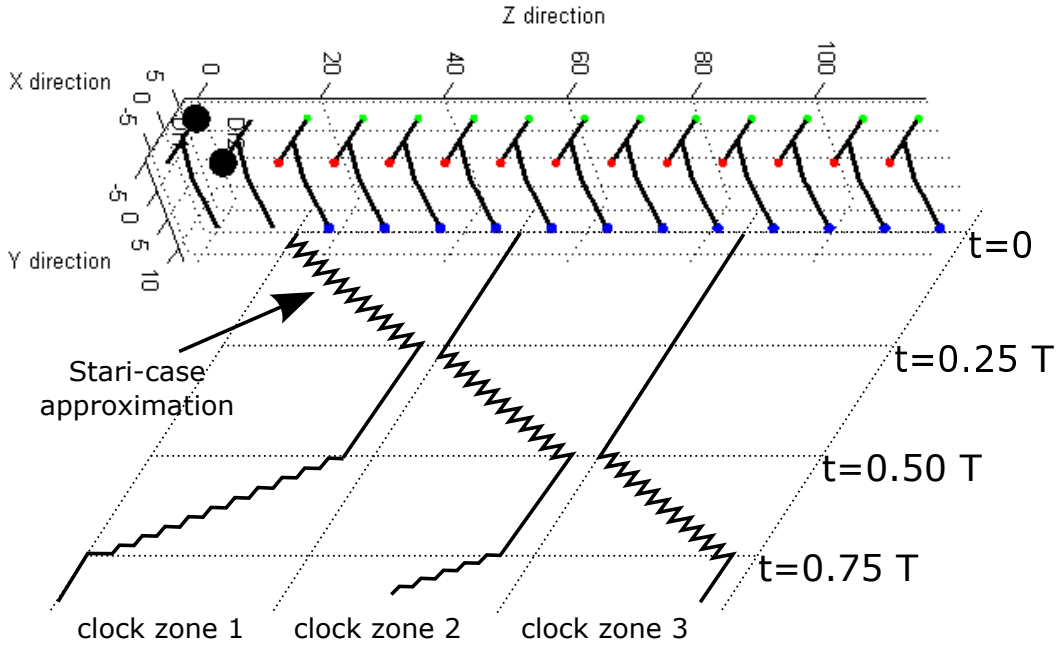

Figure 6.24 Clocked binary wire layout in algorithm and clock zones partitioned along wire with multi-phase clock signal applied.

calculation inside algorithm reducing the abrupt change of clock values. With this clock mechanism considered, the MQCA wire is expected to behave like a shifted register forwarding information from the *INPUT* cell to the end of it. The inter-molecule distance considered here is $d = 0.8nm$, since with $1.0nm$ in between, the information will be lost soon after few molecules of propagation. Obtained results in terms of aggregated dot charges on molecules are pictured in Figure 6.25 and Figure 6.26 for both logic states of *INPUT* cell considered (top view).

Similarly, the computed aggregated dot charges are represented by spheres with colors and the radius of the sphere is proportional to the quantity of dot charge. In general, it can be seen that, the binary information is transmitted following the set-up of clock signals shown in Figure 6.24. In particular, at $t = 0$ the molecules located along the whole wire are in *Relax* phase during which no switching is allowed. In this condition, the unit amount of charge of the molecule is thus mainly located on the central dot $Q3$ (blue). For example, the first molecule $M1$ near the *INPUT* cell, its aggregated charges for the logic dots ($Q1$ and $Q2$) and central dot $Q3$ are $+0.037$, $+0.019$ and $+0.944$, while its neighbor $M2$ has similar aggregated charges with values of $+0.024$, $+0.029$ and $+0.947$, see Fig 6.25 ($t = 0$), and so are those

successive molecules. Therefore, with little amount of charge left on logic dots, all molecules are in *NULL* states with no interaction phenomena observed.

Then at $t = 0.25T$, the molecules inside the *clock zone 1* are in *Switch* phase so that they have been activated slowly and begin to interact to each other following the logic state (e.g., "0") encoded by the *INPUT* cell. At the end of this phase, the aggregated charges of $M1$ are achieved with values of $+0.918$, $+0.011$ and $+0.071$, while those charges of $M2$ are $+0.039$, $+0.887$ and $+0.074$. Thus these two molecules together encode the same logic state of *INPUT* cell. This is also true for the next cell which contains $M3$ and $M4$, see Figure 6.25 ($t = 0.25T$), whereas the rest of the molecules are still in *NULL* states waiting to be activated.

By the same logic, following the change of time, the molecule inside each clock zone on wire will be either activated or dis-activated following the alternated clock phases thus propagating information throughout the wire. Moreover, the erasure of information on wire, e.g., *Release* phase at $t = 0.75T$, is not trivial, it gives the possibility to receive new information from the *INPUT* while forwarding previous information along wire. Therefore the potential throughput for MQCA is increased, i.e., pipeline mechanism in Section 8.3.

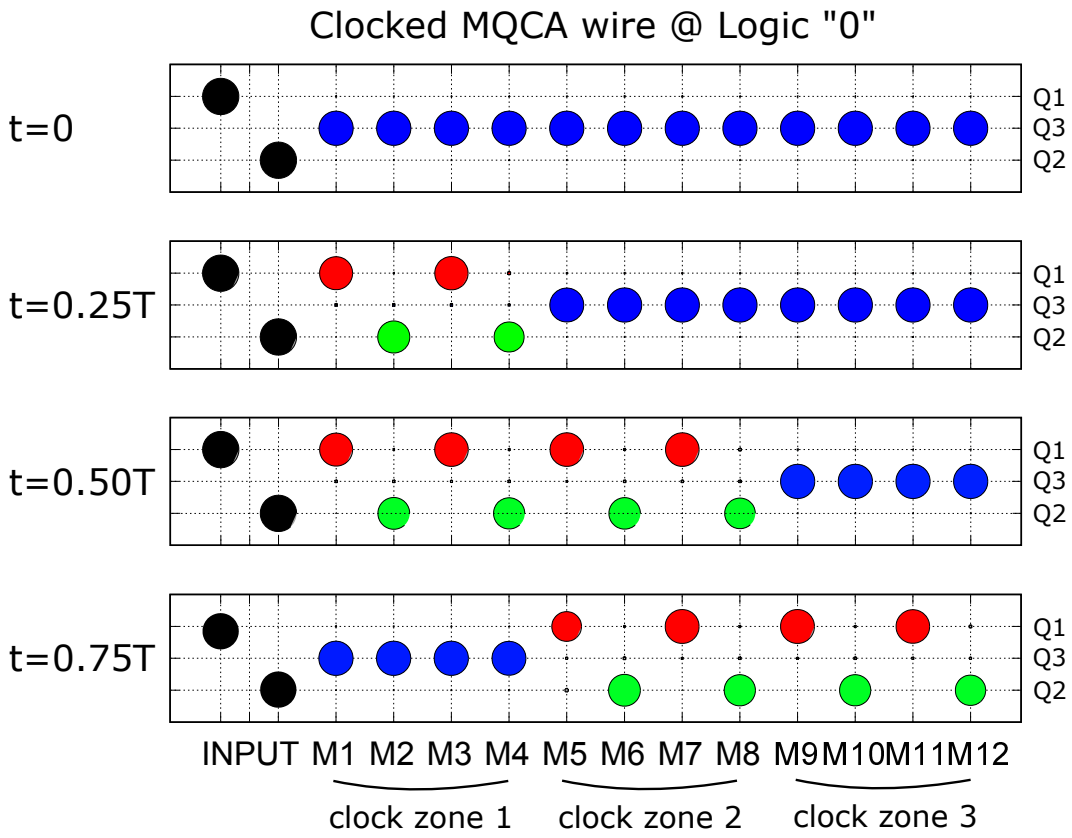

Figure 6.25 Aggregated dot charges distributed along clocked MQCA wire (logic “0”).

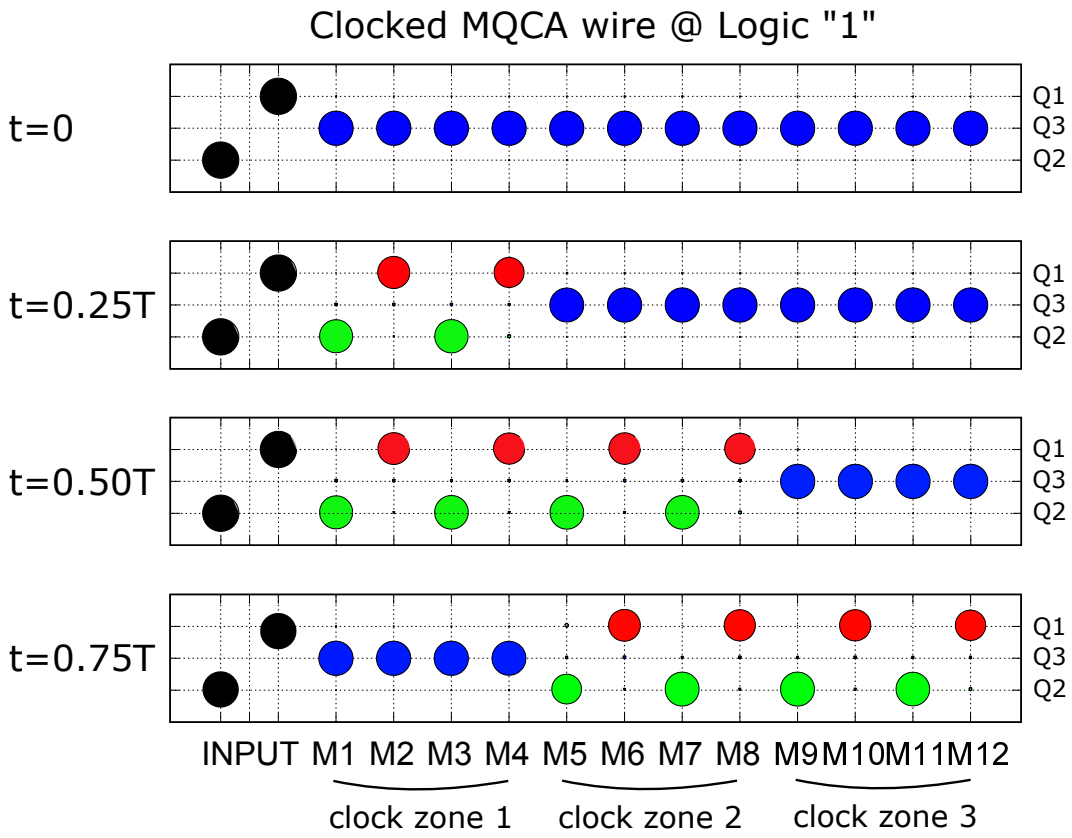

Figure 6.26 Aggregated dot charges distributed along clocked MQCA wire (logic “1”).

Chapter 7

MQCA Functional Block Analysis

The implemented algorithm for MQCA wire is turned out to be functional and the generated results have demonstrated expected performance of QCA computation. However, regarding more complex structures of MQCA, for example, majority voter, inverter, buses of wire, they are also of great importance for building MQCA devices with purpose of digital computation. Therefore, in this chapter, the introduced new method of MQCA analysis based on proposed algorithm has been extended considering more complicated structures under analysis.

7.1 Clocked MQCA Circuits Layout

In stead of binary wire which is a one-dimensional structure, the initialization stage here is capable of generating two-dimensional MQCA structures like three-input majority voter or inverter, etc.

In particular, as shown in Figure 7.1, during the initializing stage, a large plane is created, it is possible to place molecules, which are represented by its redox centers and binding thiol, as well as *INPUT* cell as drivers. Here the molecules are supposed to be deposited on the same plane, hence all molecules have identical coordinates along Y-axis. Whereas regarding the other two directions of coordinates, it is possible to be modified according to requirement. For example, the inter-molecule distance d along Z-axis and X-axis are both configurable. Figure 7.1 depicts the layout of an inverter defined inside the algorithm.

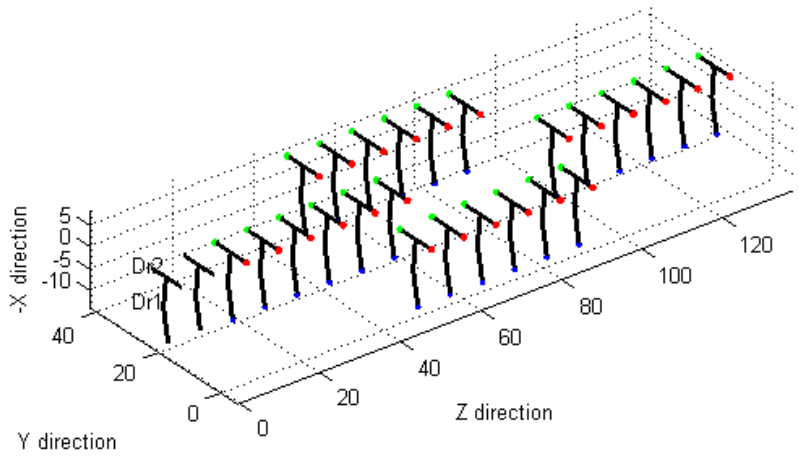

Figure 7.1 Schematic layout of MQCA inverter considered inside algorithm.

On the other hand, since large MQCA devices should be operated with clock system, the clock system assignment is also necessary. Similar as MQCA, here the two-dimensional structures are also partitioned into several clock zones with periodic multi-phase clock signal assigned to each one of them. Some examples of clock zone division together with its principle implementation are schematically shown in Figure 7.2 and Figure 7.3. Meanwhile, the clock zone partition of three-input majority voter is already shown in Figure 3.13(B).

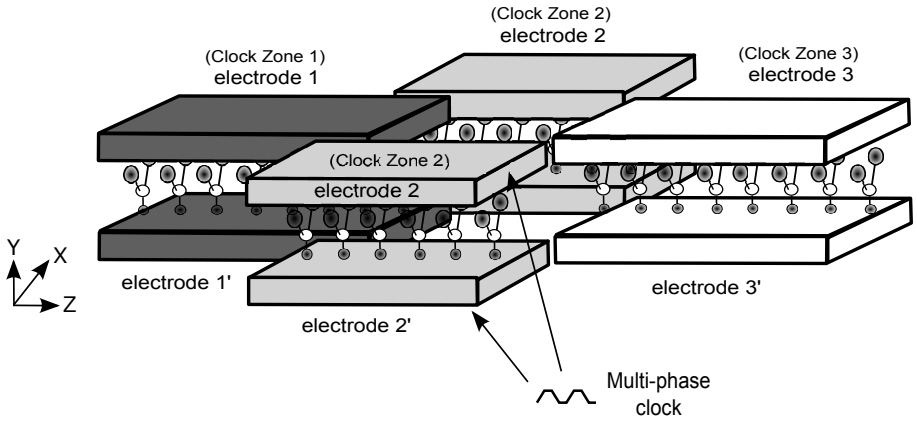

Figure 7.2 Clocked MQCA inverter.

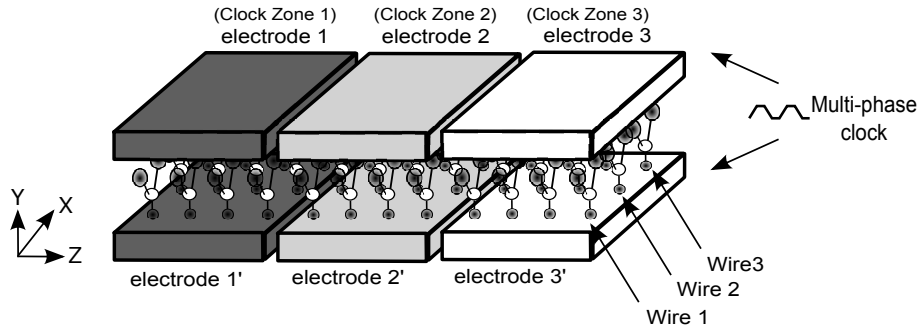

Figure 7.3 Clocked MQCA bus with three parallel wires.

Inside the algorithm, each molecule will be labeled with its assigned clock signals, those values are stored the clock matrix in pseudo code for the algorithm considering the application of clock, see Section 6.2.3. Whereas concerning the multi-phase clock signal, similar as the case of MQCA wire, the stair-case approximation is also adopted for molecular interaction calculation when smooth change of clock values is needed to avoid abrupt switching among molecules. With the presence of clock zones and multi-phase clock signals, the binary information carried by the *INPUT* could be safely guided and eventually transmitted to the *OUTPUT* of the MQCA devices for further read-out.

7.2 Interaction between Two Random Molecules

As for the second stage of molecular interaction calculation, modifications have been also performed based on these two-dimensional MQCA devices. Previously in MQCA wire condition, the interactions are considered and calculated between two well-aligned molecules and such interactions are presented in terms of a series of equivalent voltage V_{IN} from one molecule to another, as the *Driver* and the *MUT* shown in Figure 7.4. However, in cases of complex blocks, molecules could be located in an alternative way with tilted angle or misalignment along any axis, like the *MUT'* or *MUT"* depicted in Figure 7.4.

As a consequence of that, the algorithm calculates the interaction between two random molecules. To be specific, taking aggregated dot charges ($D1$. $D2$ and $D3$) of one molecule as driver. Then the generated electric field of these charges are computed. After that, first integrating the electric field components that are parallel to the dot-axis (within X-Z plane) of the *MUT* thus resulting an equivalent input

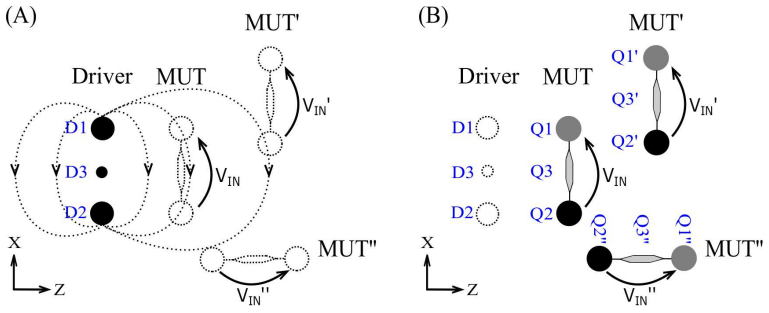

Figure 7.4 Interaction between two bis-ferrocene molecules randomly located.

voltage V_{IN}. On the other hand, integrating the electric field components that are parallel to the vertical axis of *MUT* (Y-axis), this allows to obtain another equivalent voltage $V_{vertical}$, see Figure 7.5. Although this vertical influence is not directly affecting the charge movement between logic dots as V_{IN} does, it will interference the clock signal applied perpendicularly to this molecule. In fact, the actual clock influence considered for interaction computation should be the combination between externally applied clock signal and this generated vertical voltage $V_{vertical}$. Nevertheless, it is necessary to address that in previous wire condition, the $V_{vertical}$ is not considered due to its negligible value inside wire layout. Combining both the V_{IN} and $V_{vertical}$ from the *Driver*, the *MUT* will re-arrange itself in terms of forming aggregated charges with values of $Q1$, $Q2$ and $Q3$ as a response adopting the proper trans-characteristic. Similar procedures can be also performed for computing interaction responses for *MUT'* or *MUT"*.

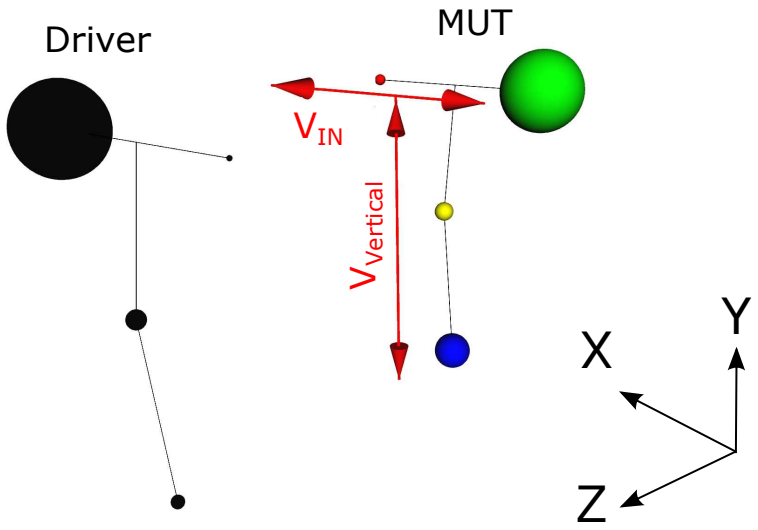

Figure 7.5 Both calculation of equivalent voltages V_{IN} and $V_{vertical}$.

In summary, regarding analysis of more complicated logic functional blocks of MQCA, the alternative method based on the proposed algorithm has been modified and expanded for more wide range of application. Specifically, its flexible design of structure layout and clock assignment, together with the improved evaluation of interaction between any two bis-ferrocene molecules localized on the device give the possibility to study MQCA device behavior from an electronic point of view. In the following section, some examples of MQCA logic functional blocks are being examined adopting the algorithm with purpose.

7.3 Generated Results

Inside the modified algorithm, it is possible to design the MQCA structure layout manipulating molecules according to requirement. Results concerning the MQCA analysis are generated adopting the algorithm and discussed in the following. In addition, it is worthy to mention that inside these MQCA functional blocks hereinafter, the distance d between two molecules, either horizontally or vertically aligned, is considered to be $d = 0.8nm$ for its optimum behavior discussed in previous Chapter 5 and Chapter 6.

7.3.1 L-Shape of Wire

The *L-Shape* of wire represent the possibility of forwarding information in alternative direction, which motivates the development of MQCA devices from one dimensional to two-dimensional. The layout designed inside algorithm is depicted in Figure 7.6. Its clock zones is partitioned based on the two segments of wire. Results provided by the algorithm regarding its QCA behavior are depicted in Figure 7.8. With the clock zones assigned, the performance of *L-Shape* of wire is verified in terms of forwarding identical information from the *INPUT* to the end of the wire.

7.3.2 T-Shape of Wire

The *T-Shape* of wire permits the propagation of information into two different directions simultaneously. Its layout considered during the calculation is shown in Figure 7.9. Similar as *L-Shape* case, the clock zones on *T-Shape* of wire is also

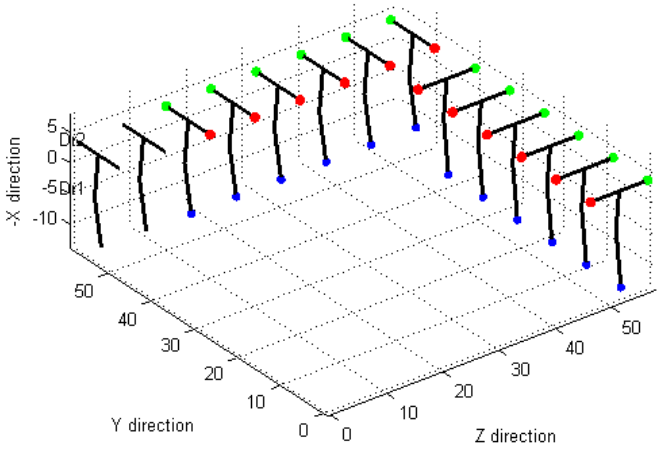

Figure 7.6 Schematic layout of *L-Shape* of wire.

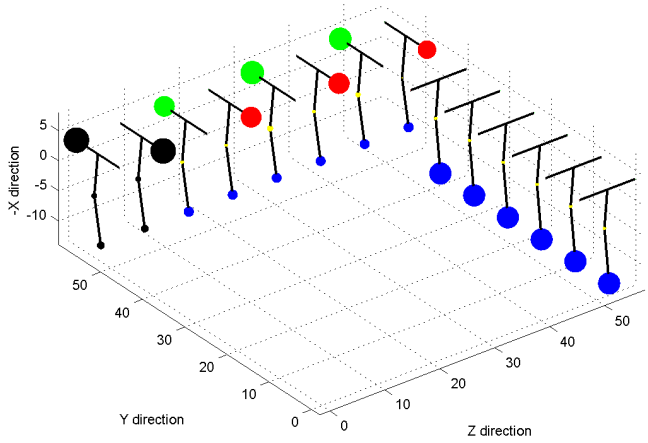

Figure 7.7 Clocked behavior of *L-Shape* of wire with *INPUT* configured to logic state "1": the horizontal segment of wire is activated.

divided based on its three segments, this can be clearly seen in Figure 7.11, where results generated from the algorithm are described. Inside this Figure, it is possible to see that information encoded by the *INPUT* has been guided to two different directions, which is useful for digital circuit design.

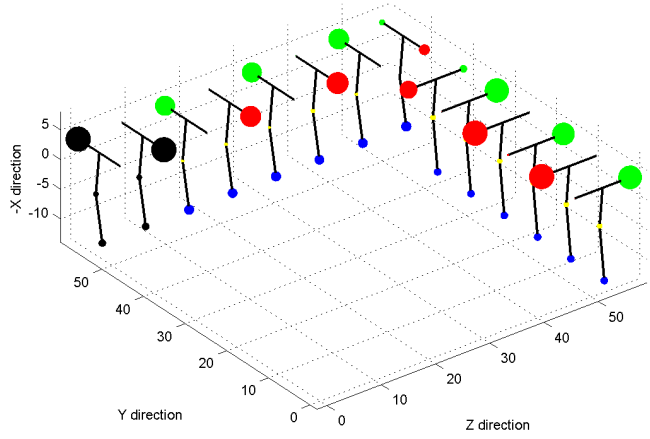

Figure 7.8 Clocked behavior of *L-Shape* of wire with *INPUT* configured to logic state "1": the vertical segment of wire is activated.

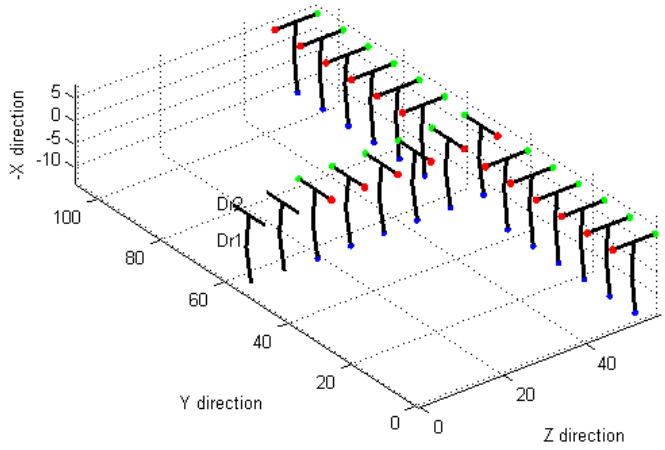

Figure 7.9 Schematic layout of *T-Shape* of wire.

7.3.3 Three-Wire Bus

A MQCA bus structure based on three parallel wires has been simulated using the developed algorithm, its layout has been demonstrated schematically in Figure 7.12, and its clock zones assignment is already shown in Figure 7.3. For example, with the *INPUT* cell set to logic state "1", results in terms of the MQCA wire bus

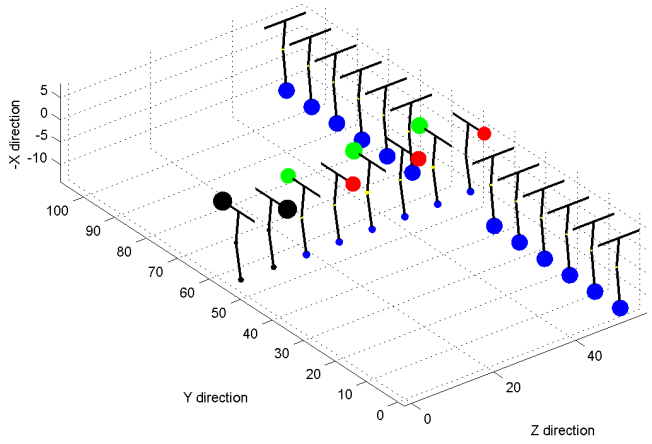

Figure 7.10 Clocked behavior of *T-Shape* of wire with *INPUT* configured to logic state "0": the horizontal segment of wire is activated.

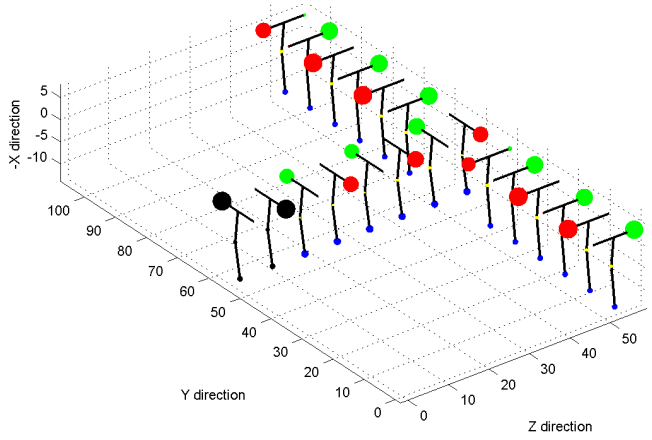

Figure 7.11 Clocked behavior of *T-Shape* of wire with *INPUT* configured to logic state "0": the two vertical segments of wire are activated.

performance are illustrated from Figure 7.13 to Figure 7.16. From which, information propagation is observed in evident.

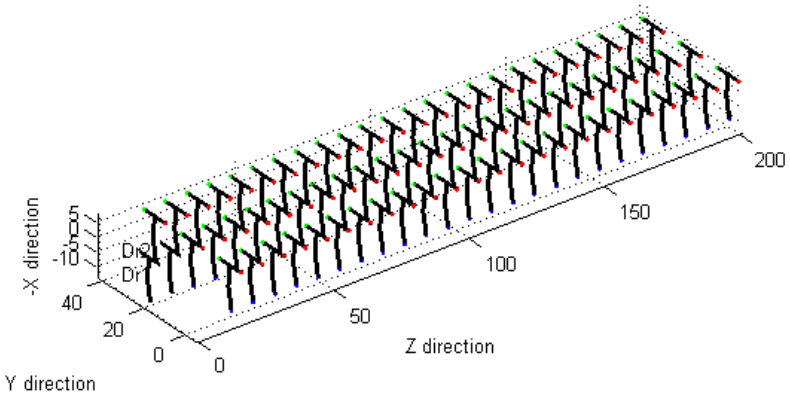

Figure 7.12 Schematic layout of a wire bus made of three parallel MQCA wires.

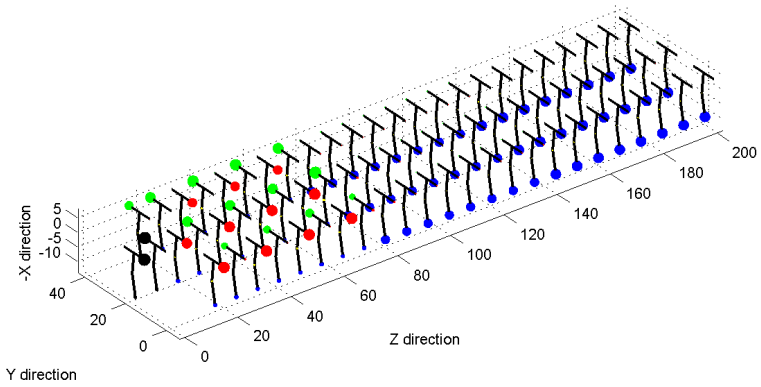

Figure 7.13 Clocked MQCA wire bus performance with *clock zone 1* activated in *Switch* phase.

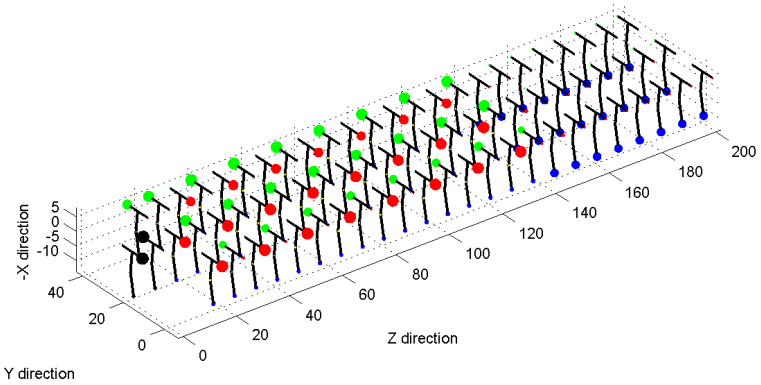

Figure 7.14 Clocked MQCA wire bus performance with *clock zone 2* activated in *Switch* phase and *clock zone 1* in *Hold* phase.

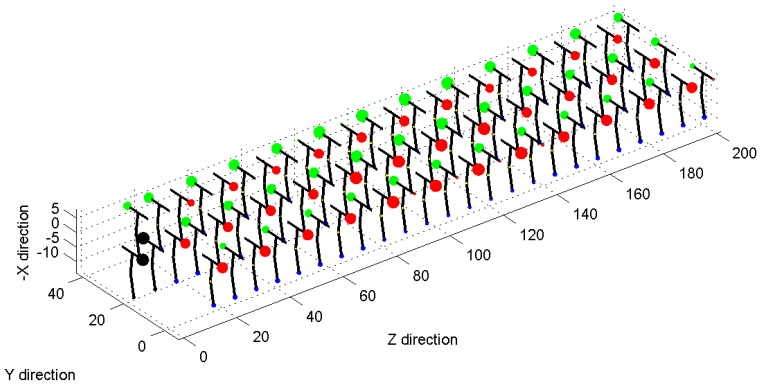

Figure 7.15 Clocked MQCA wire bus performance with *clock zone 3* activated in *Switch* phase and *clock zone 1 & 2* in *Hold* phase.

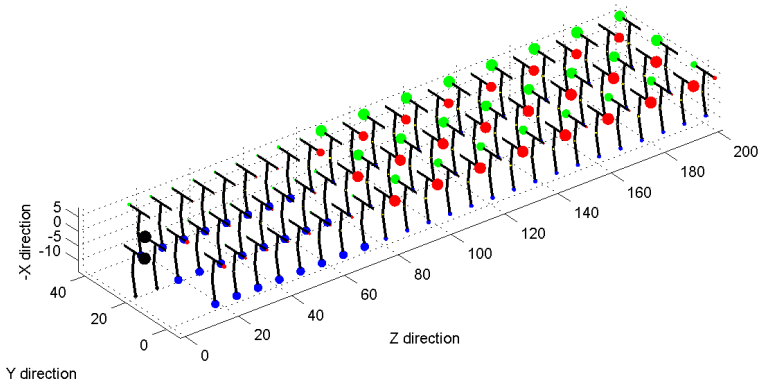

Figure 7.16 Clocked MQCA wire bus performance with *clock zone 2 & 3* in *Hold* phase and *clock zone 1* in *Release* phase.

7.3.4 Majority Voter

The simple three-input majority voter mentioned in Section 5.3.5 was implemented based on a complete MQCA cell with two molecules, whereas the majority voter considered here involves more molecules and its layout has been sketched in Figure 7.17. In particular, with three *INPUT* cells assigned to the three branches, the majority votes and outputs the majority of input logic state.

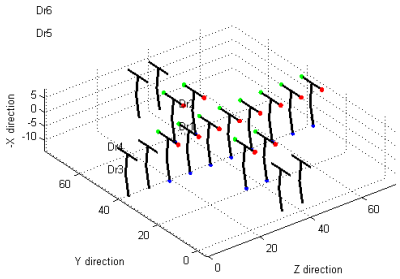

Figure 7.17 Schematic layout of a three-input majority voter

Following the clock system for majority voter, Figure 7.18 and Figure 7.19 illustrate the simulation results regarding three *INPUT* cells with logic states of "111" and "101". The propagated information eventually at the *OUTPUT* of majority voter is encoded in logic state "1" (majority of inputs) in both cases proving the proper functionality of this structure with the guidance of clock.

7.3.5 Inverter

As another fundamental logic block for building MQCA digital circuits, the inverter layout has already been sketched in Figure 7.1. Meanwhile the clock zones assigned to inverter has been demonstrated in Figure 7.2 and based on this clock, the inverting behavior is thus realized, see the example recorded in Figure 7.20.

In the end, as suggested from all the results and figures discussed in this chapter, it can be summarized that once a MQCA logic structure layout is defined with purpose, and together with proper clock zones to warrant its correct digital computation, the implemented algorithm could thus demonstrate the eventual aggregated dot charge distribution throughout the structure via counting and evaluating exiting molecular interactions.

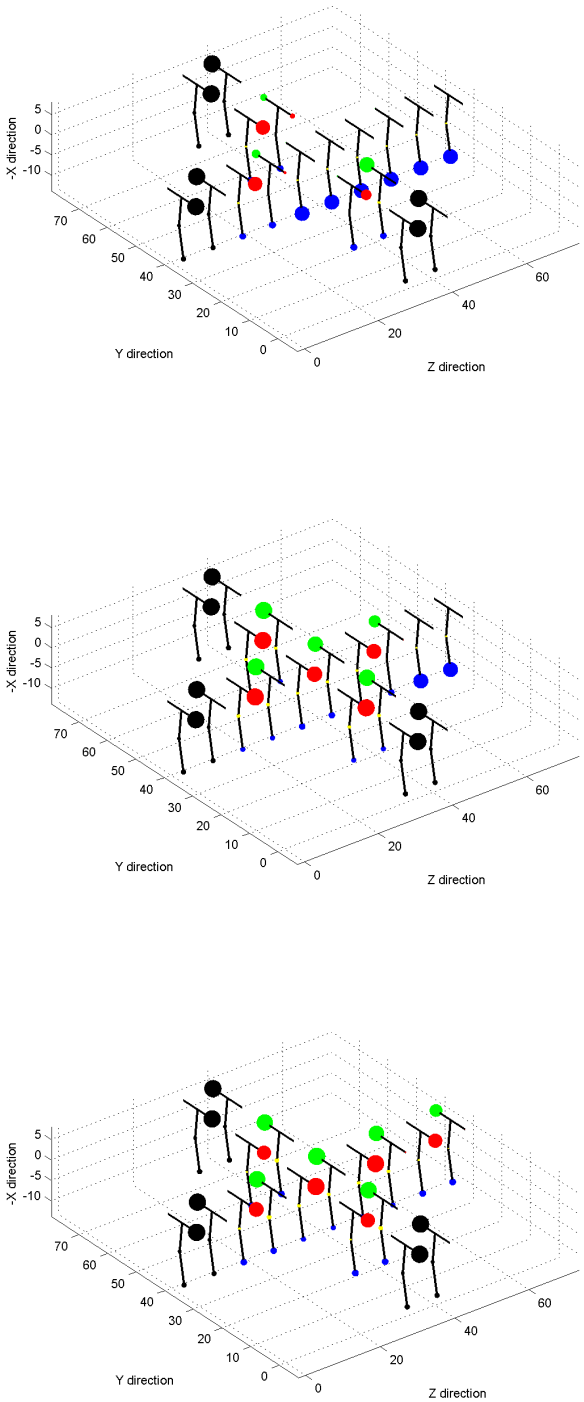

Figure 7.18 Clocked behavior of three-input majority voter with three *INPUT* cells configured into logic states “111”.

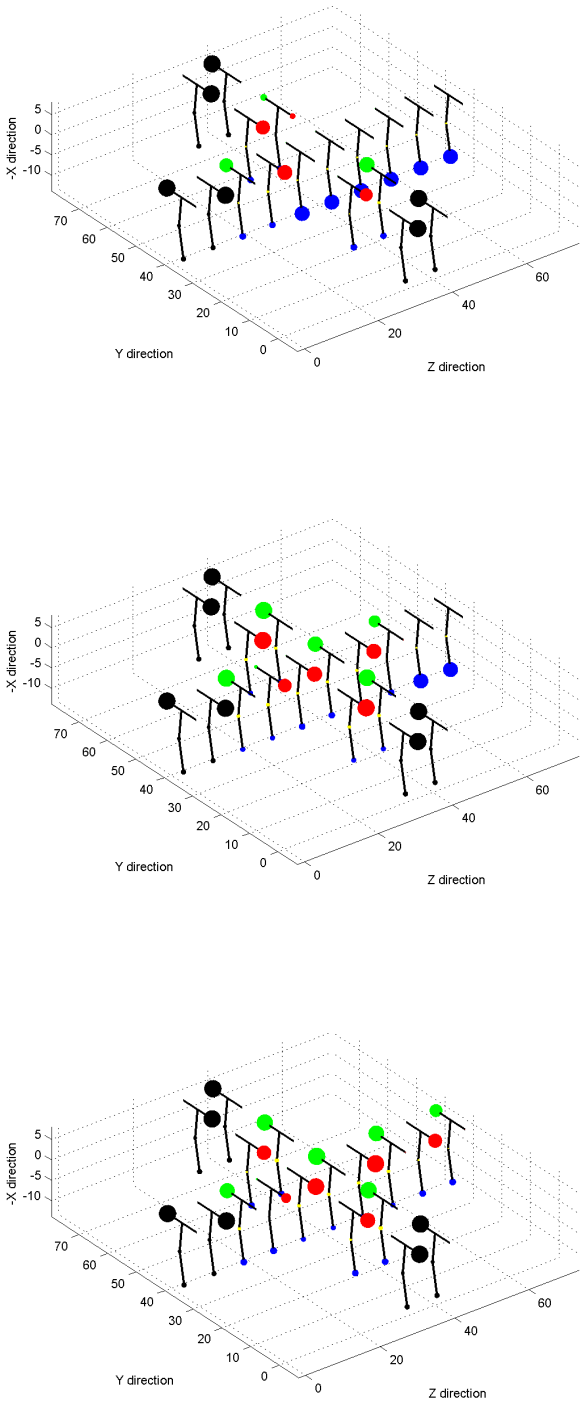

Figure 7.19 Clocked behavior of three-input majority voter with three *INPUT* cells configured into logic states “101”.

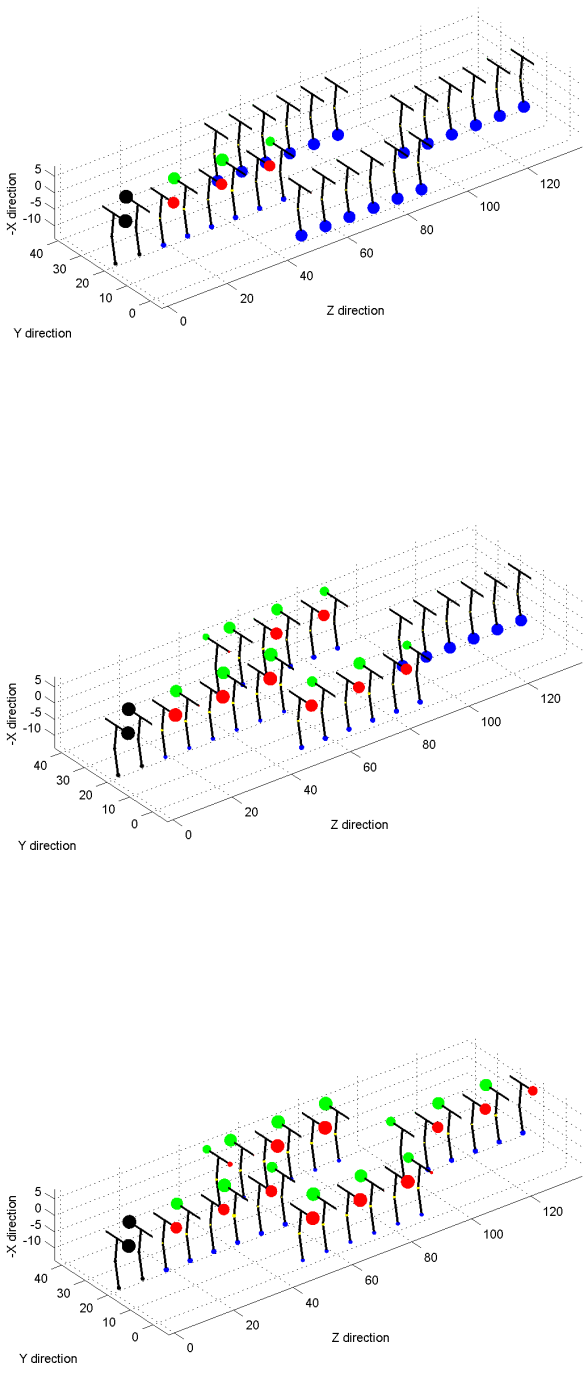

Figure 7.20 Clocked behavior of an inverter with the *INPUT* cell configured into logic states "1".

Chapter 8

New Method of Analysis Application

In this chapter, based on the new method which involves the proposed algorithm for MQCA functionality analysis, some applications are necessarily introduced that could facilitate the eventual prototype fabrication of MQCA circuits. For example, analysis of noise existing during MQCA operation, the processing variation analysis regarding defect that might occur during MQCA structure manufacture or the demonstration of a possible pipeline scheme for improving the throughput of MQCA.

8.1 Noise Analysis

The application of new method of analysis is discussed here in order to investigate the noise influence to the binary information transmission and processing along the arrays of cells. These influences could be introduced by thermal noises or electrostatic disturbances. In particular, the noise concerned here during MQCA operation in terms of breaking the balanced initial equilibrium charge distribution of bis-ferrocene molecule.

As discussed in Section 6.2, inside the new method of analysis, the algorithm starts from a balanced initial charge located on the two logic dots at equilibrium. However, it is impossible to guarantee that in reality due to existing external thermal or electric disturbance. For example, in Table 8.1, in presence of an enhancing clock signal with value of $+2V/nm$, some random noises existing between these unbalanced initial aggregated charges are illustrated along an eight-molecule MQCA

wire. These values are set in a random way representing unpredictable noisy influences in terms of re-distributing charges between two logic dots. However, we assume in this condition due to the presence of enhancing clock system, the charge left on central $Dot3$ is almost null as equilibrium and kept constant during noise assignment ($+0.054$).

Dots (Initial)	Mol 1	Mol 2	Mol 3	Mol 4
Q1 (0.+475)	+0.498	+0.275	+0.375	+0.425
Q2 (0.+471)	+0.448	+0.671	+0.571	+0.521
Q3 (0.+054)	+0.054	+0.054	+0.054	+0.054
Dots (Initial)	Mol 5	Mol 6	Mol 7	Mol 8
Q1 (+0.475)	+0.575	+0.495	+0.365	+0.595
Q2 (+0.471)	+0.371	+0.451	+0.581	+0.351
Q3 (+0.054)	+0.054	+0.054	+0.054	+0.054

Table 8.1 Noisy unbalanced initial aggregated dots charges along eight-molecule MQCA wire @ $+2V/nm$.

In the meantime, they are also assigned inside the algorithm as input parameters and should be considered throughout the whole period of interaction calculation. Therefore, inside the first stage of algorithm, not only the initial interaction from *INPUT* cell to molecules are evaluated, but the influences from one molecule's unbalanced equilibrium charges to the others are also computed and saved for further self-consistent calculations in the next stage.

Consequently, the aggregated dot charges of all molecules distributed on wire are recorded in Figure 8.1 for both inter-molecule distances $d = 1.0nm$ and $d = 0.8nm$ with *INPUT* cell configured into logic state "1". The achieved results suggest that with $d = 1.0nm$ as inter-molecule distance, the noises could be a serious problem resulting total loss of information, as shown in Figure 8.1(A), the difference between two logic dots is not sufficient for encoding logic state starting from the first molecule ($Mol1$) on wire. Whereas with shorter distance $d = 0.8nm$, as usual, the stronger interactions compensate the noisy influence in term of preserving the correct polarity for each molecule on wire hence forwarding the encoded information in safety.

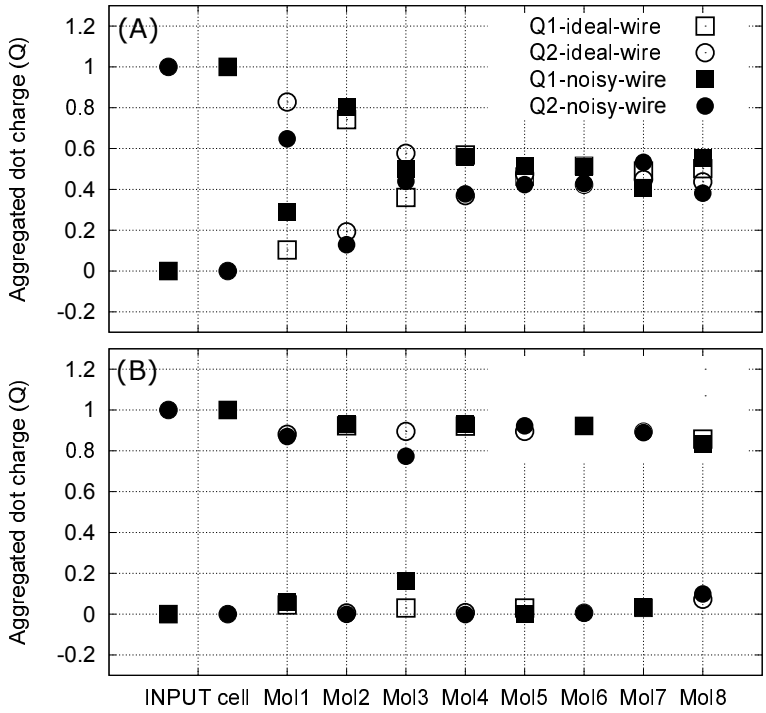

Figure 8.1 Aggregated dot charges distributed along eight-molecule MQCA wire: (A)$d = 1.0nm$; (B)$d = 0.8nm$.

8.2 Process Variation

This section concerns the most important application of the new method of analysis, i.e., the process variation. During the all the discussions in Chapter 6 and Chapter 7, the layouts of MQCA binary wire or other logic gates are in terms of ideal condition, namely all molecules are uniformly aligned in the same plane with identical distance between them following the designed patterns, as the example of inveter depicted in Figure 7.1. In addition, from the code level point of view, all the molecules are "deposited" in a matrix, the position of molecule together with its logic dots and central dot ($Dot\,i$, where i=1, 2, 3), is at the position (h, k) on the Y-Z plane with respect to the reference molecule at the origin. In Table 8.2, the data concerning molecule at the origin is shown.

	Coordinates		
	x [Å]	**y** [Å]	**z** [Å]
Dot 1	−3.622	−5.062	−0.094
Dot 2	−3.588	+5.083	−0.094
Dot 3	+3.133	−0.011	−0.755
Bind ele.	+11.776	−0.053	+0.409

Table 8.2 Coordinates of reference molecule at the origin.

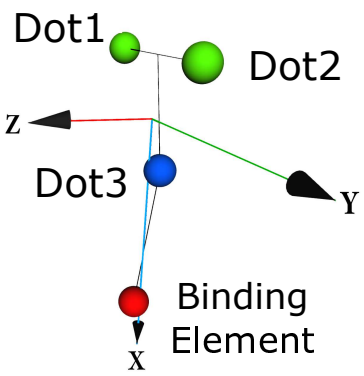

Therefore the coordinates are defined by Equation 8.1 for other shifted molecular dots. The vertical axis of molecule is along the X-axis, whereas the $dist_Y$ and $dist_Z$ represent the two-dimensional shifts along Y-axis and Z-axis for aligning molecules, see Figure 8.2. Furthermore, the $dist_Z$ has a value that is equal to the previous referred inter-molecule distance d, whereas the $dist_Y$ is the sum of inter-molecule distance d and the width of bis-ferrocene molecule.

$$\begin{cases} Dot\_i_{X,new} = Dot\_i_{x,ref} \\ Dot\_i_{Y,new} = Dot\_i_{y,ref} + (k-1)\cdot dist_Y \\ Dot\_i_{Z,new} = Dot\_i_{z,ref} + (h-1)\cdot dist_Z \end{cases} \tag{8.1}$$

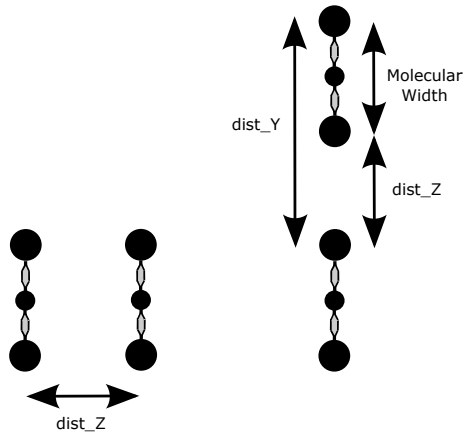

Figure 8.2 Representation of two-dimensional shifts $dist_Y$ and $dist_Z$ in algorithm (top view).

Actually, in the future manufacture of MQCA structures, molecules are required to be attached to substrate, e.g. a gold nanowire. Notice that the interference between metal nanowire and the bis-ferrocene molecules during molecular deposition

or information transmission is not currently addressed in this work. However, during the procedure of gold substrate fabrication for the nanowire and bis-ferrocene molecule deposition, these experimentally related defects might occur, like mis-alignment in all possible directions or non ideal parallelism between two nearby molecules, as highlighted in Figure 8.3. They are considered to be harmful to the correct behavior of the molecular QCA circuits in terms of influencing information propagation. To be specific, they are discussed as follows.

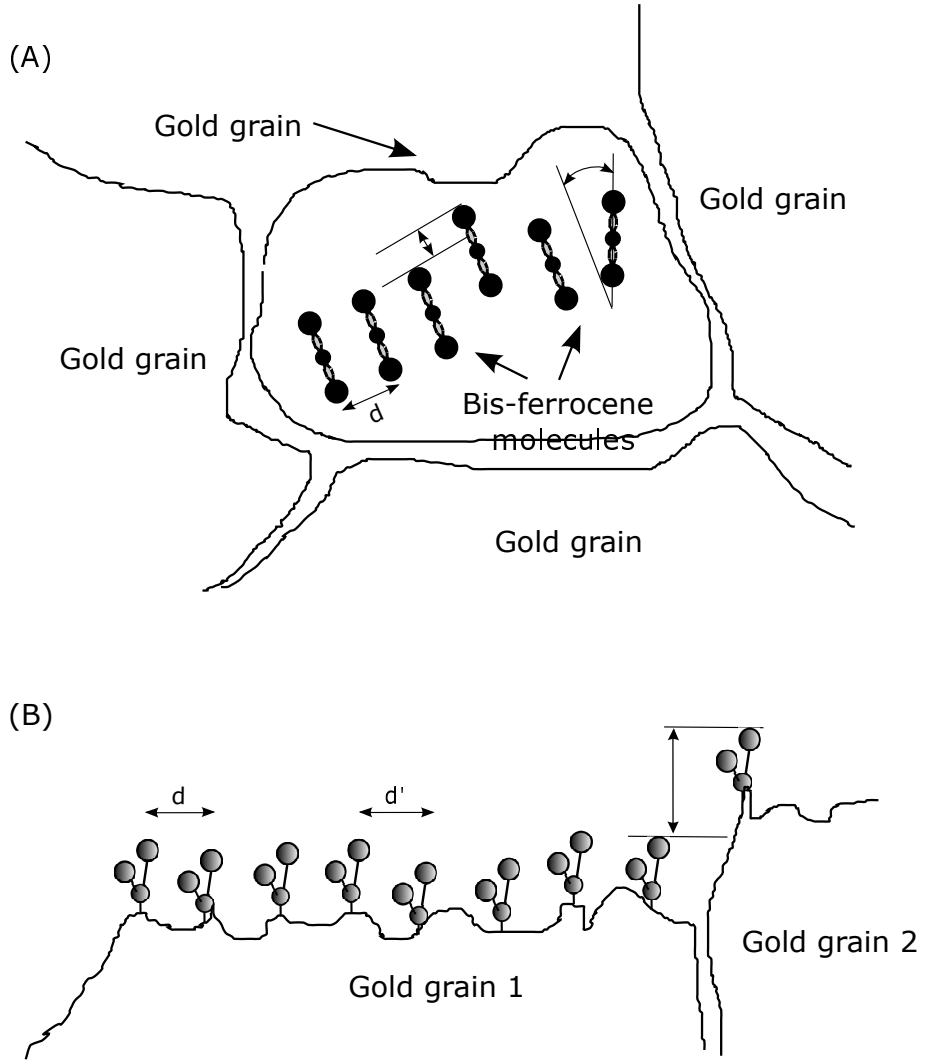

Figure 8.3 Possible defects existing on MQCA manufacturing: (A)Horizontal mis-alignments and tilting angle between two neighboring bis-ferrocene molecule; (B)Horizontal mis-alignments and vertical mis-alignment between two molecules due to different gold grains in presence.

8.2.1 Defects Modeling: Rotation of Molecule

During the molecule deposition, the perfect alignment can not be ensured in terms parallelism between nearby molecule, there might be a tilting angle between them, see Figure 8.3(A). In addition, Figure 8.4 also illustrates that this rotation might be also three-dimensional. In order to set-up the coordinates of a rotated bis-ferrocene molecule (*Mol*), located at position (h, k), into the algorithm for calculation, we first rotate the reference molecule at the origin thus the resulting shifts along three axes for three dots of molecule are achieved with equations in Equation 8.2.

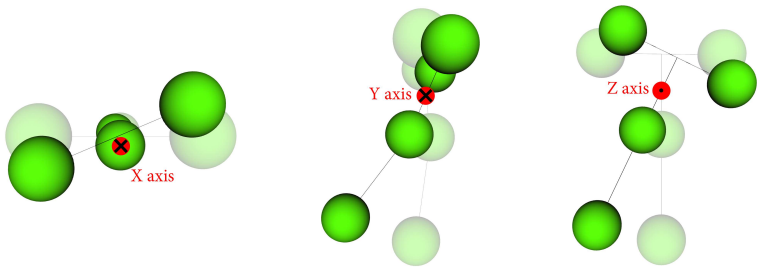

Figure 8.4 Representation of a three-dimensional rotation with respect to X, Y, Z axes.

$$
\begin{cases}
R_X = \begin{bmatrix} 1 & 0 & 0 \\ 0 & \cos(rot_X(Mol)) & -\sin(rot_X(Mol)) \\ 0 & \sin(rot_X(Mol)) & \cos(rot_X(Mol)) \end{bmatrix} \\
R_Y = \begin{bmatrix} \cos(rot_Y(Mol)) & 0 & \sin(rot_Y(Mol)) \\ 0 & 1 & 0 \\ -\sin(rot_Y(Mol)) & 0 & \cos(rot_Y(Mol)) \end{bmatrix} \\
R_Z = \begin{bmatrix} \cos(rot_Z(Mol)) & -\sin(rot_Z(Mol)) & 0 \\ \sin(rot_Z(Mol)) & \cos(rot_Z(Mol)) & 0 \\ 0 & 0 & 1 \end{bmatrix} \\
dot\_1_{new,[X,Y,Z]} = R_X \cdot R_Y \cdot R_Z \cdot dot\_1_{ref,[X,Y,Z]}; \\
dot\_2_{new,[X,Y,Z]} = R_X \cdot R_Y \cdot R_Z \cdot dot\_2_{ref,[X,Y,Z]}; \\
dot\_3_{new,[X,Y,Z]} = R_X \cdot R_Y \cdot R_Z \cdot dot\_3_{ref,[X,Y,Z]};
\end{cases}
\tag{8.2}
$$

Where parameters like $rot_X(Mol)$, $rot_Y(Mol)$ and $rot_Y(Mol)$ are the dihedral rotation angles for the molecule of interest Mol with respect to three axes. Then, the rotated molecule Mol is moved to its correct position (h, k) in the matrix using Equation 8.3.

$$
\begin{cases}
dot\_i_{X,rot} = dot\_i_{x,new} \\
dot\_i_{Y,rot} = dot\_i_{y,new} + (k-1) \cdot dist_Y \\
dot\_i_{Z,rot} = dot\_i_{z,new} + (h-1) \cdot dist_Z
\end{cases}
\tag{8.3}
$$

8.2.2 Defects Modeling: Misalignment of Molecule

The misalignment is due to the presence of roughness on the gold substrate or huge gaps between nearby gold grains. They could be found in any direction of axis, as depicted in Figure 8.3. In general, they are classified into three conditions following X, Y, and Z-axis inside the algorithm, see Figure 8.5.

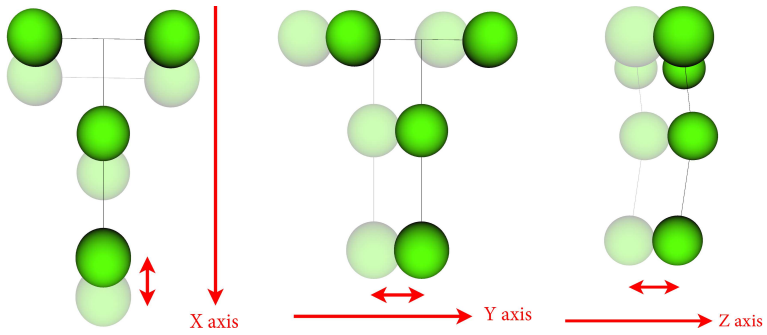

Figure 8.5 Representation of a three-dimensional misalignment along X, Y, Z axes.

In this way, it is possible to combine these two types of defects in terms of rotation and misalignment together and the eventual coordinates for molecule Mol are obtained with Equation 8.4, where the parameters like $shift_X(Mol)$, $shift_Y(Mol)$ and $shift_Z(Mol)$ represents the above mentioned misalignment along three axes for molecule Mol.

$$\begin{cases} dot\_i_{X,final} = dot\_i_{X,rot} + shift_X(Mol) \\ dot\_i_{Y,final} = dot\_i_{Y,rot} + shift_Y(Mol) \\ dot\_i_{Z,final} = dot\_i_{Z,rot} + shift_Z(Mol) \end{cases} \tag{8.4}$$

Figure 8.6 and Figure 8.7 sketch example layouts of an inverter and a eight-molecule wire considered inside the algorithm with misalignment and rotation of molecules taken into account.

8.2.3 Example of Application

As an example of the algorithm application concerning process variation, the behavior of an eight-molecule MQCA wire is analyzed. Theoretically, the molecular wire is schematically anchored on the surface of a gold nanowire, on top of which the molecules could be bound through the thiol element. Therefore it is necessary to prepare the gold surface and model possible existing defects into the algorithm.

An experimental scheme has been proposed for depositing molecular wire and mentioned in Section 3.2. The idea is to fabricate a gold nanowire upon which the bis-ferrocene molecules could be bound through the thiol end-group element. Whereas, the exact experiment procedure to prepare a smooth gold substrate for

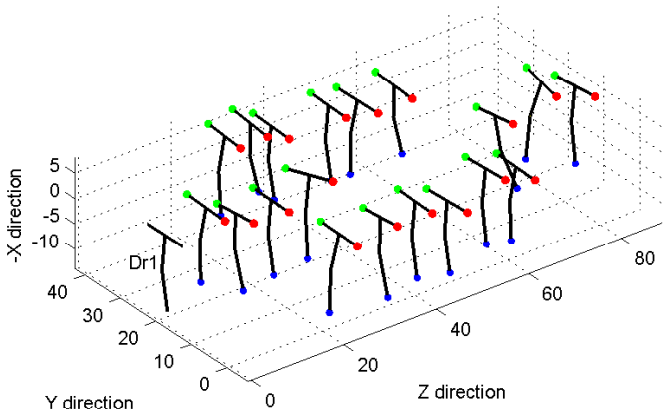

Figure 8.6 A possible layout of MQCA inverter in presence of misalignment and rotation of molecules that might occur during molecular deposition.

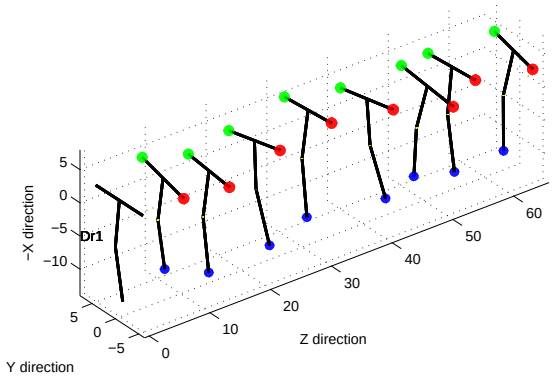

Figure 8.7 A possible layout of MQCA wire in presence of misalignment and rotation of molecules that might occur during molecular deposition.

the nanowire and to realize bis-ferrocene molecular QCA wire deposition has been described in detail in [52, 65–67].

According to the need of smooth gold substrate surface, a low-rough gold substrate was reported by authors in [52], in which a clean glass microscope slide was smoothed. Figure 9.9 depicts that two profiles are chosen within the same gold grain. They highlight the appearance of the gold substrate surface. This sample of gold substrate is with a dimension of $500nm \times 500nm$. After examining their smooth-

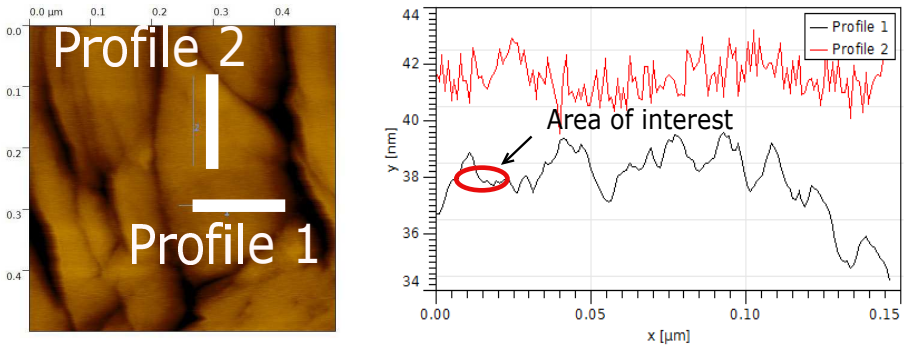

Figure 8.8 Two proposed profiles regarding gold nanowire smoothness on a sample of gold grain.

ness, the length range from $0.015um$ to $0.025um$ of the first profile ($Profile1$) is collected for simulating the molecular behavior.

Based on the exact profile of gold substrate involved here, the major defect in terms of vertical misalignment, denoted as δX since X-axis is the vertical axis in the algorithm, is considered. So that, if an eight-molecule MQCA wire with $d = 1.0nm$ as inter-molecule distance is simulated based on this profile, the roughness of the surface is hence assigned to each molecule on the wire. Taking the first molecule as reference at the origin, the vertical misalignment for the rest of molecules is listed in Table 8.3.

Molecule number	Mol 1	Mol 2	Mol 3	Mol 4
$\Delta X(nm)$	0.00	+0.65	+0.05	-0.65
Molecule number	Mol 5	Mol 6	Mol 7	Mol 8
$\Delta X(nm)$	-0.45	-0.35	+0.15	+0.40

Table 8.3 Vertical shifts ΔX for molecules located on wire ($d = 1.0nm$) with respect to origin due to roughness on the sample of gold grain.

After that, transferring these vertical shifts into molecular coordinates, the molecular wire performance is thereby analyzed adopting the algorithm with this gold surface in presence. The *INPUT* cell is configured into logic state "1" and no clock system is applied. Obtained results are plot in Figure 8.9.

In addition, if the simulated wire has a shorter inter-molecule distance $d = 0.8nm$, its performance can be also examined by the same logic. Table 8.4 records the vertical misalignment for molecules along the shorter wire, whereas generated

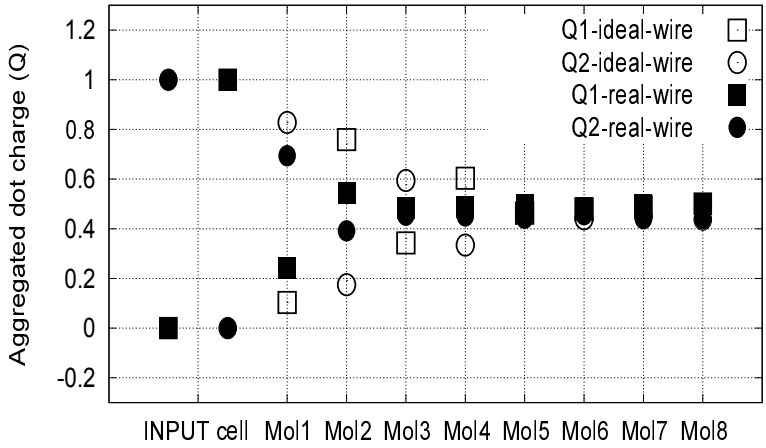

Figure 8.9 Aggregated dot charges of molecules along wire ($d = 1.0nm$) in presence of a low-rough gold substrate.

results in terms of charge distribution for the same *INPUT* cell state is shown in Figure 8.10.

Molecule number	Mol 1	Mol 2	Mol 3	Mol 4
$\Delta X(nm)$	0.00	+0.75	+0.15	-0.58
Molecule number	Mol 5	Mol 6	Mol 7	Mol 8
$\Delta X(nm)$	-0.49	-0.38	+0.10	+0.38

Table 8.4 Vertical shifts ΔX for molecules located on wire ($d = 0.8nm$) with respect to origin due to roughness on the sample of gold grain.

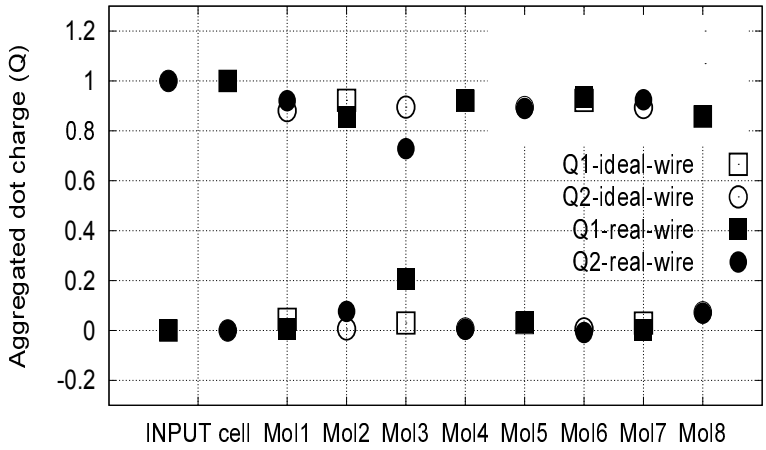

Figure 8.10 Aggregated dot charges of molecules along wire ($d = 0.8nm$) in presence of a low-rough gold substrate.

From the values reported in Figure 8.9 and Figure 8.10, it can be summarized that with for 1.0*nm* molecular wire, the roughness existed on the sample of the gold substrate sabotages the ability of MQCA wire for transmitting information, the aggregated charges are no more distinguishable except for the first cell with $Mol1$ and $Mol2$. On the contrary, in the case of 0.8*nm* molecular wire, although the roughness exists, the aggregated dot charges are preserved for all molecules and they are switching properly thus propagating the identical information carried by *INPUT* cell.

In the end, both noises and experimentally existing defects could affect the quality of information propagation among MQCA structure. In this part of analysis, we demonstrate their influence in evidence in case of a MQCA wire. Moreover, as a not-too-distant future work, it could be useful to define a *Safe-Operating-Area (SOA)* of MQCA operation by means of evaluating the fault tolerance of MQCA logic gates.

8.3 Pipeline Mechanism

Here a possible pipeline mechanism has been embedded into the algorithm with the aim of exploring the potential of high throughput of MQCA devices. In particular, it is realized assigning properly the clock phases. After the erase of previous information transmitted along clock zone on MQCA device during *Release* phase, a new logic state of *INPUT* cell is thus applied inside the coming *Relax* phase and waiting to be activated again. Meanwhile, the algorithm computes the influence due to the absence of previous input subtracting the previous mentioned initial interactions ($V_{IN-to-Moli}$, where *i*=1,2,...,*MolNum*) from *INPUT* cell to other molecules. Correspondingly, this would break the convergent status of molecules localized on MQCA devices thus further interaction computation is performed self-consistently until reaching the new steady-state.

Following the same clock zone division and multi-phase clock assignment discussed in Chapter 6 and Chapter 7, some examples of MQCA structure performances with applied pipeline mechanism have been demonstrated in cases like binary wire and three-input majority gate, see Figure 8.11 and Figure 8.12.

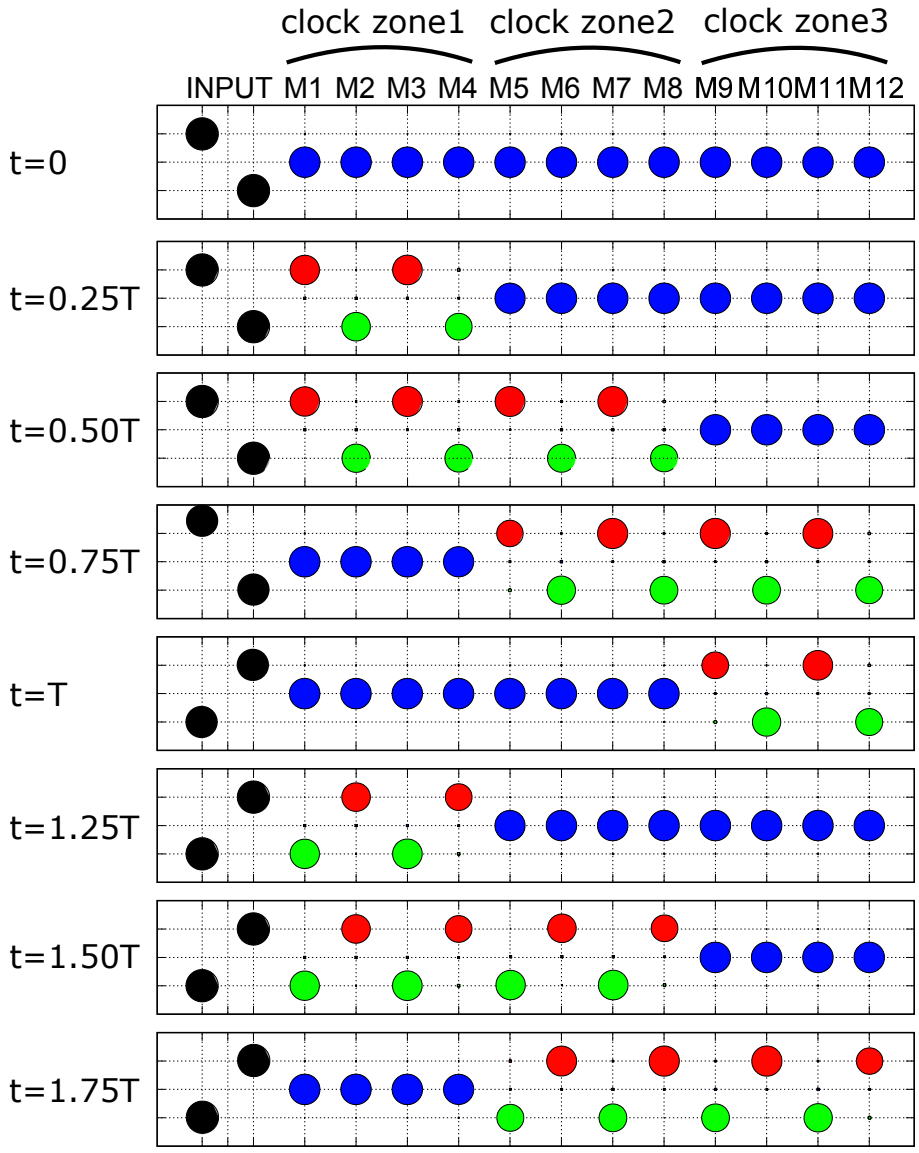

Figure 8.11 Clocked MQCA binary wire with pipeline mechanism applied changing *INPUT* cell logic state from "0" to "1" at $t = T$.

For the clocked MQCA wire, the results shown in Figure 8.11 is an extension of Figure 6.25 in Section 6.4.3 considering also the application of pipeline mechanism. The logic state of *INPUT* changes from "0" to "1" at $t = T$ after deleting previous propagated information. As a result of that, it can be observed that the binary information transmitted to the end of wire at $t = 0.75T$ and $t = 1.75T$ is with opposite values. Similar as before, the aggregated dot charges are represented by colored spheres.

As for case of three-input majority gate, in Figure 8.12, the MQCA majority voter behavior guided by the clock zones is depicted. Similar as the binary wire analyzed before, depending the *INPUT* cells assigned at the beginning, e.g., "0-1-0", the device outputs the majority of them, which is logic state “0” to the deciding molecules in the middle. Then, this information is transferred along the circuit following the clock signals to the end.

More specific, at $t = 0$, all the molecules are in *Relax* phase. For instance, inside the molecular cell near *INPUT* cell $IN1$, the aggregated charges for molecules $M1$ and $M2$ are respectively $+0.022$, $+0.034$, $+0.944$ and $+0.017$, $+0.054$, $+0.929$. Nearly all amount of the charge for each molecule is localized on the central dot. Then in the next clock phase ($t = 0.25T$), the first clock zone is activated. Hence the corresponded molecules switch according to the three *INPUT* cells $IN1$, $IN2$ and $IN3$. For example, the aggregated charges of $M3$ and $M4$ are respectively $+0.059$, $+0.868$, $+0.073$ and $+0.930$, $+0.004$, $+0.066$ thus encoding logic state “1” of *INPUT* cell $IN2$; whereas the aggregated charges of $M5$ and $M6$ are $+0.938$, $+0.011$, $+0.051$ and $+0.189$, $+0.744$, $+0.067$ encoding logic state “0” of *INPUT* cell $IN3$.

After that, at time $t = 0.50T$, both the first two clock zones are activated, and most importantly the deciding molecules located in the second clock zone eventually switch to logic state “0”, which is the majority logic states of the three inputs. However, due to reciprocal feedback effects during molecular interaction, the difference of aggregated charge between logic dots for $M2$, $M4$ and $M5$ are reduced.

At last, the binary information inside the majority voter propagated to the output cell distributed at the end and at $t = T$, the pipeline mechanism is applied in terms of changing new inputs (e.g. "1-1-1") when the previous information is deleted at $t = 0.75T$. As a consequence of that, the majority voter is capable to generate again the corresponding output with logic state “1” within another cycle of clock ($t = 1.75T$).

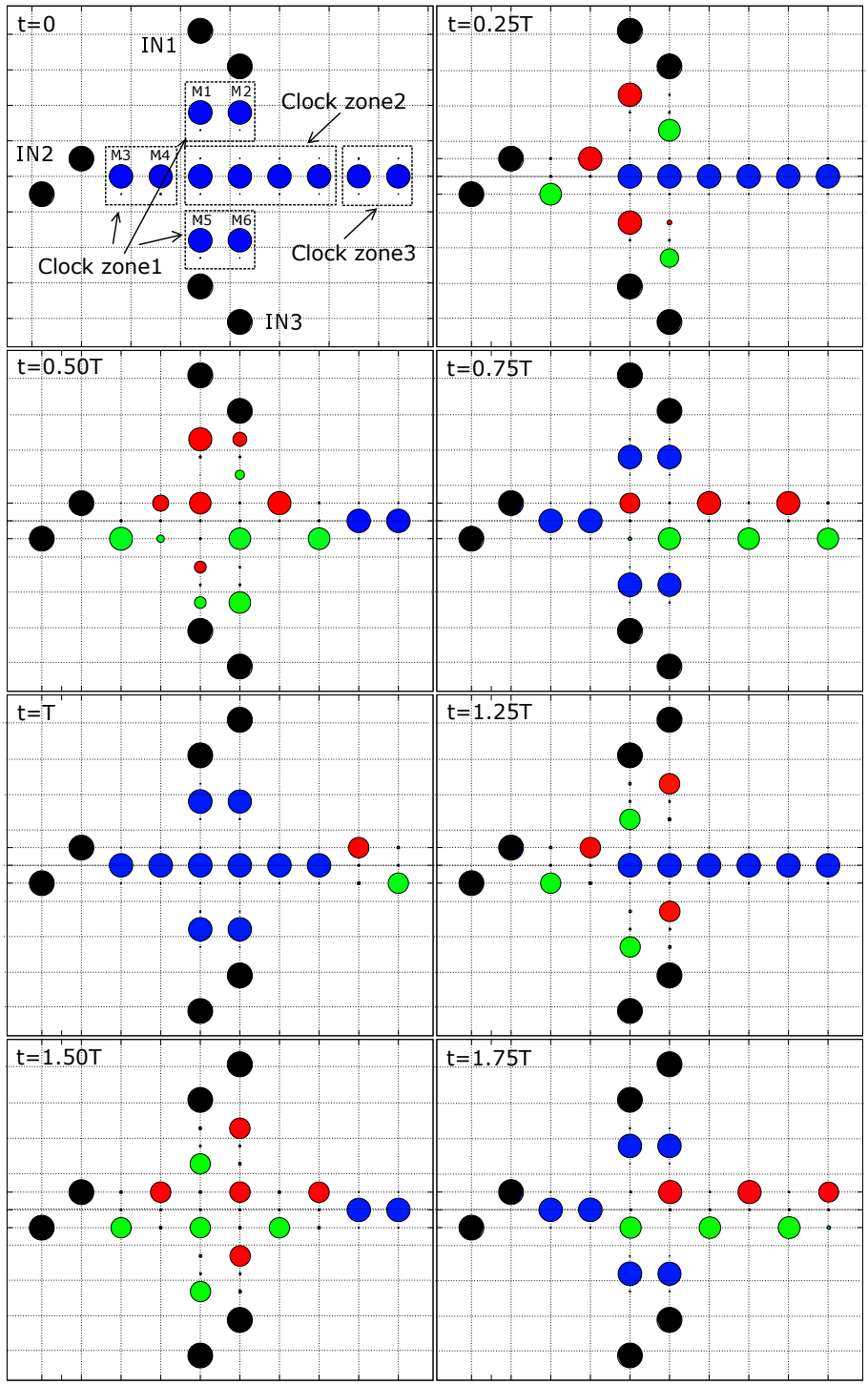

Figure 8.12 Clocked three-input majority gate with pipeline mechanism applied changing *INPUT* cells logic states from "010" to "111" at $t = T$.

Chapter 9

Ongoing and Future Work

Following large amount of work, there is general consensus that QCA networks are capable of Boolean computation, and that particularly the molecular solution is feasible and prone to ambient temperature operation. However, an implementation at the molecular scale has not yet been demonstrated. Therefore, in this part, we address some ongoing as well as some future work in order to promote the progress in terms of prototype fabrication.

9.1 On-going Work

9.1.1 Noise Influence and Process Variation

As one of the most important application for the implemented novel method including those algorithms, the noise influence analysis based on external disturbance is under investigation. Till now, analysis have already been done for disturbances in terms of unbalanced initial charges localized on molecule in ground state. Nevertheless, more complicated aspects should be modeled and addressed in detail. For example, thermal-dynamic influences and electrostatic interference, their effects might be random and continuous during the whole information propagation period along MQCA circuits.

As for the experimental related process variation, now inside the algorithm for analysis, these process variations in terms of mis-alignments among molecules are modeled as three-dimensional shifts and rotations regarding their coordinates. They

are based on the experimental data, like roughness of gold substrate. However, regardless of external data, a *Safe-Operating-Area (SOA)* has been determined for single bis-ferrocene molecule to be properly influenced from other molecules nearby [41]. Moreover, starting from that, a more complex SOA could be defined for the whole structure of MQCA devices thus determining their fault tolerance with respect to correct QCA operation. This could be extremely useful for choosing the precision of instruments during finally fabrication of device at molecular level. On the other hand, defects related to missing or extra molecules are also going to be considered during the initialization stage of the algorithm, see Section 6.2.2, in which MQCA device layout patterns are carefully described.

9.1.2 General-Purpose Application

The proposed novel method, including the ab-initio simulations, post-processing of simulation data, for MQCA circuit analysis is based on the developed effective algorithms. Particularly, such algorithms are prepared for MQCA devices made of bis-ferrocene molecules since it integrates the trans-characteristic curves of this candidate molecule.

Nevertheless, as mentioned in Section 2.4, during the journey of exploring the breakthrough of the field in MQCA, many molecules have been recommended as possible solutions, such as a simple example which represented by a methylene group placed between two phenyl rings, the three allyl groups connected by alkyl bridges in a "V" shape discussed in [25], the dially butane simulated in [14] and [68], the decatriene and bis-ferrocene molecule analyzed in [69]. Therefore, all of these types of molecule candidates could be actually considered inside our method rendering this whole package tool the ability to examine and to screen molecular candidates with QCA purpose for building MQCA devices as well as widening its range regarding application. Moreover, with different molecular structures, a Graphical User Interface (GUI) could be designed in order to facilitate the user to pick-and-place molecules and to design MQCA structure layout according to various requirements, as illustrated in Figure 9.1 and Figure 9.2. Then, these designed layout information would be converted into physical data of each molecule, e.g. coordinates, rotational angle or initial charge distribution for further MQCA computation.

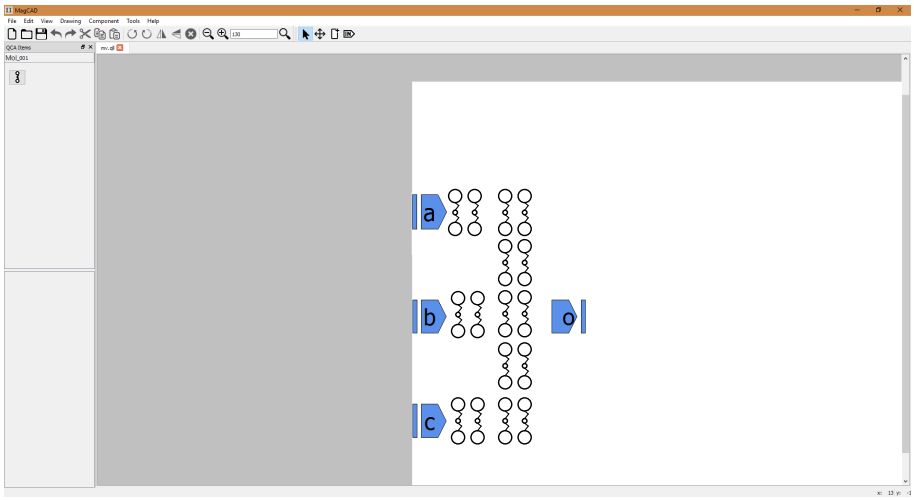

Figure 9.1 A three-input majority gate designed by pick-and-place of candidate molecules.

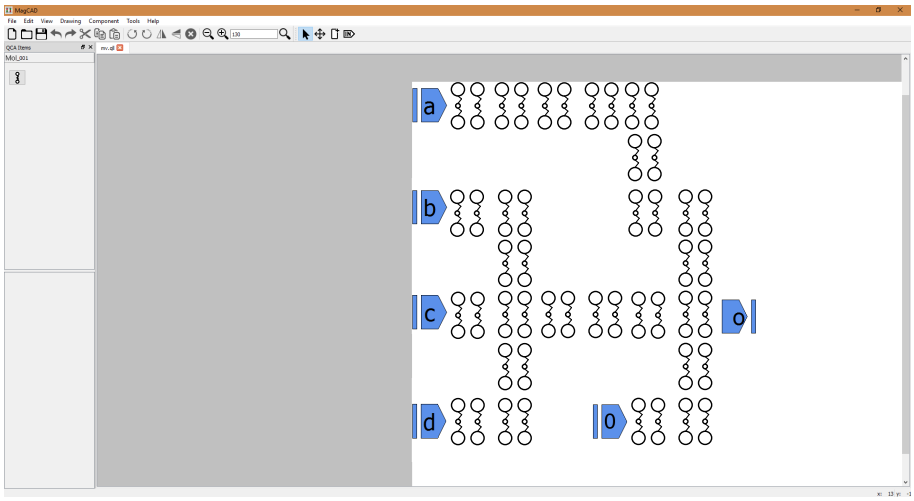

Figure 9.2 A more complicated MQCA structure consists of L-shape structure and three-input majority gate designed by pick-and-place of candidate molecules.

9.1.3 Experimental Set-up

The requirement for further MQCA application includes also the development of patterning techniques to have the molecules aligned and positioned in a controlled fashion, to which the observed trend to align to the crystallographic lines of gold is a favorable clue. As a consequence of that, the gold nanowires with comparable resolution with respect to nanometer-size is critical for forming molecular devices. Thus as an ongoing work, experimental demonstration of MQCA wire patterns, de-

position of metal substrate as well as deposition of clock and write-in electrodes are in progress. All these work are performed in *London Centre for Nanotechnology*.

9.1.3.1 Demonstration of MQCA Metal Wire Patterns

First of all, it turns out that this kind of technology, due to the molecular dimensions involved (1.0*nm* of width and 1.8*nm* of height), requires to work in the field of nanometer scales. These are very high resolutions to achieve through standard semiconductor processes. In particular, the device functioning requires to deposit the molecules sequentially along the wire. At the same time, it is important to avoid parallel depositions since the additional charges could induce interference among the electric fields. Currently, some macro-molecules can be deposited through single-molecule vapor deposition techniques and similar processes would being studied for smaller molecules. This means that the wire width plays a fundamental role: the narrower it is, the higher is the probability of having a sequential displacement of molecules along it. All these procedures involve the FIB equipment that is available in the clean room laboratory of the *London Center for Nanotechnology (LCN)*. Some fundamental trials regarding wire patterns (seen via Scanning Electron Microscope (SEM)) in terms of the production of trenches on a Silicon substrate through the FIB tool have been demonstrated in Figure 9.3 and Figure 9.4. Although the precision may be not achieved yet, it is meaningful as trial for demonstration of fabrication procedure.

9.1.3.2 Deposition of Metal Substrate

After the silicon patterning, the next step is to realize the metal substrate to which the thiol group (binding element) of a bis-ferrocene molecule can be anchored to. The bis-ferrocenes are very narrow molecules, thus the substrate needs to be as narrow to avoid parallel depositions. There exist several processes to perform metal deposition, such as evaporation, sputtering or Chemical Vapor Deposition (CVD). In this case, the FIB is provided with a gas injection system for ion implantation, that is a technique by which ions of a material are accelerated in an electric field and impacted into a target surface. Some obtained results are shown in Figure 9.5.

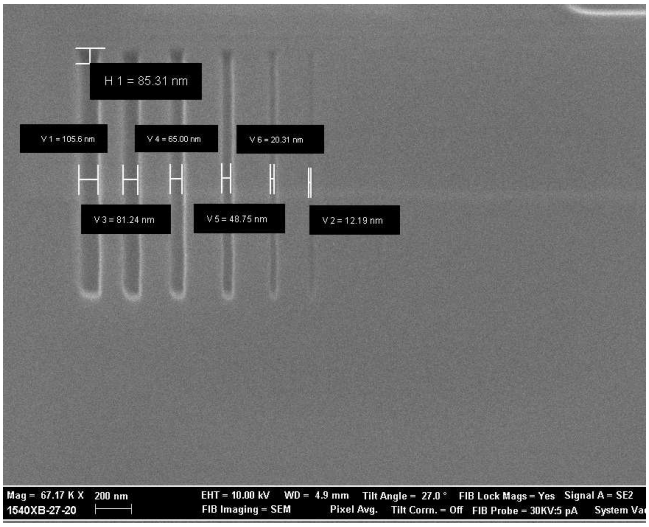

Figure 9.3 SEM image of wire pattern in terms of several trenches with height set to 80*nm* and variable widths.

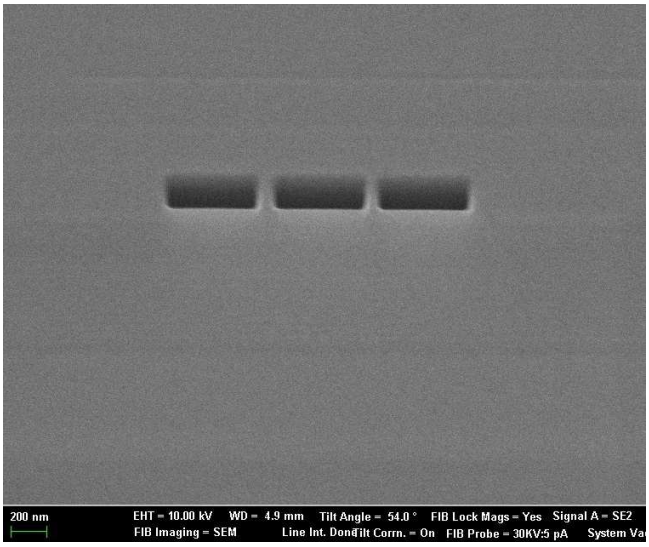

Figure 9.4 SEM image of wire pattern partitioned into clock zones in terms of three sequential trenches with small gaps in between.

9.1.3.3 Deposition of Electrodes

The following step is the deposition of metal strips which act as electrodes thus implementing the clock system and the write-in stage, as introduced previously in Section 3.2.2. Before actual experiments, the exact models in terms of aspect ratios and electrodes dimension are carefully designed and verified using *COMSOL Multiphysics*. Specifically, as demonstrated in Figure 9.6, it has been aimed at producing

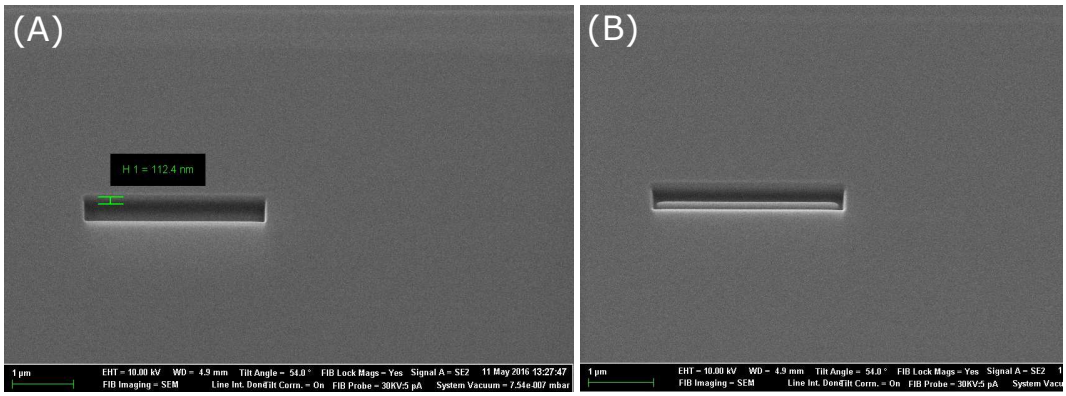

Figure 9.5 SEM images of (A) trenches (wire) patterned on Silicon substrate and (B) following deposition of Pt lines inside them.

lines as narrow as possible for the clock electrodes. The image shows a wire made of three clock zones, where the clock electrodes are separated by a small gap.

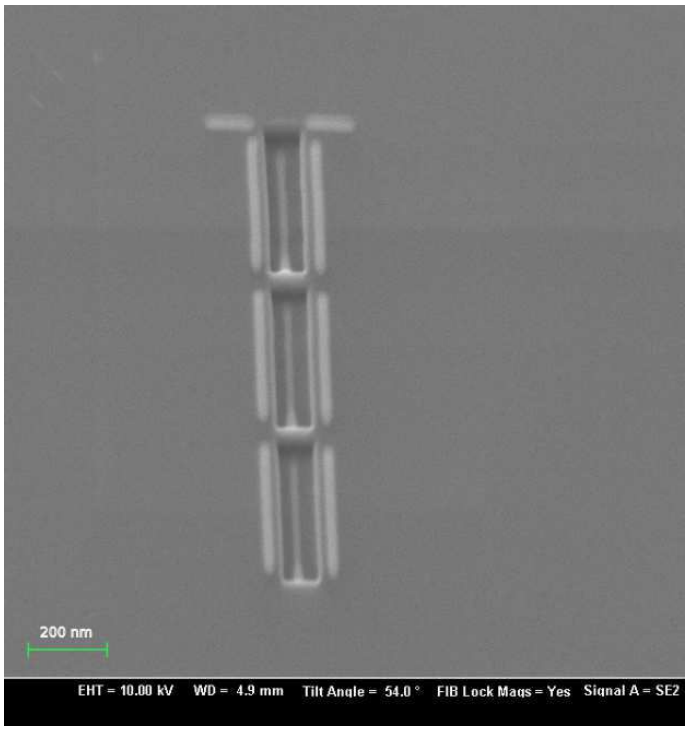

Figure 9.6 SEM image of clock electrodes deposited over the trench sides.

On the other hand, the same process is performed to realize the write-in system which is responsible for assigning proper binary information to MQCA devices, and the results are illustrated in Figure 9.7. By the same logic, the lines should be also as narrow as possible because the field components of write-in system must affect only

the first few molecules on the wire. Moreover, it is crucial for write-in electrodes to avoid interference with the voltage applied to the clock electrodes.

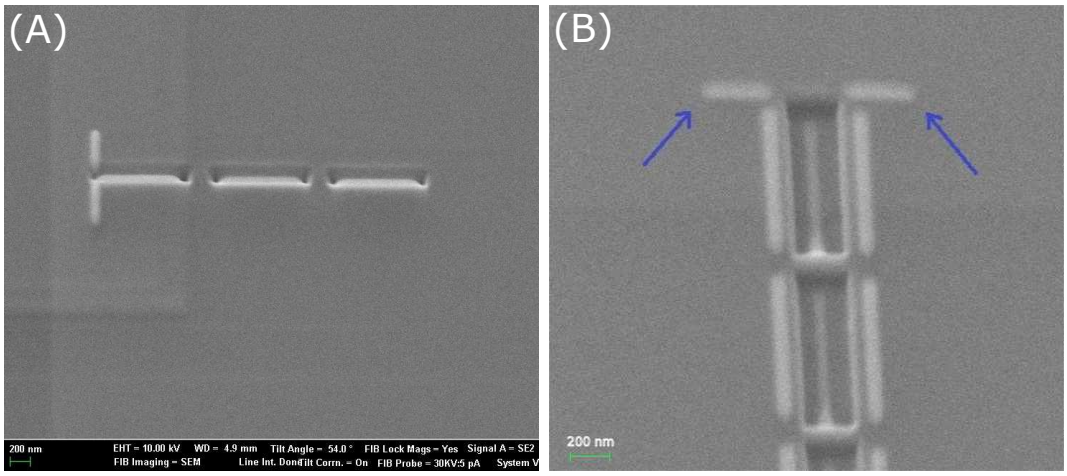

Figure 9.7 SEM images of write-in electrodes realized by FIB deposition on a wire made of three clock zones.

9.1.3.4 Deposition of Gold Nanowire for MQCA

Considering bis-ferrocene as the molecule candidate for implementing MQCA circuits, gold nanowire on the substrate is thus needed in terms of binding molecules via self-assembly. In this experimental procedure, based on the previously obtained results in 9.1.3.1, a new method is introduced with a higher resolution (sub-20nm) compared to the ion implantation mentioned previously in Section 9.1.3.2.

In particular, this new method starts with the wire patterns on silicon in Figure 9.3, then the selected trench is deposited with a layer of insulator, e.g. alumina (Al_2O_3), using thermal evaporator. After that, on top of the insulator, a layer of gold is deposited via *Physical vapour deposition (PVD)* sputtering. At last, a planarization process through FIB tool is performed removing the higher part of the gold nanowire, as shown in Figure 9.8. With this new procedure involved, the width resolution of fabricated nanowire could reach a value of 19.05nm with 42.86nm as wire height, see Figure 9.9. Although the currently achieved metal nanowire still not yet reaches the nanometer size resolution, these experimental data indicates the methodology for fabrication is executable and turned out to be of great importance for eventually scaling down of nanowire to molecular scale.

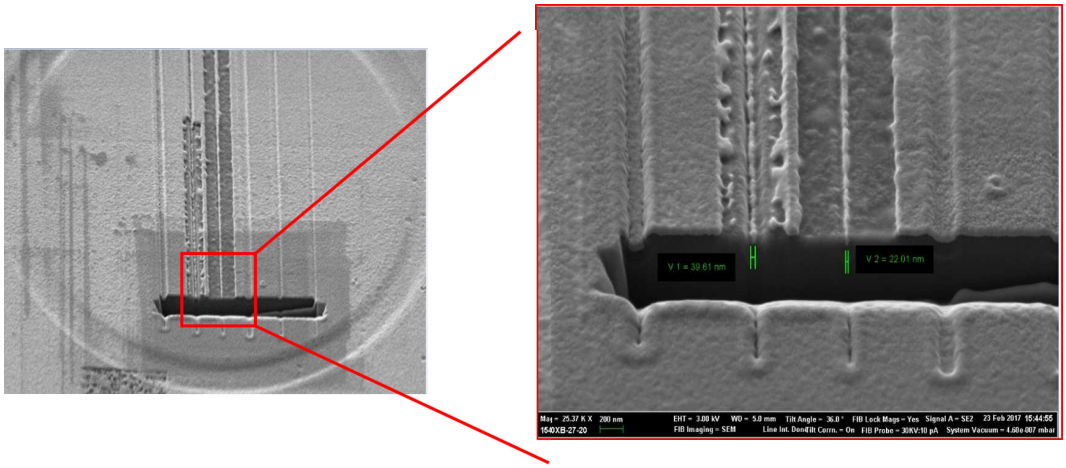

Figure 9.8 SEM images of gold nanowire fabricated considering the new method.

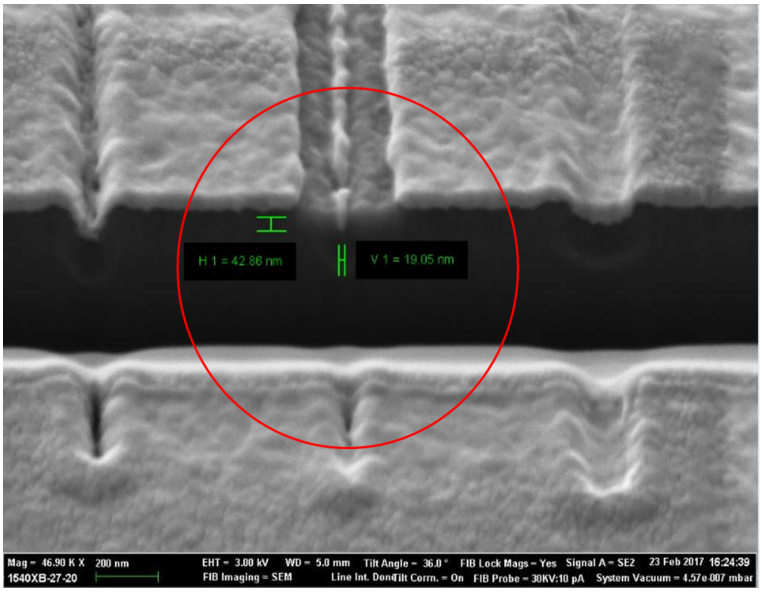

Figure 9.9 SEM images of a high-resolution (sub-20nm) gold nanowire fabricated using new method.

9.2 Future Work

9.2.1 Screening Effect During Molecular Behavior

Similar as the example introduced in Section 8.2.3, inside MQCA device, the information propagated among molecules deposited on metal nanowires. Thence, it is necessary to mention that interference between metal nanowire and the bis-

ferrocene molecules during molecular wire deposition and information transmission, i.e. the *Screening Effect*. In general, the so-called *Screening Effect* can be mainly divided into two aspects within the field of MQCA application.

Firstly, the screening effect between molecules and the substrate. Many molecules proposed in literature have the problem, even though partially solved, in terms of attaching molecules to proper substrate, those analysis seem not useful for experiments. If somehow the problem has been solved, e.g. the thiolated bis-ferrocene molecule could be anchored to the gold substrate self-assembly, which is good for massive production reducing the cost for creating molecular logic arrays, one should take into account the screening effect between the deposited molecules and metal nanowires on the substrate.

As known to all, if the quantum-dot is surrounded by dielectric or conducting medium (silicon or metal), the bare Coulomb interaction potential between two electrons localized inside the cell is screened due to moving of electrons and impure sprayed charges of the medium. Since the shape of the quantum dot is not isotropic, it is usually impossible to characterize the strength of the screening by one parameter, screening length. However, since the screening is effective for larger distances, it would be not bad to choose a screening length which is appropriate in-the-plane of the dot. And we use an approximated screened Coulomb potential,

$$U(\overrightarrow{r}) = \frac{e^2}{4\pi\varepsilon_0 r} e^{-\frac{r}{\lambda}}. \tag{9.1}$$

where λ is the screening length parameter [70]. Depending on different circumstances, e.g. the electron density of the conductor or superconductor around the quantum-dot, there are different models to calculate the screening length parameter, for example the *Debye–Hückel* approximation [71, 72] or the *Fermi-Thomas* approximation [73]. Therefore, this screened Coulomb potential is obtained by multiplying the Coulomb potential with an exponential damping term, with the strength of the damping factor given by the magnitude of $1/\lambda$, also called the Debye or Fermi-Thomas wave vector [74].

Secondly, the screened effect can be also existed between cells which would decrease the coupling interactions between nearby cells. This is because the screening action of the electronic clouds of the ligand atoms between redox centers may determine too large a suppression of the electrostatic interaction [76].

In the current work, we consider the Coulomb interaction among molecules deposited on the nanowire to be ideal neglecting the interference between molecule and nanowire or themselves. This is due to the molecular level of QCA cells in which we may no longer have screening effect by the semiconductor [10]. Although our procedure does not involve this issue, the results are remained acceptable since quantum chemistry simulation have shown that bi-stable properties can be obtained, as well as sufficient electrostatic interaction between neighboring bis-ferrocene molecules. Meanwhile, the main goal of this work is to introduce an alternative way of describing MQCA performance based on exact circuit layout patterns and to examine the possibility of using candidate molecule to create complex MQCA structures, and eventually to ensure the quality of information propagation.

However, when comes to experimentally set up of molecular devices, those mentioned analysis seems more reliable in terms of foreseeing MQCA behavior if contribution of screening effects are added to our methodology since there are analytical models for describing these effects, e.g. the authors derived in [75]. These models describe the reduction of inter-cell or intra-cell Coulomb interaction. In specific, they can be integrated inside the algorithms for evaluating the electrostatic interaction among nearby molecules, which before is ideally computed. Moreover, these calculations adopt exact physical parameters (size, temperature of operation, etc) of substrates and nanowires for evaluating the screening parameter in the equation 9.1. Once those values are carefully assigned from measurements, the screened Coulomb interactions can be evaluated in self-consistent way similar as before thus determining the final charge distribution on molecules.

On the other hand, considering the second screening action, it is more plausible to be found inside molecules which possess four or six redox centers representing a whole QCA cell structure. The electronic cloud of ligands atoms between redox centers, the logic dots or central dot whatsoever, could lead to a decreasing interaction. As a solution to that, the half-cell concept should be well explored and used, in particular aimed at the ultimate miniaturization, with which cells consisting single molecules [76]. Furthermore, another promising enhancement could be, instead of approximating the presence of bis-ferrocene molecule as rigid container with four aggregated charges describing its electrostatic property, using the more precise ninety-one atomic charges obtained from ab-initio simulations (ESP charge). With empirical choice of computational method and basis set, this solution

may consider the ligand atoms influence during the calculation of state switching inside molecules.

9.2.2 Switching Frequency and Energy Analysis

It is noteworthy that during all the analysis in this work, it is regardless of timing issue, e.g. the speed of switching among molecules or the time required for molecules to reach steady ground state from another degenerated one are not addressed. We are assuming the electrostatic interaction among molecules and information propagation is time-independent. Currently, molecular dynamics simulations (via *Material Studio*) based on bis-ferrocene molecule together with biasing conditions, e.g. electric field, are being performed in order to determine its molecular performance in terms of logic state switching. In the meantime, the timing parameter is also inserted for observation. However, in future work, attentions should be paid to time-dependent issues in terms of molecular dynamics and molecular device switching frequency in order to realize MQCA operation from circuit level point of view.

On the other hand, any digital device designed to represent data and perform computation, regardless of the physics principles it exploits and materials being used for implementation, must have two fundamental properties: distinguishability and conditional change of state, the latter implying the former. This means that such a device must have barriers that make it possible to distinguish between states and that it must have the ability to control these barriers to perform conditional change of state. For example, in a digital electronic system, transistors play the role of such controllable energy barriers, making it extremely practical to perform computing on them. As a consequence of that, the energy analysis in terms of electrostatic potential energy is necessary for assessing the performance of MQCA from a computational point of view.

During some ongoing work, since the communication based on MQCA technology happens without involving charge transportation, thus regarding the electrostatic energy, we referred to analyze the potential energy stored in a static charge distribution of the molecular system. Therefore during the calculation, we assumed that the charges in the molecular system were moved slowly enough making the their kinetic energy was neglected and any loss due to electromagnetic radiation

effects, significant if rapid charge accelerations occur, would be neglected. Figure 9.10 highlights some molecular orbitals calculated during switching of states for bis-ferrocene molecule. Particularly, the HOMOs, i.e. Highest Occupied Molecular Orbitals are mostly localized on the ferrocenes, as expected in a MQCA cell which, when no clocking is applied, must store a definite Boolean state; conversely, if a prohibiting clock is applied, the HOMO is well localized on the central carbazole encoding the *NULL* state.

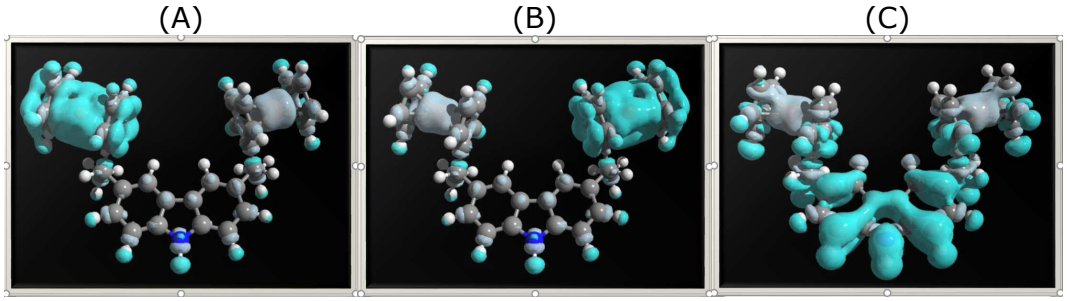

Figure 9.10 Some calculated molecular orbitals (HOMOs) for bis-ferrocene molecule during state switching: (A) Logic state "1"; (B) Logic state "0"; (C) *NULL* state.

For example, concerning the atomic charges distributed on the molecule at equilibrium which were obtained from ab-initio simulations, the electrostatic energy can be recognized as the work needed to bring those static charges from infinity and assemble them in such required formation for MQCA computation. When the molecule is switched from the equilibrium condition, the total electrostatic energy changes and the difference with respect to the equilibrium case can be considered as the energy which would be released to the molecule in order to realize the switch of logic states, e.g. cell-to-cell interaction, hence making the information propagated through MQCA devices.

Chapter 10

Conclusion

Since 1965, Moore's law dictates that the number of devices integrated on a single die doubles every year and a half. However, intensive studies indicate also since 2012 the CMOS transistor hit the physical scaling limits which inhibit this aggressive packing of devices. Therefore pondering near this edge, the Molecular Quantum-dot Cellular Automata (MQCA) has been, promisingly, advocated as an emerging device architecture of great potential for field-coupled nanocomputing with purpose of computation.

As most of the research articles about MQCA, in which properties of different molecule candidates regarding their non-linear behavior, bi-stable interaction between molecules on which the essential device performance depends, were thoroughly discussed, but things like layout and patterning, input/output stage, appropriate circuit architecture based on candidate molecules, clocked control, screening effect, or the speed of molecular switching response are not addressed. The majority analysis of these intensive researches are by means of theoretically solving the many-electron *Schroedinger Equation* self-consistently or adopting computational chemistry software. Meanwhile, from experimental point of view, most of the discussed molecules possessed the difficulty to be attached to a substrate, e.g. due to the reactivity of the allyl groups. Hence they do not seem likely candidates for MQCA experimental demonstration.

Oppositely, the aim of this work is to demonstrate and analyze the performance of MQCA devices made of the so-called *Bis-ferrocene* molecule, which is firstly artificially synthesized for a MQCA cell prototype, from an electronic point of view

hence modeling these molecules as components for electronic devices and foreseeing their performance taking into account potential thermal noises and experimental-related process variations, e.g. mis-alignments between molecules or missing one or more of them.

In particular, a two-stage procedure based on quantum chemistry ab-initio simulations with empirical choices of computational method and basis set, and post-processing of simulation data has been carried out in order to characterize the bis-ferrocene molecule and to examine its possibility for building MQCA devices. The obtained results suggest that the bis-ferrocene molecule, especially in its oxidized form with counterion in presence, is one such suitable candidate due to: (i) its bi-stable capability of confining charge on two lateral quantum logic dots (the ferrocenes) for logic state encoding; (ii) the ability to confine charge on both logic dots shows its sensitive response with respect to externally applied biasing conditions like electric field or point charges implying the successful write-in stage implementation and excellent switching property while information propagates; (iii) its middle carbazole which acts as the central dot is sensitive to the clock signal in terms of confining charge encoding *NULL* state between logic states switches, e.g. pipeline mechanism; (iv) the good stability when immobilized in the solid state with thiolated element during SAM. Similar results in terms of bi-stable condition with sufficient electrostatic interaction and clocking control have also been achieved in the case of complete MQCA cell with two bis-ferrocene molecules aligned together.

Whereas regarding analysis for MQCA logic functional blocks that are composed of bis-ferrocene molecules, methods based on quantum chemistry demonstrates their limitations in terms of unexpected charge movement and intensive computation. Therefore, a new alternative method has been introduced and implemented for complicated MQCA structure study. This new method procedure is come up with effective algorithms, which rely on single molecule characterization results achieved from ab-initio simulations and reciprocal models of describing and evaluating electrostatic interactions among molecules, based on which binary information could be determined and transmitted. To be specific, it is necessary to characterize single bis-ferrocene molecule in terms of deriving a trans-characteristic (Charge vs. Voltage). Such relationship is important to illustrate the ability of one molecule to response to other molecules in presence. In stead of adopting classic molecular dipole moment or charge polarization, new figures of merits, i.e., *Aggregated Charge* and *Equivalent-Input-Voltage* V_{in} have been defined for more directly

picturing such relationship. On the other hand, with respect to computing molecular interactions, the *Cause* & *Effect* evaluation procedure, which models the reciprocal electrostatic interactions among molecules on wire, is iterated back-and-forth in a self-consistent way until reach convergence, during which the molecules are modeled as rigid charge containers to represent their electrostatic state and furthermore, the Coulomb interaction among neighboring molecules is assumed to be ideal without considering screening effects for sake of approximation and reducing computational resources. Eventually, the algorithms output aggregated charges distribution along the whole MQCA structure highlighting the steady ground state with minimum energy after molecule switching following properly defined input condition.

Our proposed method adopted here breaks the limitation of using quantum chemistry simulation to analyze MQCA device behavior as well as solves one of the gap which is preventing those molecules from being recognized as elements in a digital circuit. With the proposed new method of analysis based on effective algorithms, the results generated are not only schematic but also quantitative since the highlighted dot size is proportional to the aggregated dot charge. They are convincing and somehow make the prediction regarding the switching of molecules that forwards binary information possible. As a consequence of that, the study of MQCA with actually synthesized molecules has also moved from the single molecule (or cell) level to systematic circuitry level. In addition, with the method used for applications like thermal noises analysis and process variations concerning fabrication related physical constrains, the fault tolerance for guaranteeing the quality of MQCA device operation is thereby provided.

On the other hand, although our study is based on bis-ferrocene molecule, the proposed methodology and analysis procedure is not only concentrated on one specific candidate molecule. The whole analyzing package discussed above is both fundamental and generic, which provides also the possibility to examine other potential candidate molecules that might be suitable or not with purpose of MQCA computation. More importantly, as future work, more precise molecular interaction modeling mechanism, e.g. ninety-one atomic charge emulation of present molecule, screening effects between molecules and conduction metal nanowires or among molecule themselves as well as dynamic switching response of molecules should be involved increasing the accuracy of our modeling methods. In this way, important feedback would have been created between circuit designers and QCA technol-

ogists. Such strong link would eventually facilitate the experimental demonstration of computationally interesting circuits implemented with MQCA technology.

Bibliography

[1] Disco. Cornelius, Van der Meulen. Barend, *Getting new technologies together*, New York: Walter de Gruyter. pp.206-207. ISBN 3-11-015630-X. OCLC 39391108. Retrieved August 23, 2008.

[2] *Overall Technology Roadmap Characteristics*, International Technology Roadmap for Semiconductors. 2010. Retrieved 2013-08-08.

[3] Moore, Gordon (March 30, 2015). *Gordon Moore: The Man Whose Name Means Progress, The visionary engineer reflects on 50 years of Moore's Law*. IEEE Spectrum: Special Report: 50 Years of Moore's Law (Interview). Interview with Rachel Courtland. "We won't have the rate of progress that we've had over the last few decades. I think that's inevitable with any technology; it eventually saturates out. I guess I see Moore's law dying here in the next decade or so, but that's not surprising."

[4] Von Trapp, Francoise, *Executive Interview: Bill Bottoms Talks about Revamping the ITRS Roadmap*, 3D InCites. 3D InCites. Retrieved April 14, 2015.

[5] James A. Hutchby, George I. Bourianoff, Victor V. Zhirnov, and Joe E. Brewer, *Extending the road beyond CMOS*, IEEE circuits and devices magazine, March, 2002

[6] Semiconductor Industry Association, International Technology Roadmap of Semiconductors 2.0, 2015 Edition, Emerging research Device (ERD).

[7] N.G. Anderson, S. Bhanja (eds.), Field-Coupled Nanocomputing: Paradigms, Progress, and Perspectives., LNCS, vol. 8280. Springer, Heidelberg, 2014.

[8] Craig S. Lent, P. Douglas Tougaw, and Wolfgang Porod, *Quantum Cellular Automata* Nanotechnology, vol. 4, pp. 49-57, 1993.

[9] C.S. Lent, P.D. Tougaw and W. Porod, *Bistable saturation in coupled quantum dots for quantum cellular automata*, Appl. Phys. Lett., vol. 62, p. 714, 1993.

[10] C.S. Lent, P.D. Tougaw and W. Porod, *Quantum cellular automata: the physics of computing with arrays of quantum dot molecules*, PHYSCOMP 94 Proceedings, pp. 5-13, 1994.

[11] Y. Lu and C S Lent, *A metric for characterizing the bistability of quantum-dot cellular automata*, Nanotechnology, vol. 19, 2008.

[12] G. Toth and C.S. Lent, *Quasi-adiabatic Switching for Metal-Island Quantum-dot Cellular Automata*, Journal of Applied Physics, vol. 85, pp. 2977-2984, 1999.

[13] P.D. Tougaw and C.S. Lent, *Logical devices implemented using quantum cellular automata*, Journal of Applied Physics, vol. 75, pp. 1818-1825, 1994.

[14] C.S. Lent, B. Isaksen and M. Lieberman, *Molecular quantum-dot cellular automata*, J. Am. Chem. Soc., vol. 125, pp. 1056-1063, 2003.

[15] Wei Wang, K. Walus, G.A. Jullien, *Quantum-dot cellular automata adders*, IEEE-NANO 2003, vol. 2, pp. 461- 464, 2003.

[16] H. Cho and EE. Swartzlander, *Adder designs and analyses for quantum-dot cellular automata*, Nanotechnology, IEEE Transactions on, vol. 6, no. 3, pp. 374-383, 2007.

[17] H. Cho and E E. Swartzlander, *Adder and multiplier design in Quantum-dot Cellular Automata*, Computers, IEEE Transactions on, vol. 58, no. 6, June, 2009.

[18] M.T. Niemier, M.J. Kontz and P.M. Kogge, *A design of and design tools for a novel quantum dot based microprocessor*, Proceedings of 27th Design Automation Conference, pp. 227-232, 2000.

[19] K. Walus, M. Mazur, G. Schulhof and G.A. Jullien, *Simple 4-bit processor based on quantum-dot cellular automata (QCA)*, Application-Specific Systems, Architecture Processors, 16th IEEE International Conference on, 2005.

[20] C.S. Lent and P.D. Tougaw, *A Device Architecture for Computing with Quantum Dots*, Proceedings of the IEEE 85, pp. 541-557, 1997.

[21] A.O. Orlov, I. Amlani, R.K. Kummamuru, R. Ramasubramaniam, G. Toth, C.S. Lent, G.H. Bernstein and G.L. Snider, *Experimental demonstration of clocked single-electron switching in quantum-dot cellular automata*, App. Phys. Lett., vol. 77, pp. 295-297, 2000.

[22] V. Vankamamidi, M. Ottavi, F. Lombardi, *Clocking and Cell Placement for QCA*, IEEE-NANO 2006, vol. 1, pp. 343- 346, 2006.

[23] Douglas Tougaw, *A clocking strategy for scalable and fault-tolerant QDCA signal distribution in combinational and sequential devices*, in N.G. Anderson, S. Bhanja (eds.), Field-Coupled Nanocomputing: Paradigms, Progress, and Perspectives., LNCS, vol. 8280. Springer, Heidelberg, 2014.

[24] V. Vankamamidi, M. Ottavi, F. Lombardi, *Two-Dimensional Schemes for ClockingTiming of QCA Circuits*, Computer-Aided Design of Integrated Circuits and Systems, IEEE Transactions on , vol.27, no.1, pp.34,44, Jan. 2008.

[25] C.S. Lent and B. Isaksen, *Clocked molecular quantum-dot cellular automata*, Electron Devices, IEEE Transactions on, vol. 50, pp. 1890-1896, 2003.

[26] A. O. Orlov, I. Amlani, R. Kummamuru, R. Rajagopal, G. Toth, J.Timler, C. S. Lent, G. H. Bernstein, and G. L. Snider, *Power gain in a Quantum-dot Cellular Automata latch*, Appl. Phys. Lett., vol. 81, pp.1332-1334, 2002.

[27] J. Timler and C. S. Lent, *Dissipation and gain in quantum-dot cellular automata*, J. Appl. Phys., vol. 91, pp. 823-831, 2002.

[28] C.S. Lent and P.D. Tougaw, *Bistable saturation due to single electron charging in rings of tunnel junctions*, Journal of Applied Physics, vol. 75, pp. 4077-4080, 1994.

[29] I. Amlani, A.O. Orlov, G.L. Snider, C.S. Lent and G.H. Bernstein, *Demonstration of a functional quantum-dot cellular automata cell*, Journal of Vacuum Science and Technology B, vol. 16, pp 3795-3799, 1998.

[30] G.H. Bernstein, I. Amlani, A.O. Orlov, C.S. Lent and G.L. Snider, *Observation of switching in a quantum-dot cellular automata cell*, Nanotechnology, vol. 10, pp. 166-173, 1999.

[31] M. Mitica, M. C. Cassidy, K. D. Peterssonb, R. P. Starrett, E. Gauja, R. Brenner, R. G. Clark, and A. S. Dzurak C. Yang and D. N. Jamieson, *Demonstration of a silicon-based quantum cellular automata cell*, Appl. Phys. Lett. 89, 013503 (2006); doi: 10.1063/1.2219128.

[32] F. Perez Martineza, I. Farrer, D. Anderson, G. A. C. Jones, D. A. Ritchie, S. J. Chorley, and C. G. Smith, *Demonstration of a quantum cellular automata cell in a GaAs/AlGaAs heterostructure*, Appl. Phys. Lett. 91, 032102 (2007); doi: 10.1063/1.2759257.

[33] G. Csaba and W. Porod, *Simulation of field coupled computing architectures based on magnetic dot arrays*, Journal of Computational Electronics, vol. 1, pp. 87-91, 2002.

[34] A. Orlov, A. Imre, G. Csaba, L. Ji, W. Porod, and G. H. Bernstein, *Magnetic quantum-dot cellular automata: Recent developments and prospects*, J. Nanoelec- tron. Optoelectron., vol. 3, no. 1, pp. 55-68, 2008.

[35] E. Varga, A. Orlov, M.T. Niemier, X.S. Hu, G.H. Bernstein and W. Porod, *Experimental demonstration of fanout for nanomagnetic logic*, IEEE Trans. Nanotechnol., vol. 9, no. 6, pp. 668-670, 2010.

[36] C.S. Lent, *Molecular Electronics: Bypassing the Transistor Paradigm*, Science, vol. 288, pp. 1597-1599, 2000.

[37] K. Hennessy and C.S. Lent, *Clocking of molecular quantum-dot cellular automata*, Journal of Vacuum Science and Technology B, vol. 19, pp. 1752-1755, 2001.

[38] Y. Lu and C.S. Lent, *Theoretical Study of Molecular Quantum-Dot Cellular Automata*, Journal of Computational Electronics, vol. 4, pp. 115-118, 2005.

[39] M.T. Niemier, *The effects of a New Technology on the Design, Organization, and Architectures of Computing System*, Ph.D. Dissertation.

[40] Christie, et al., *Synthesis of a Neutral Mixed-Valence Diferrocenyl Carborane for Molecular Quantum-Dot Cellular Automata Applications*, Angewandte Chemie 127, 15668-15671, 2015.

[41] A. Pulimeno, M. Graziano, A. Antidormi, R. Wang, A. Zahir and G. Piccinini, *Understanding a Bisferrocene Molecular QCA wire*, in N.G. Anderson, S. Bhanja (eds.), Field-Coupled Nanocomputing: Paradigms, Progress, and Perspectives., LNCS, vol. 8280. Springer, Heidelberg, 2014.

[42] M. Graziano, M. Vacca, A. Chiolerio, M. Zamboni, *A NCL-HDL Snake-Clock Based Magnetic QCA Architecture*, IEEE Transaction on Nanotechnology, vol. 10 n. 5, pp. 1141-1149, 2011.

[43] John Timler and Craig S. Lent, *Power gain and dissipation in quantum-dot cellular automata*, Journal of Applied Physics, Vol. 91, No. 2, 2002.

[44] Y. Lu, M. Liu and C.S. Lent, *Molecular quantum-dot cellular automata: From molecular structure to circuit dynamics*, Journal of Applied Physics, vol. 102, 2007.

[45] H. Qi, S. Sharma, Z. Li, G.L. Snider, A.O. Orlov, C.S. Lent and T.P. Fehlner, *Molecular quantum cellular automata cells. Electric field driven switching of a silicon surface bound array of vertically oriented two-dot molecular quantum cellular automata*, J. Am. Chem. Soc., vol. 125, pp. 15250-15259, 2003.

[46] Y. Lu and C.S. Lent, *Self-doping of molecular quantum-dot cellular automata: mixed valence zwitterions*, Phys. Chem. Chem. Phys., vol. 13, pp. 14928-14936, 2011.

[47] R. Quardokus, Y. Lu, N.A. Wasio, C.S. Lent, F. Justaud, C. Lapinte and S.A. Kandel, *Through-Bond versus Through-Space Coupling in Mixed-Valence Molecules: Observation of Electron Localization at the Single-Molecule Scale*, J. Am. Chem. Soc., vol. 134, pp. 1710-1714, 2012.

[48] V. Arima, M. Iurlo, L. Zoli, S. Kumar, M. Piacenza, F. Della Sala, F. Matino, G. Maruccio, R. Rinaldi, F. Paolucci, M. Marcaccio, P.G. Cozzi and A.P. Bramanti, *Toward quantum-dot cellular automata units: thiolated-carbazole linked bisferrocenes*, Nanoscale, vol. 4, pp. 813-823, 2012.

[49] L. Zoli, *Active bis-ferrocene molecules as unit for molecular computation*, PhD dissertation, 2010.

[50] A. Pulimeno, M. Graziano, C. Abrardi, D. Demarchi, and G. Piccinini, *Molecular QCA: A write-in system based on electric fields*, IEEE Nanoelectronics Conference (INEC), June 2011.

[51] A. Pulimeno, M. Graziano, and G. Piccinini, *Molecule Interaction for QCA Computation*, IEEE NANO2012 12th International Conference on Nanotechnology, Birmingham (UK), 20-23 August 2012.

[52] A. Pulimeno, M. Graziano, A. Sanginario, V. Cauda, D. Demarchi and G. Piccinini, *Bis-ferrocene molecular QCA wire: ab-initio simulations of fabrication driven fault tolerance*, IEEE Transactions on Nanotechnology, vol. 12, pp. 498-507, 2014.

[53] R. Wang, A. Pulimeno, M. Ruo Roch, G. Turvani, M. Graziano and G. Piccinini, *Effect of a clock system on bis-ferrocene molecular QCA*, IEEE Transactions on Nanotechnology, vol. 15, No.4, 2016.

[54] A. Pulimeno, M. Graziano, D. Demarchi, and G. Piccinini, *Towards a molecular QCA wire: simulation of write-in and read-out systems*, Solid State Electronics, Elsevier, vol. 77, pp. 101-107, 2012.

[55] M.J. Frisch et al. *Gaussian09 Revision A.1*, Gaussian Inc. Wallingford CT 2009.

[56] U. C. Singh, P. A. Kollman, *An approach to computing electrostatic charges for molecules*, Journal on Computational Chemistry, vol. 5, pp 129 - 145, 1984.

[57] A. T. B. GILBERT and P. M.W. GILL, *A point-charge model for electrostatic potentials based on a local projection of multipole moments*, Molecular Simulation, Vol. 32, No. 15, 30 December 2006, 1249-1253.

[58] MathWorks@MATLAB, https://it.mathworks.com/products/matlab.html. 2016

[59] Octave community, *GNU Octave 3.8.1*, www.gnu.org/software/octave/, 2014.

[60] A. Pulimeno, M. Graziano, R. Wang, D. Demarchi and G. Piccinini, *Charge distribution in a molecular QCA wire based on bis-ferrocene molecules*, NANOARCH, pp. 42-43, 2013.

[61] Konard Walus, Timothly J. Dysart, Graham A. Jullien and Arief R. Budiman, *QCADesigner: A Rapid Design and Simulation Tool for Quantum-Dot Cellular Automata*, IEEE Transactions on Nanotechnology, Volume. 3, Issue, 1, March 2004.

[62] M. Momenzadeh, M. Ottavi and F. Lombardi, *Modeling QCA Defects at Molecular-level in Combinational Circuits*, Proc. of 20th IEEE international Symposium on Defect and Fault Tolerance in VLSI Systems (DFT05), 2005.

[63] Tahoori, M., J. Huang, M. M., and Lombardi, F, *Testing of Quantum Cellular Automata*, IEEE TRANSACTIONS ON NANOTECHNOLOGY, VOL. 3, NO. 4, DECEMBER 2004

[64] M. Graziano, A. Pulimeno, R. Wang, X. Wei, M. Ruo Roch, G. Piccinini, *Process Variability and Energy Analysis of Molecular QCA*, ACM Journal on Emerging Technologies, Volume 12 Issue 2, August 2015.

[65] M. R. Casu, M. Graziano, G. Masera, Member, IEEE, G. Piccinini and M. Zamboni, *An Electromigration and Thermal Model of Power Wires for a Priori High-Level Reliability Prediction*, IEEE Transaction on VLSI system, vol. 12, No. 4, 2004.

[66] L.D. Eske and D.W. Galipeau, *Characterization of SiO2 surface treatments using AFM, contact angles and a novel dewpoint technique*, Colloids and surface A: Physicochemical and Engineering Aspects, vol. 154, pp 33-51, 1999.

[67] V. Svorcik, J. Siegel, P. Sutta, J. Mistrik, P. Janicek, P. Worsch and Z. Kolska, *Annealing of gold nanostructures sputtered on glass substrate*, Applied Physics A: Materials Science & Processing, vol. 102, no. 3, pp 605-610, 2011.

[68] doi:10.1186/1556-276X-7-274 Rahimi and Nejad, *Quasi-classical modeling of molecular quantum-dot cellular automata multi-driver gates*, Nanoscale Research Letters, 2012, 7:274.

[69] A. Pulimeno, M. Graziano and G. Piccinini, *Effectiveness of Molecules for QCA*, submitted.

[70] McComb, W.D., *Renormalization methods : a guide for beginners*, Oxford University Press, ISBN 978-0199236527, 2007.

[71] Escande. D.F., Elskens.Yves and Doveil. F, *Direct path from microscopic mechanics to Debye shielding, Landau damping and wave-particle interaction*, Plasma Physics and Controlled Fusion, DOI:10.1088/0741-3335/57/2/025017, 2015.

[72] P. Debye and E. Hückel, *The theory of electrolytes. I. Lowering of freezing point and related phenomena*, Physikalische Zeitschrift, 24: 185–206.

[73] N. W. Ashcroft and N. D. Mermin, Solid State Physics (Thomson Learning, Toronto, 1976).

[74] Escande, D.F., Doveil. F and Elskens. Yves, *N-body description of Debye shielding and Landau damping*, Plasma Physics and Controlled Fusion, DOI:10.1088/0741-3335/58/1/014040.

[75] H. Ouerdane, *Analytic model of effective screened Coulomb interactions in a multilayer system*, JOURNAL OF APPLIED PHYSICS, DOI:10.1063/1.3646482, 2011.

[76] Rainer Waser, *Nanotechnology: Volume 4: Information Technology II*, ISBN:978-3-527-31737-0, 2008.